Observational Cosmology

The Cosmic Microwave Background

Part IV: CMB detectors, CMB secondary anisotropies

Kaustuv Basu

Course website:
https://www.astro.uni-bonn.de/~kbasu/ObsCosmo

CMB detectors, space- and ground-observations

CMB receiver types

Coherent receivers:

Phase-preserving amplification
Correlation of different polarization

- Correlation/Pseudocorrelation receiver (e.g. WMAP, CAPMAP)
- Interferometer (e.g. DASI, CBI)

Incoherent receivers (bolometers):

Direct detection of radiation,
No phase information kept
Large arrays!

- Bolometers (e.g. ACBAR, Boomerang, BICEP, Clover, Planck)

Interferometers for CMB

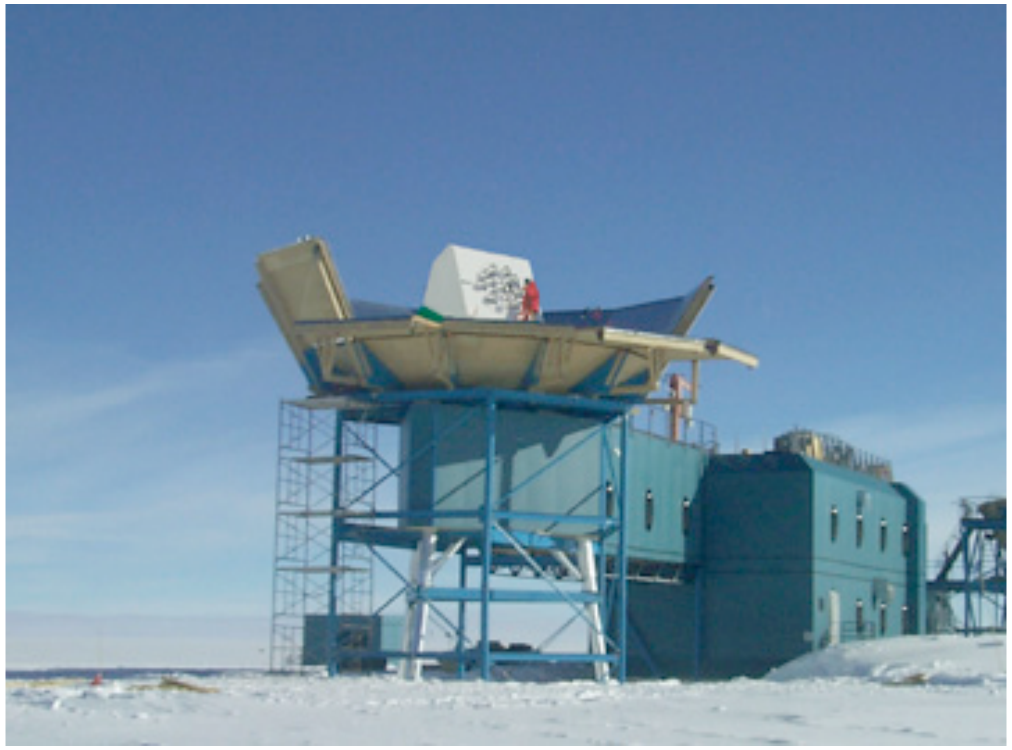

DASI in South Pole

CBI in Atacama desert

Coherent receivers: Can be configured so that the output is the correlation of two input signals.
HEMT (High Electron Mobility Transistor) allow coherent amplification with low noise and high gain.

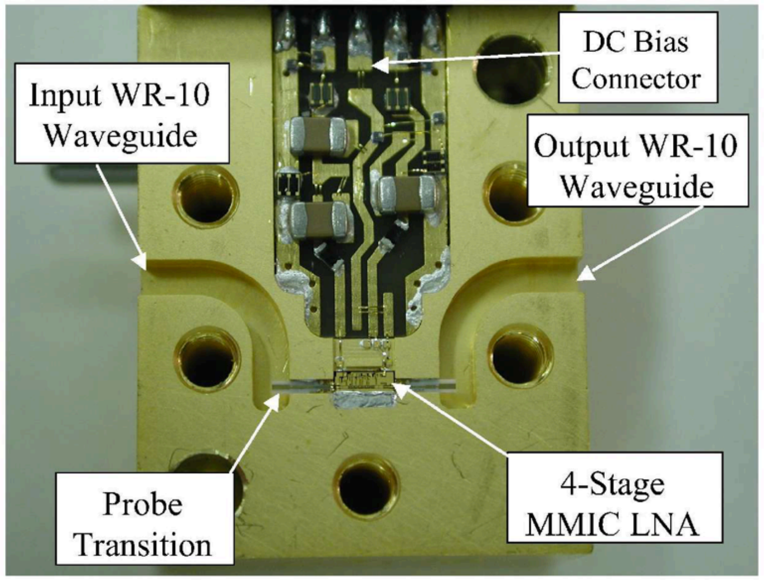

Interferometric measurement

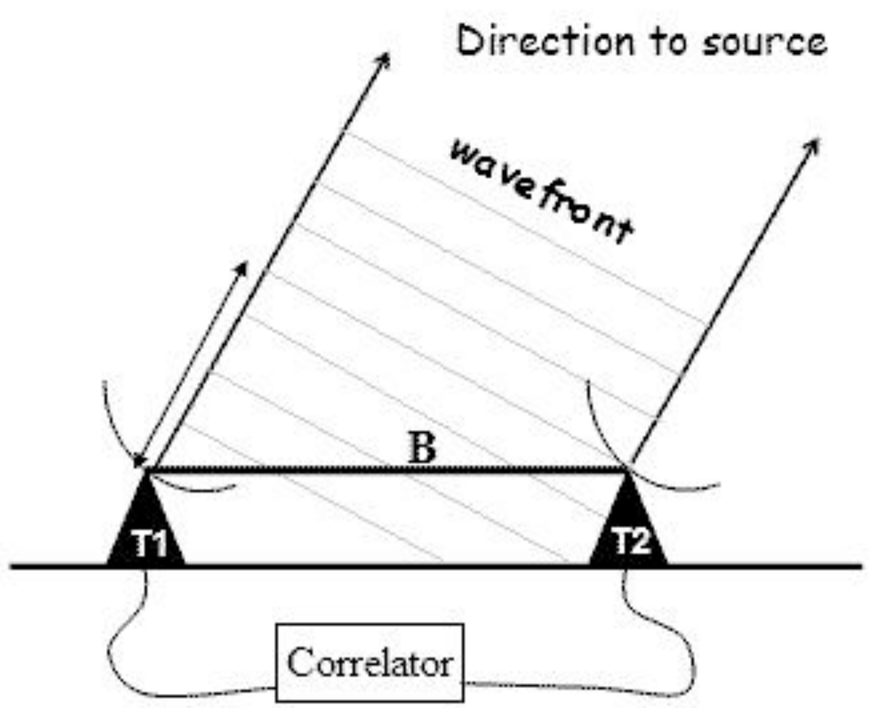

Properties of interferometers that make them ideally suited for CMB observation:

- Automatic subtraction of the mean signal
- Intrinsically stable (no skynoise)
- Beamshape is easy to obtain (and is not as important as in single dish observations)
- Direct measurement of visibilities (which are very nearly the Fourier transform of sky brightness distribution)
- Precision radiometry and polarimetry
- Repeated baselines allow variety of instrumental checks

Bolometers (heat detectors)

ACBAR

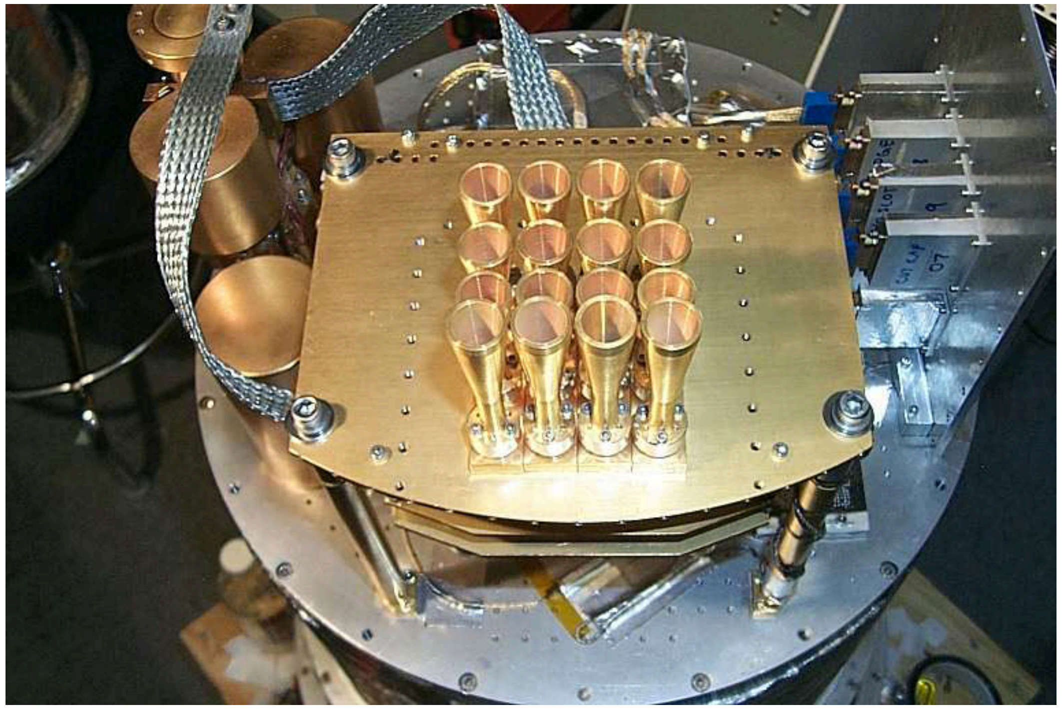

Boomerang

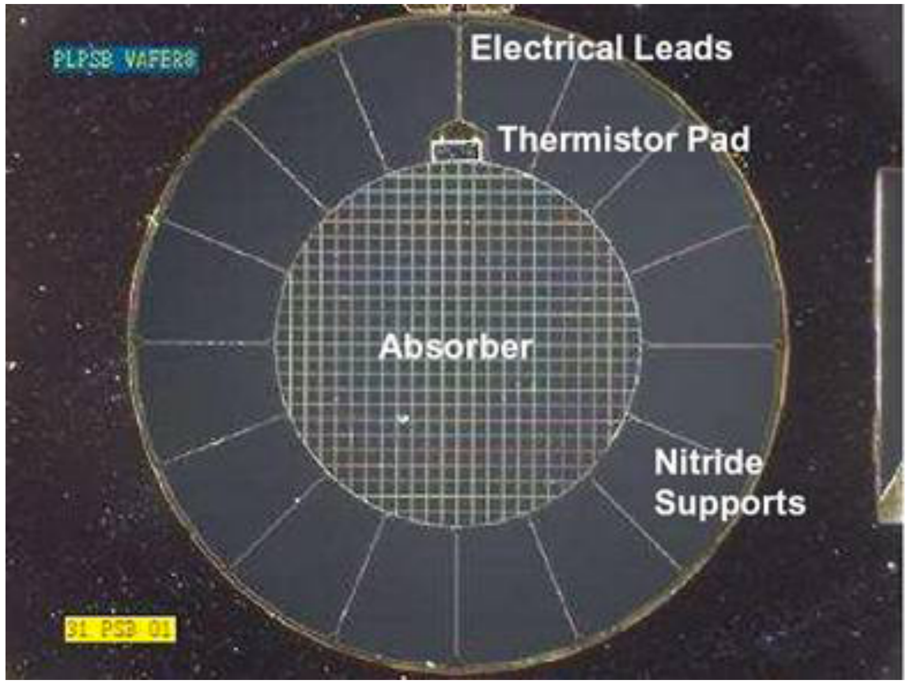

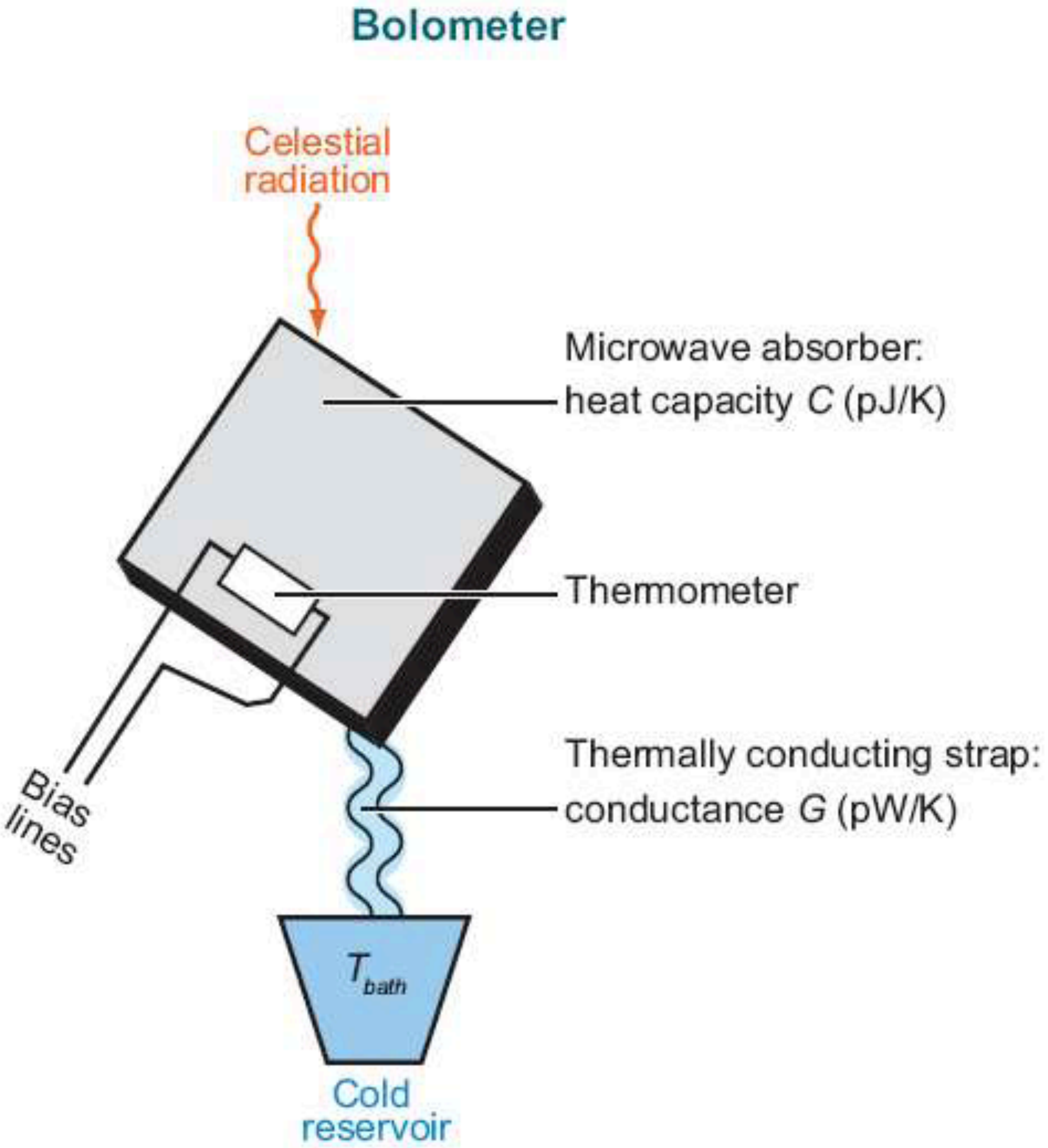

Bolometer and HEMT sensitivities

Fluctuations in the arrival rate of CMB photons impose a fundamental limit of ~30 μK√(sec) for detection of a single mode of radiation in a fractional bandwidth of 25% from ~30 to 220 GHz. This is called the **photon noise limit**.
Modern bolometers are essentially photon noise limited.

	2005[b]		2010[c]	
Freq.	**Bolometer**	**HEMT $/\sqrt{2}$**	**Bolometer**	**HEMT $/\sqrt{2}$**
[GHz]	**[$\mu K_{cmb}\sqrt{s}$]**	**[$\mu K_{cmb}\sqrt{s}$]**	**[$\mu K_{cmb}\sqrt{s}$]**	**[$\mu K_{cmb}\sqrt{s}$]**
30	**–**	**93**	**57**	**48**
40	**–**	**115**	**51**	**51**
60	**–**	**175**	**44**	**60**
90	**67**	**224**	**40**	**75**
120	**–**	**–**	**40**	**93**
150	**48**	**–**	**43**	**–**
220	**68**	**–**	**64**	**–**
350	**224**	**–**	**220**	**–**

(about a decade ago)

(CMB Task Force Report)

Bolometer and HEMT sensitivities

	Bolometers	MMIC HEMTs
• Sensitivity	great	good @ < 100 GHz
• Response time	~ msec -> sub-msec	fast
• Frequency Coverage	comprehensive	limited
• Cooling Requirements	little P at low T	large P at higher T
• Linearity	adequate	excellent
• Gain Stability	excellent	poor
• Offset Stability	excellent	good
• Focal Plane Density	better	feedhorn limited
• Polarization Sensitivity	good	good
• EMI / RFI / B-field / microphonic susceptibility	adequate	better
• Array Uniformity	good	???

(Slide from Andrew Lange)

Example of a modern bolometer array

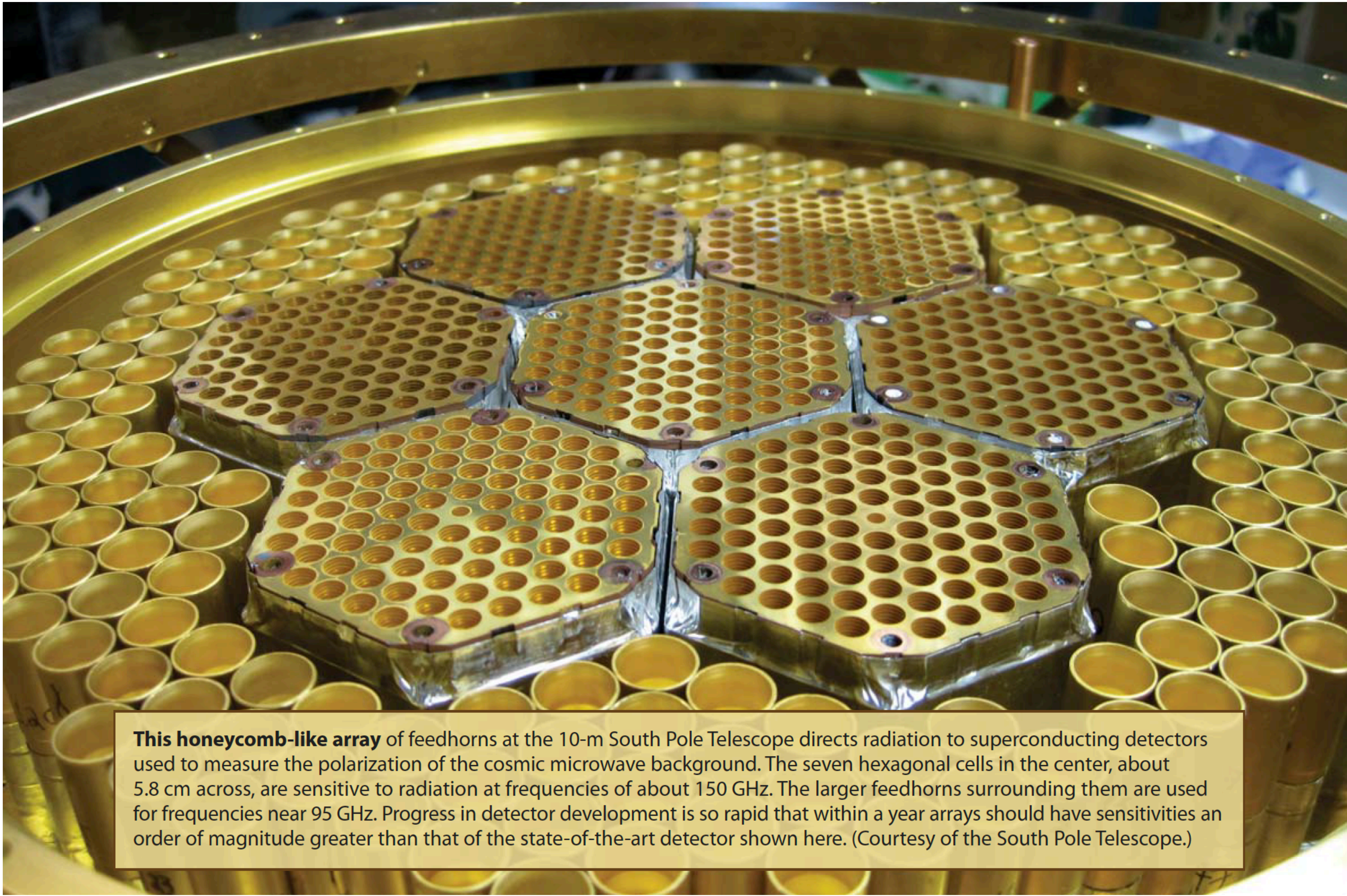

This honeycomb-like array of feedhorns at the 10-m South Pole Telescope directs radiation to superconducting detectors used to measure the polarization of the cosmic microwave background. The seven hexagonal cells in the center, about 5.8 cm across, are sensitive to radiation at frequencies of about 150 GHz. The larger feedhorns surrounding them are used for frequencies near 95 GHz. Progress in detector development is so rapid that within a year arrays should have sensitivities an order of magnitude greater than that of the state-of-the-art detector shown here. (Courtesy of the South Pole Telescope.)

Ground- and space-based experiments

From Delabrouille et al., CORE mission paper

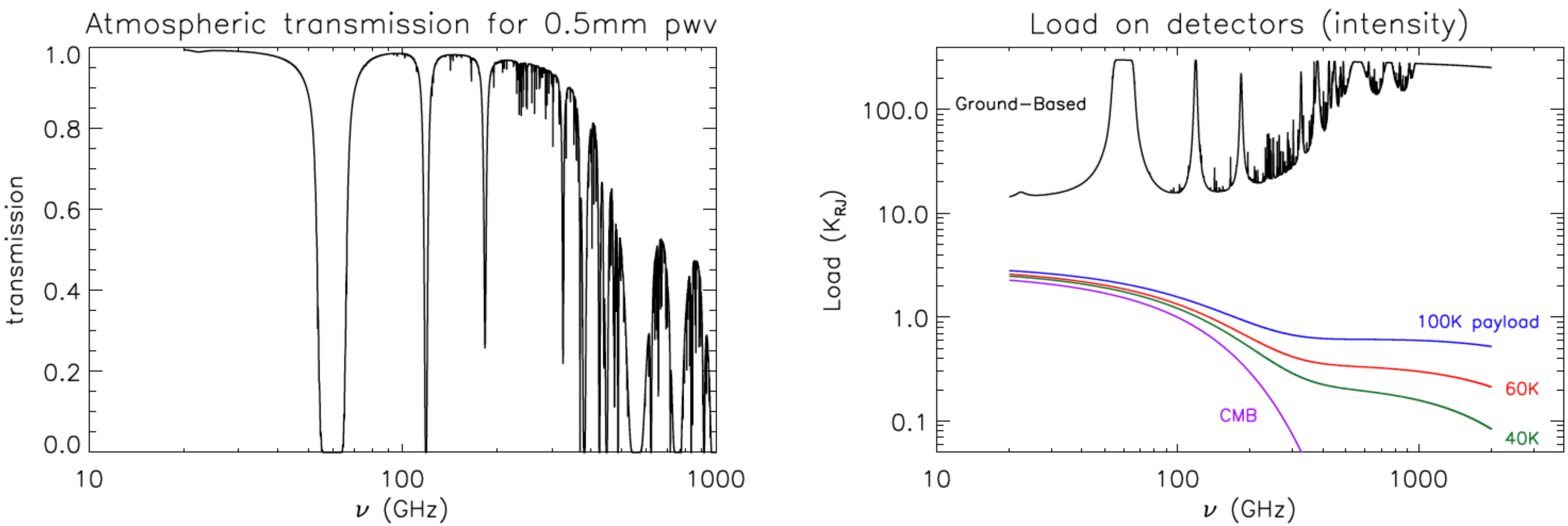

Figure 11. *Top left*: Typical atmospheric transmission from the Atacama plateau at 60° elevation, for an average of half a millimetre of integrated precipitable water vapour. *Top right*: Load on a detector for a ground-based instrument (black) and for a space-borne instrument with various payload temperatures.

A single space-borne detector can reach a sensitivity equivalent to 100-1000 ground-based detectors (depending on frequency).

Ground- and space-based experiments

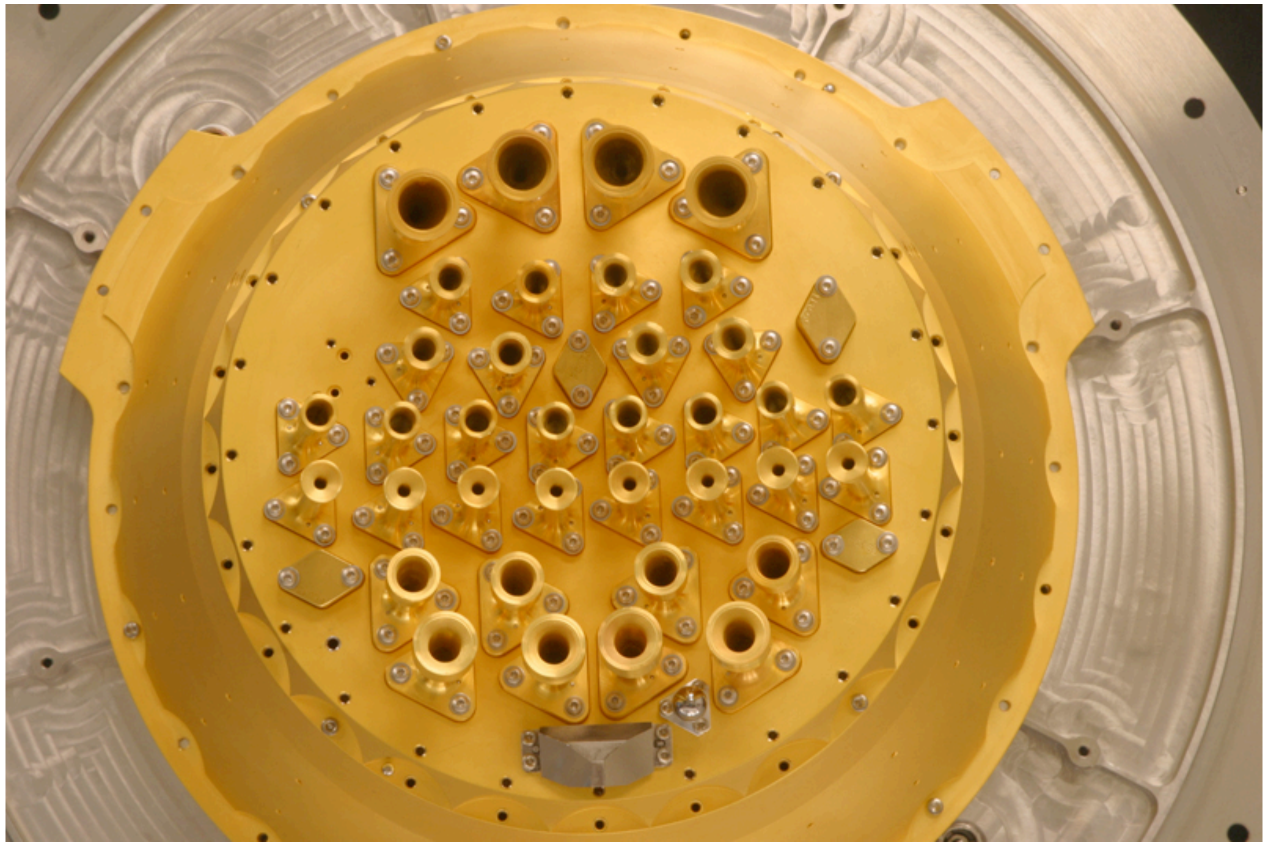

Planck HFI focal plane, showing the feed horns for 32 bolometer detectors

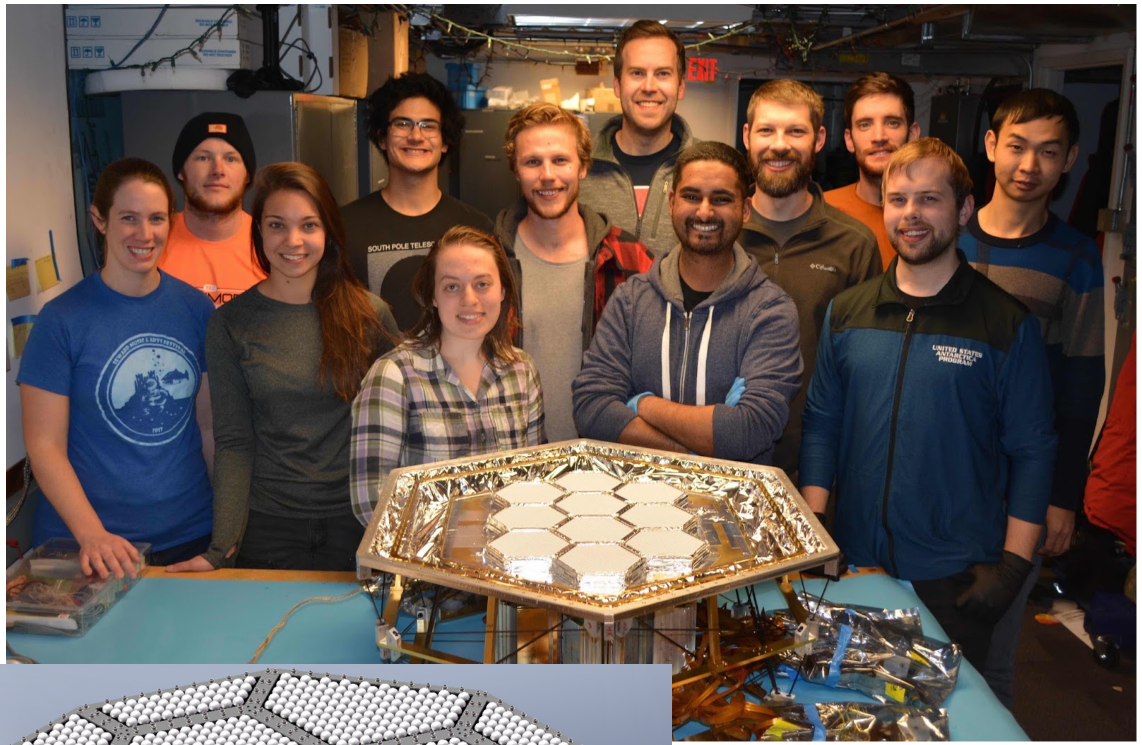

SPT-3G collaboration
Dec 2017

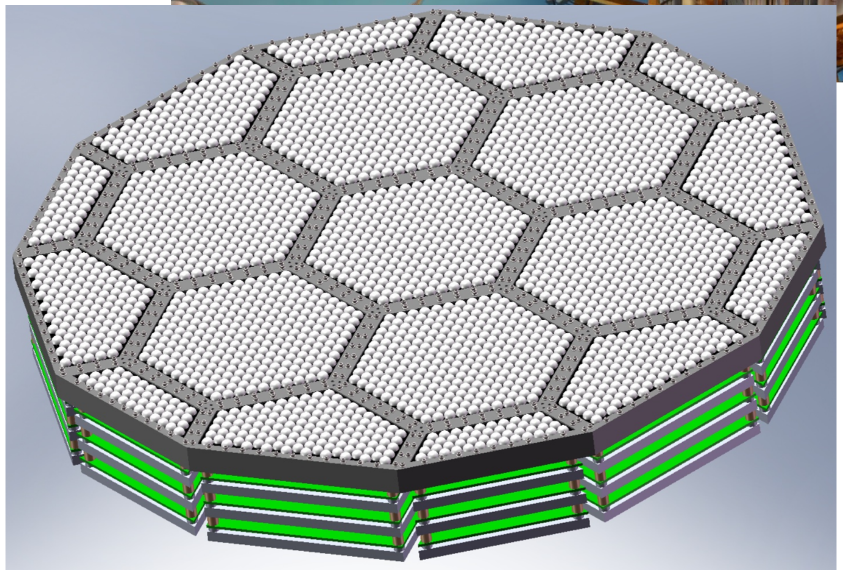

SPT-3G focal plane, with over 15 000 detectors (0.5 m diameter)

Detectors for the ground-based telescopes

(Credit: SPT collaboration)

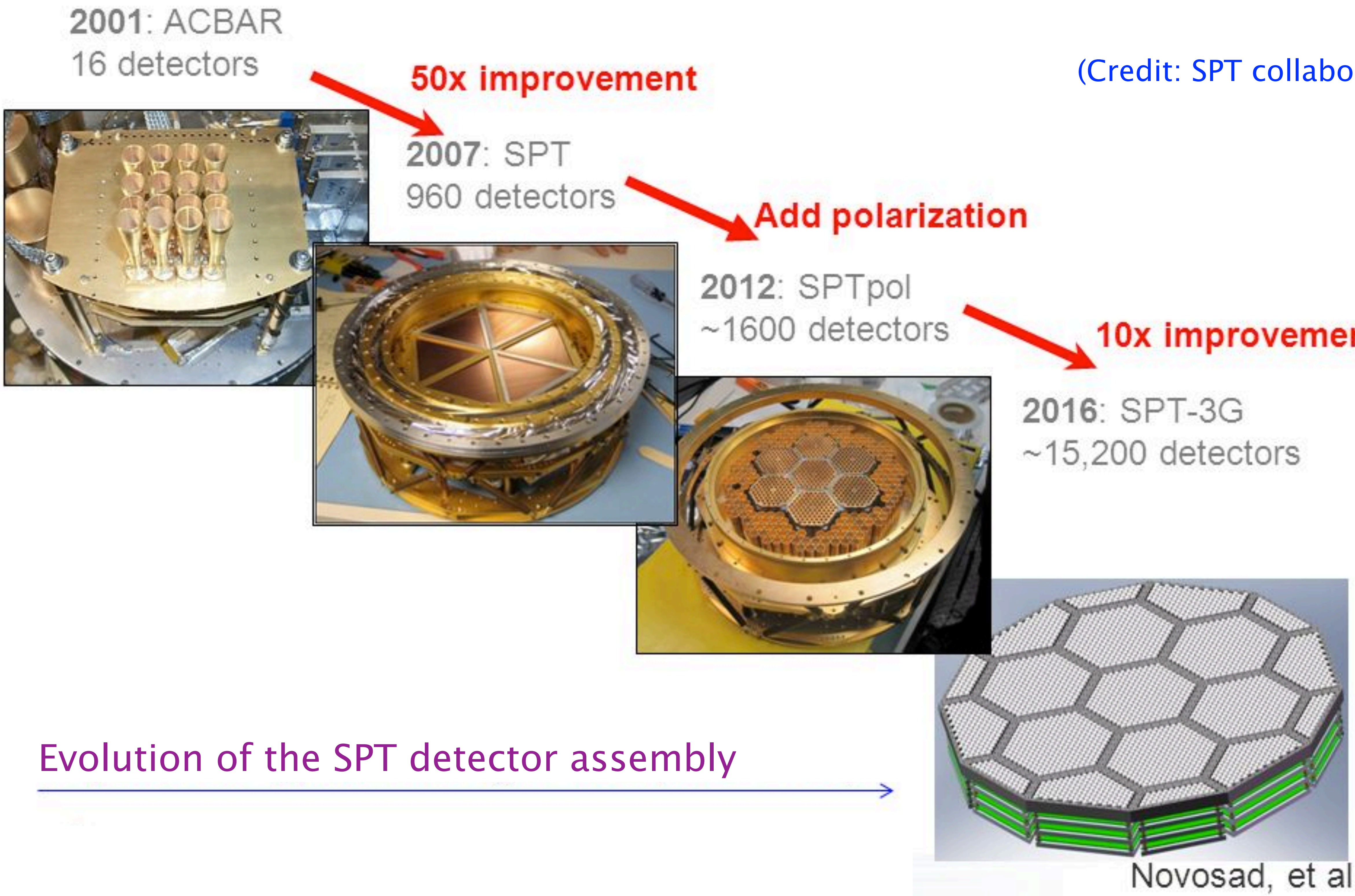

Evolution of the SPT detector assembly

Moore's law for CMB detectors

CMB-S4
Next Generation CMB Experiment

CMB Stages

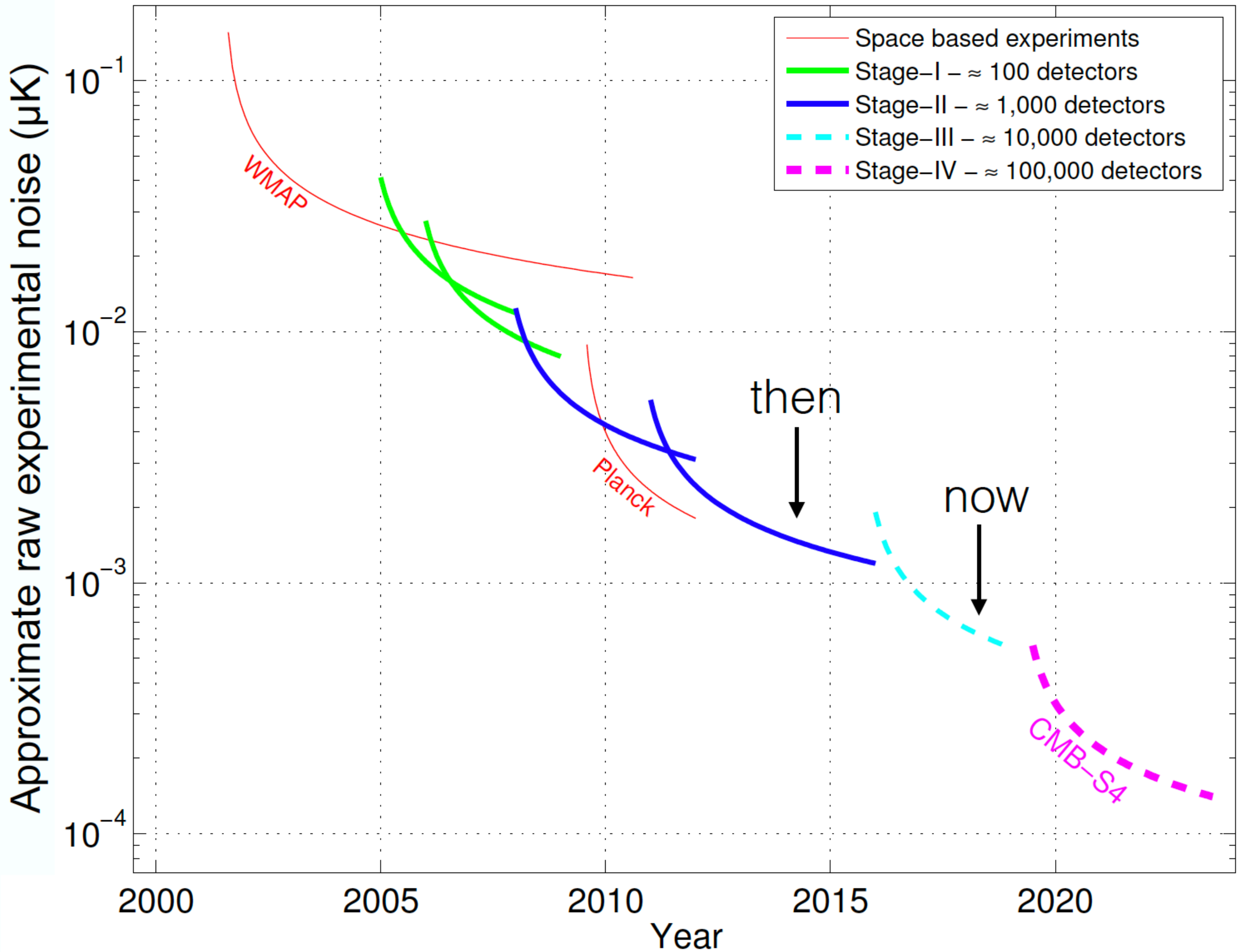

Maybe this will fly to space!

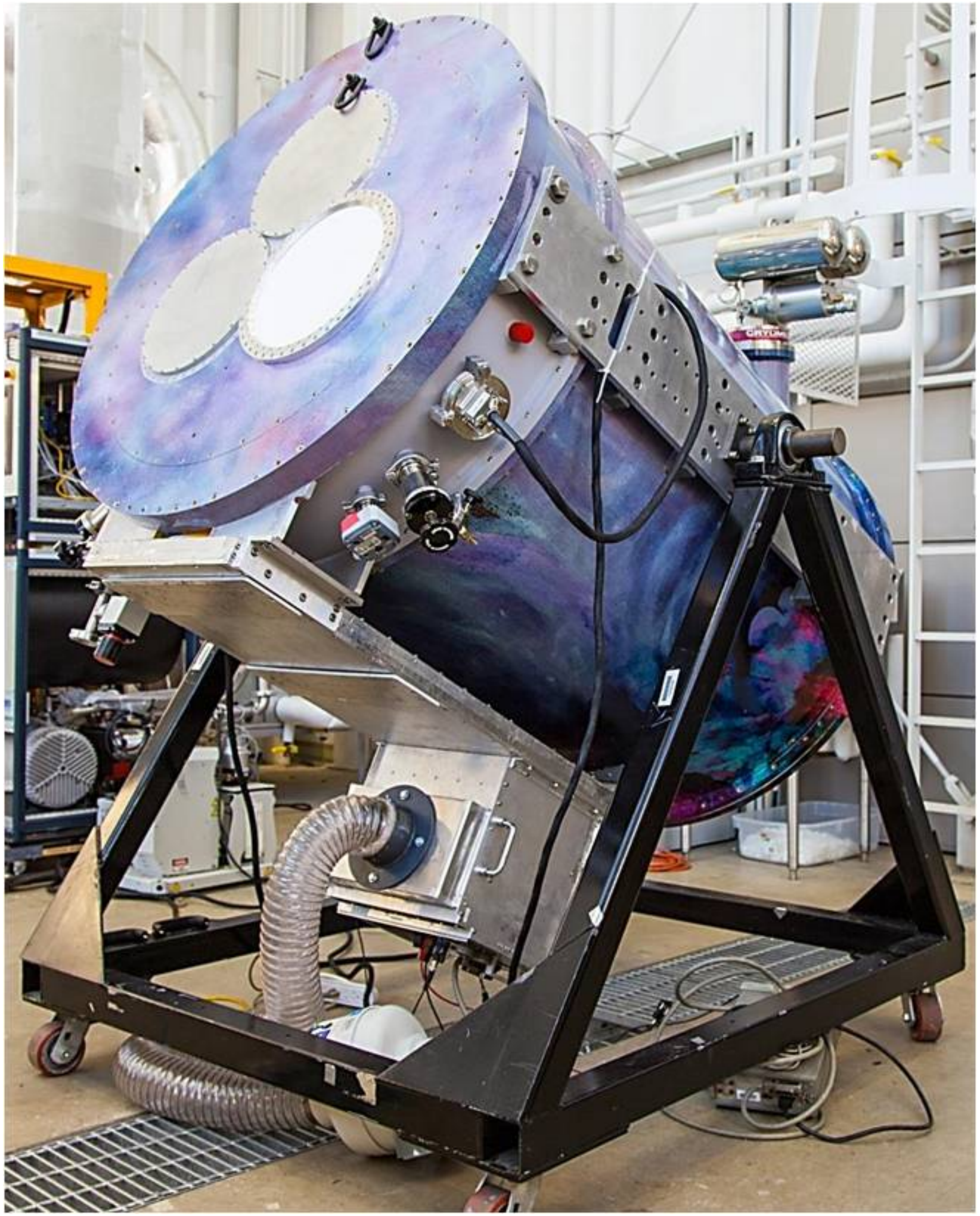

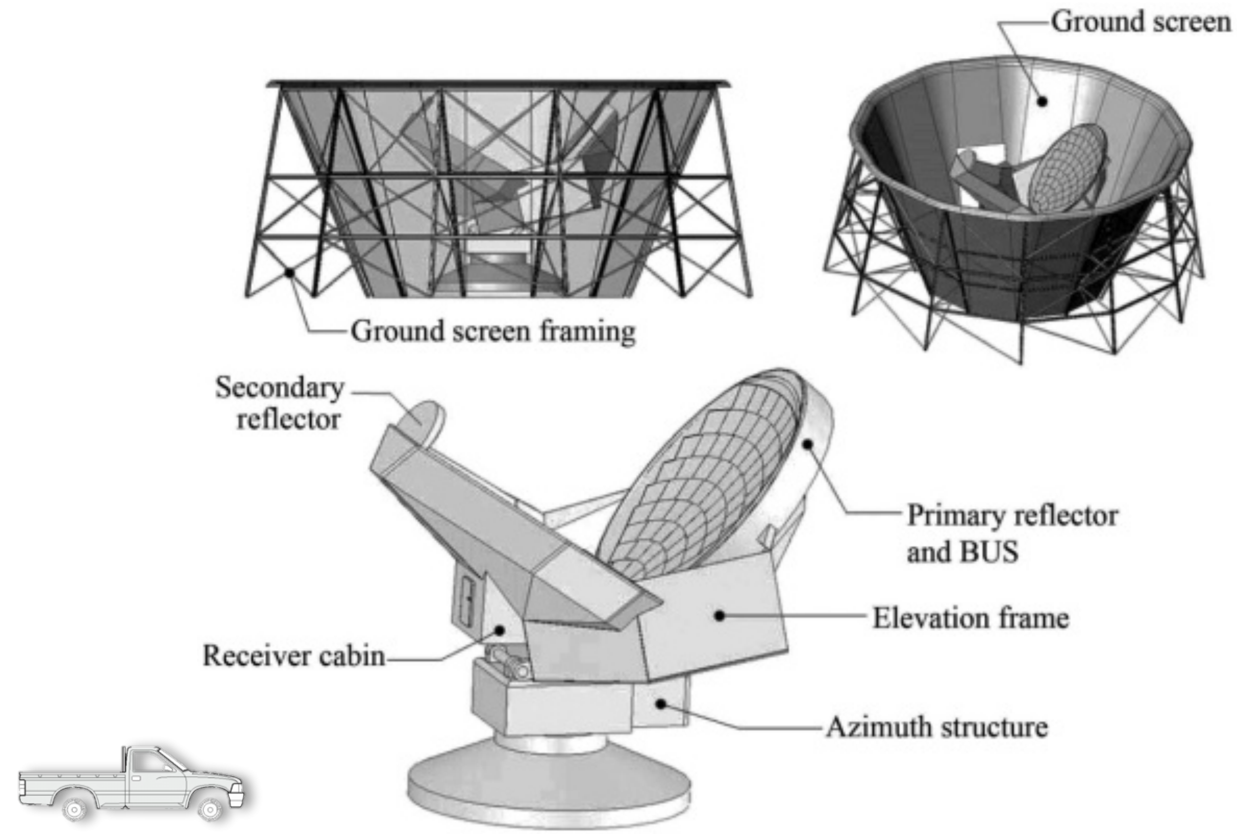

Next generation ground-based telescopes

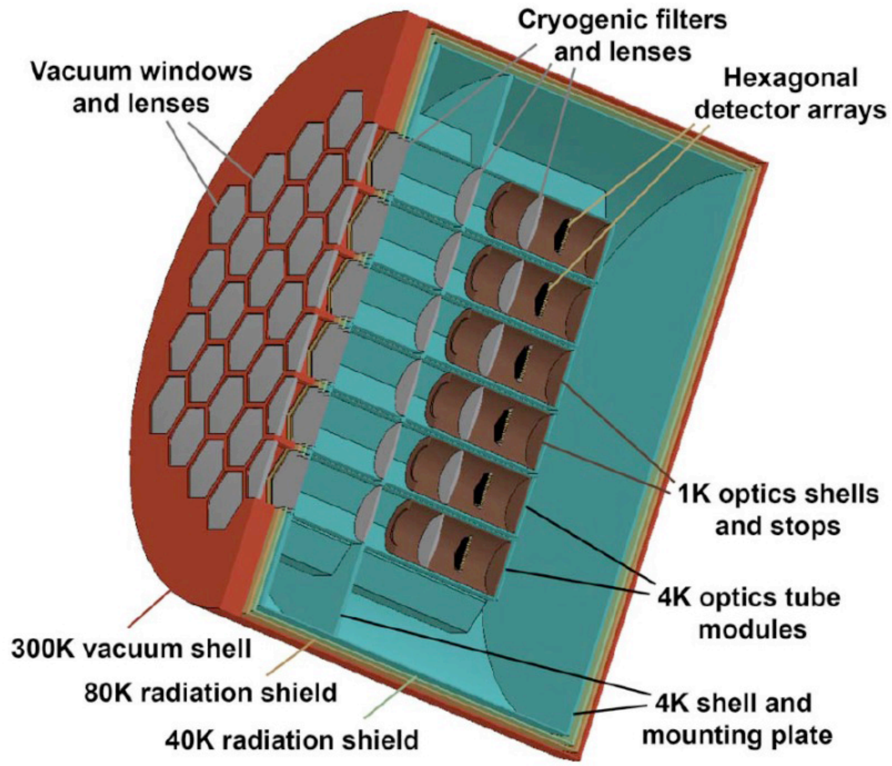

CCAT-prime

6 meter aperture and *extreme large* field-of-view sub-millimeter telescope on the Cerro Chajnantor (at 5600m) Chile

Partners: Cornell, **Bonn**-Cologne-Munich, Canadian universities

2.5 m diameter bolometer receiver

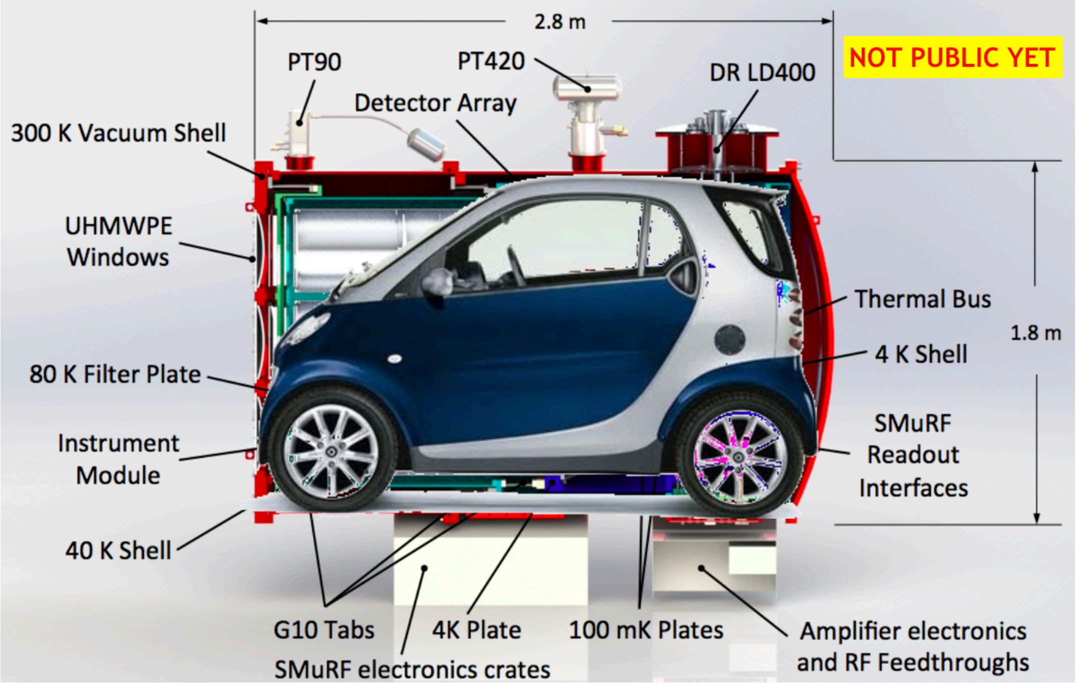

CMB measurements from ground

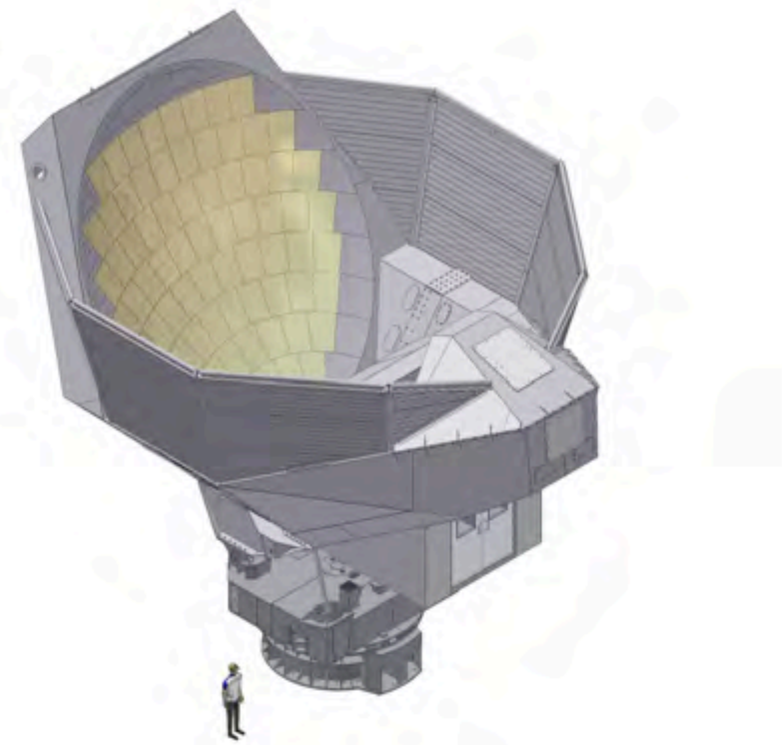

Atacama Cosmology Telescope

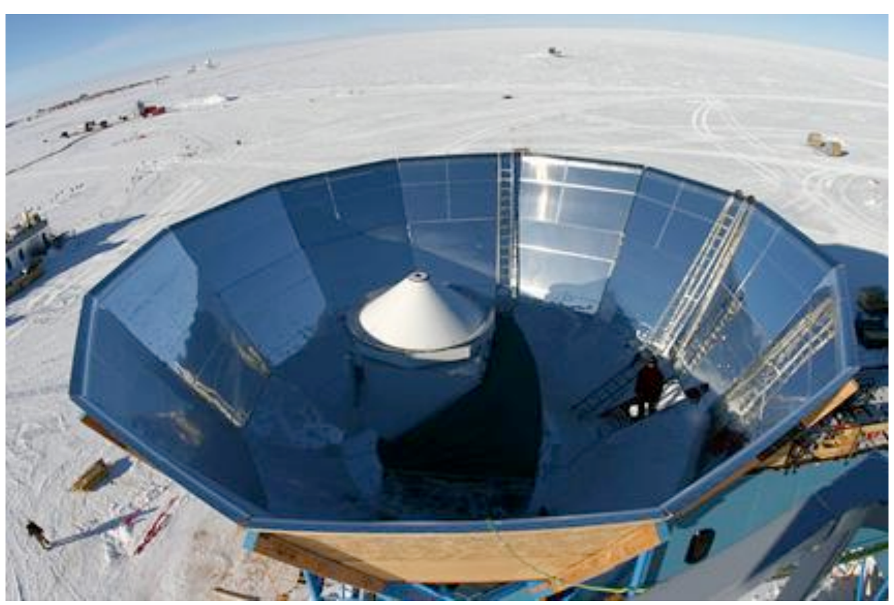

QUaD at south pole

Since 3 K << 300 K, CMB measurements are sensitive to thermal emission from their environments.

CMB telescopes are specially designed to be very directional, but 300 K in the sidelobes is always a worry.

A receiver has system temperatre T_{sys}

$$T_{sys} = T_{rec} + T_{CMB} + T_{atm} + T_{ground} + \ldots$$

The radiometer equation is: $\delta T = \frac{b T_{sys}}{\sqrt{\Delta\nu\, \tau}}$

Planck detectors

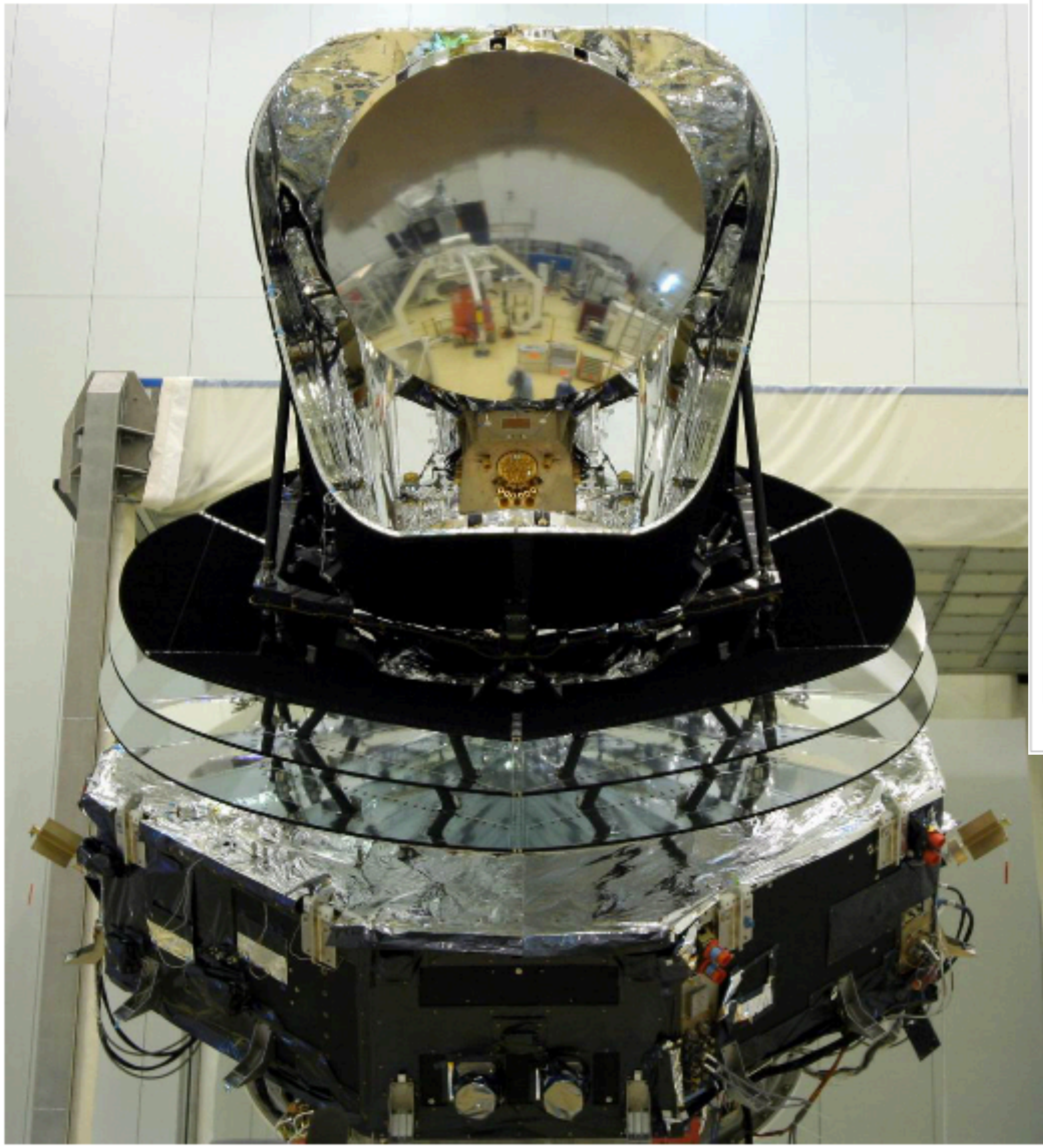

The fully assembled Planck satellite a few days before integration into the Ariane 5 rocket. Herschel is visible by reflection on the primary reflector.

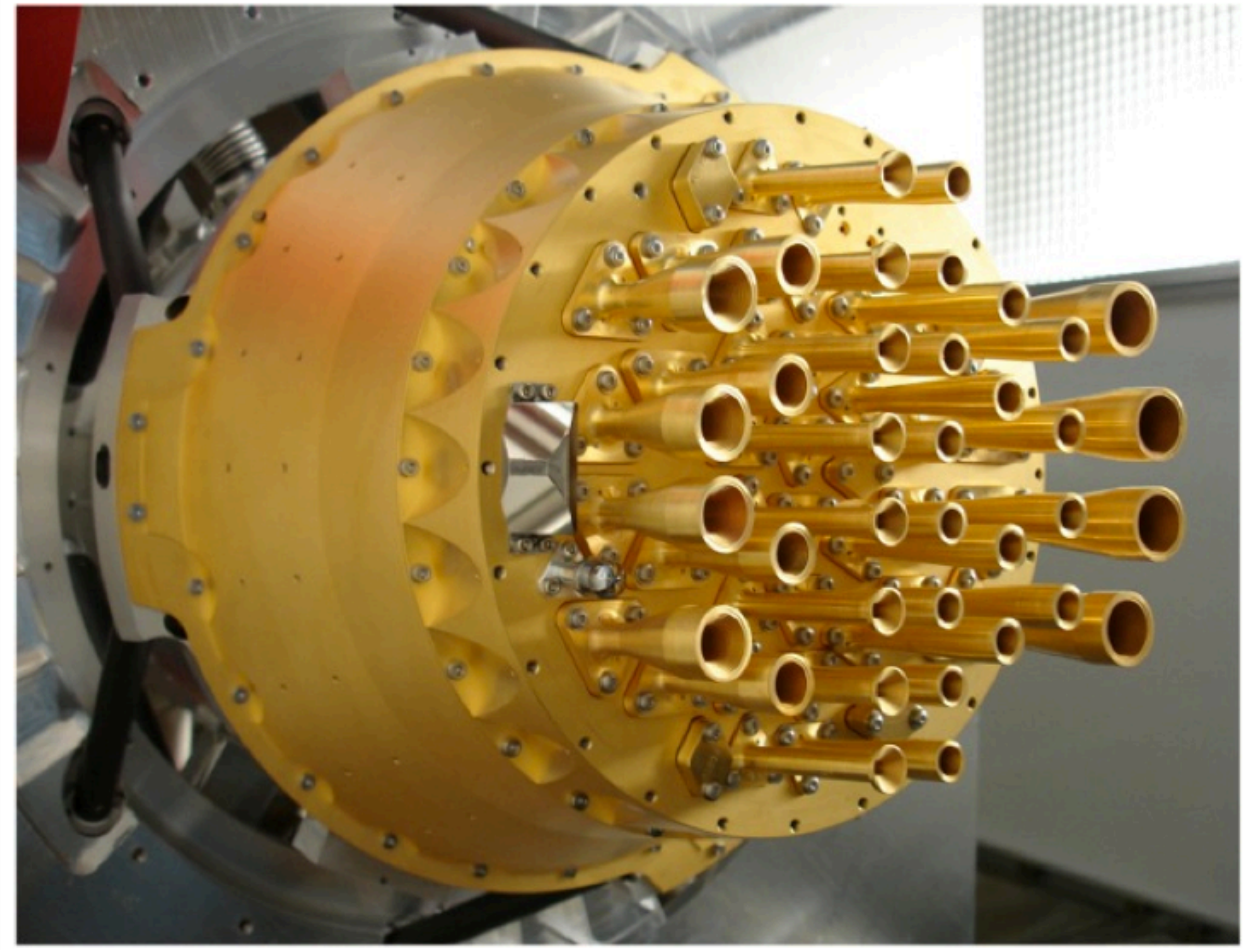

The HFI focal plane optics and 4K thermo-mechanical stage

Planck

- 20K HEMT amplifiers at 30, 45, 70 GHz
  - ~ 20 amplifiers
- 100 mK bolometers at 100 -> 850 GHz
  - ~ 50 bolometers

Planck detectors

Instrument Characteristic	LFI			HFI					
Detector Technology	HEMT arrays			Bolometer arrays					
Center Frequency [GHz]	30	44	70	100	143	217	353	545	857
Bandwidth ($\Delta\nu/\nu$)	0.2	0.2	0.2	0.33	0.33	0.33	0.33	0.33	0.33
Angular Resolution (arcmin)	33	24	14	10	7.1	5.0	5.0	5.0	5.0
$\Delta T/T$ per pixel (Stokes I)[a]	2.0	2.7	4.7	2.5	2.2	4.8	14.7	147	6700
$\Delta T/T$ per pixel (Stokes Q &U)[a]	2.8	3.9	6.7	4.0	4.2	9.8	29.8	...	...

[a] Goal (μK/K, 1σ), 14 months integration, square pixels whose sides are given in the row "Angular Resolution".

Planck Bluebook

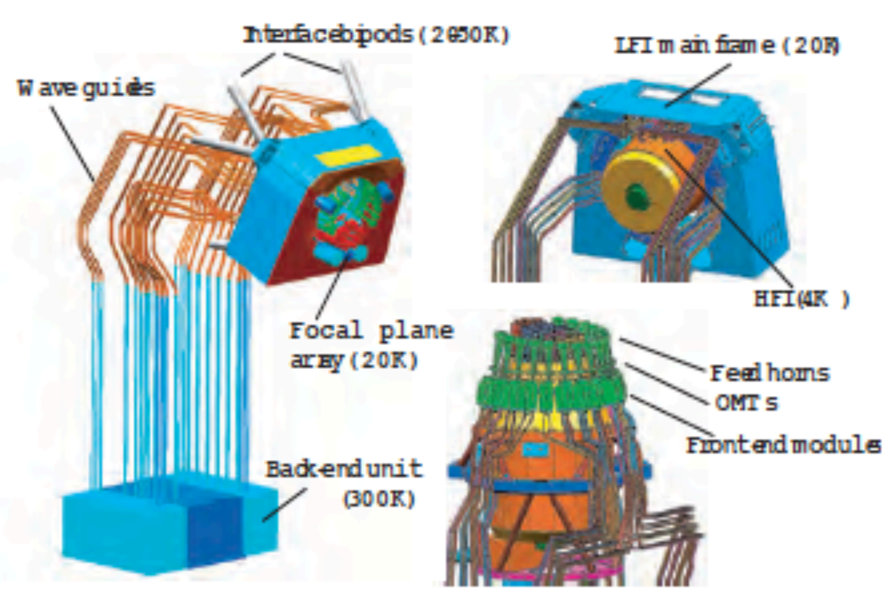

Planck Bluebook

Thales/Alenia Space+ESA

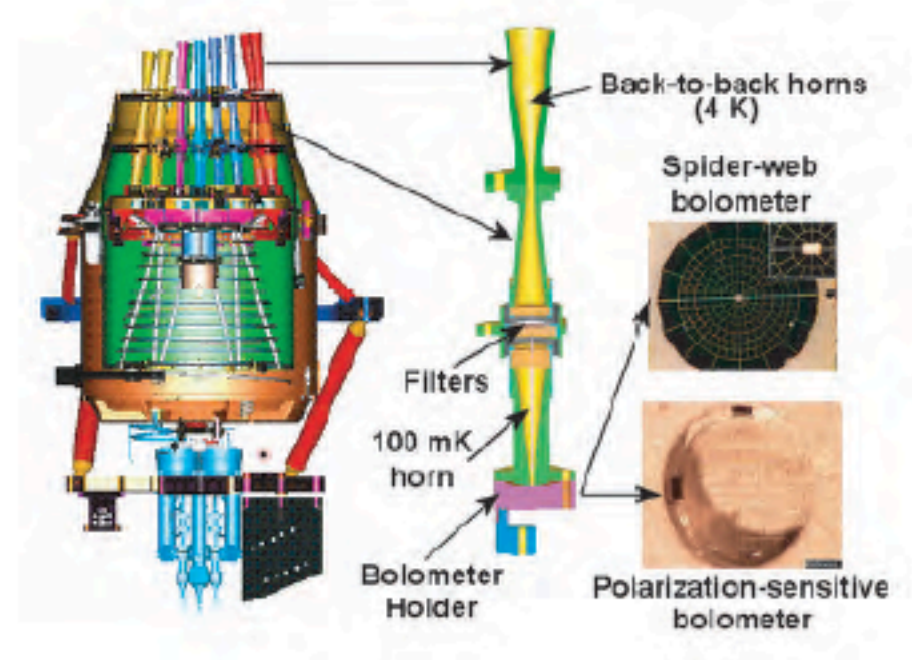

Planck Bluebook

Planck: polarization sensitivity

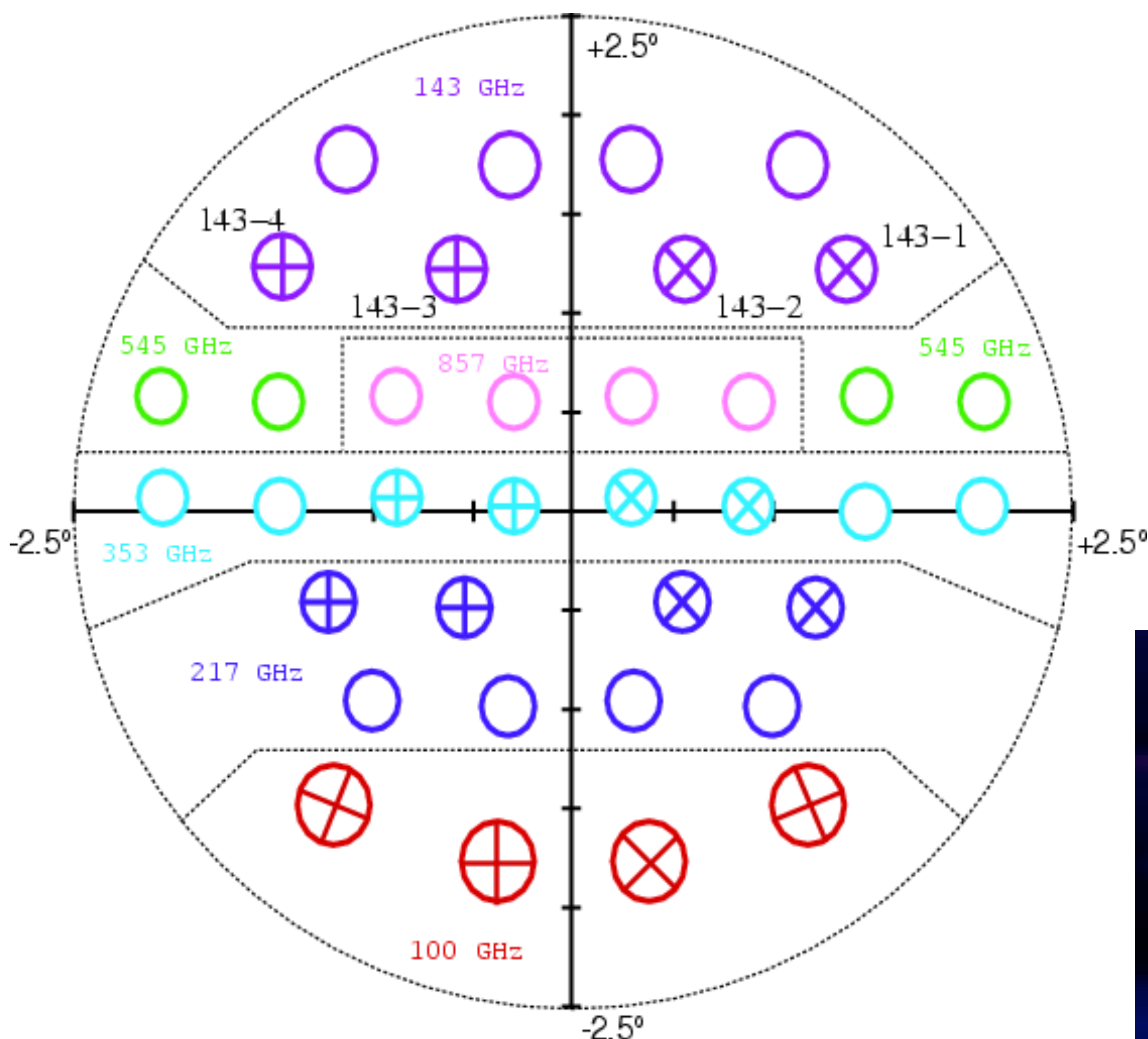

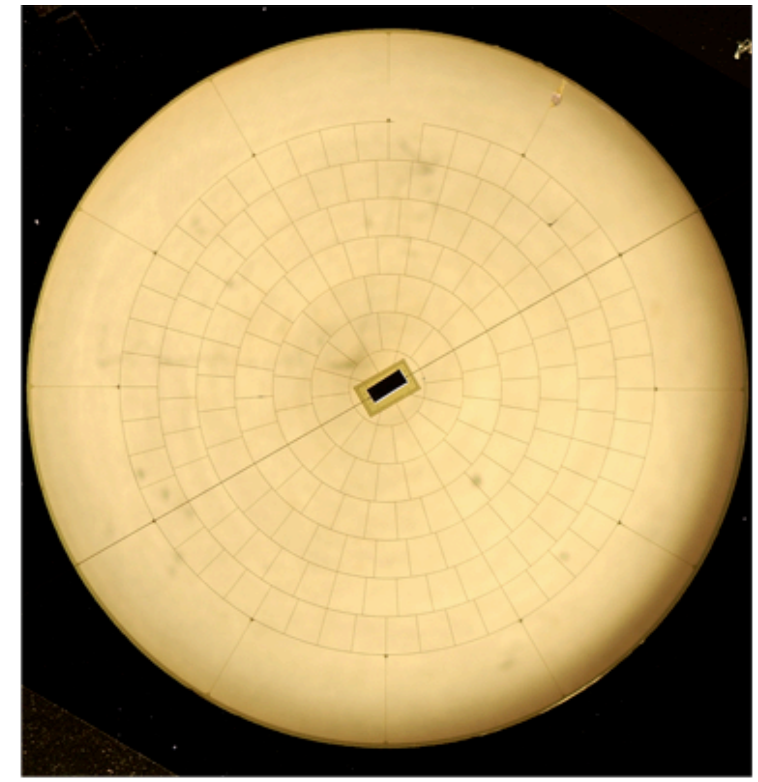

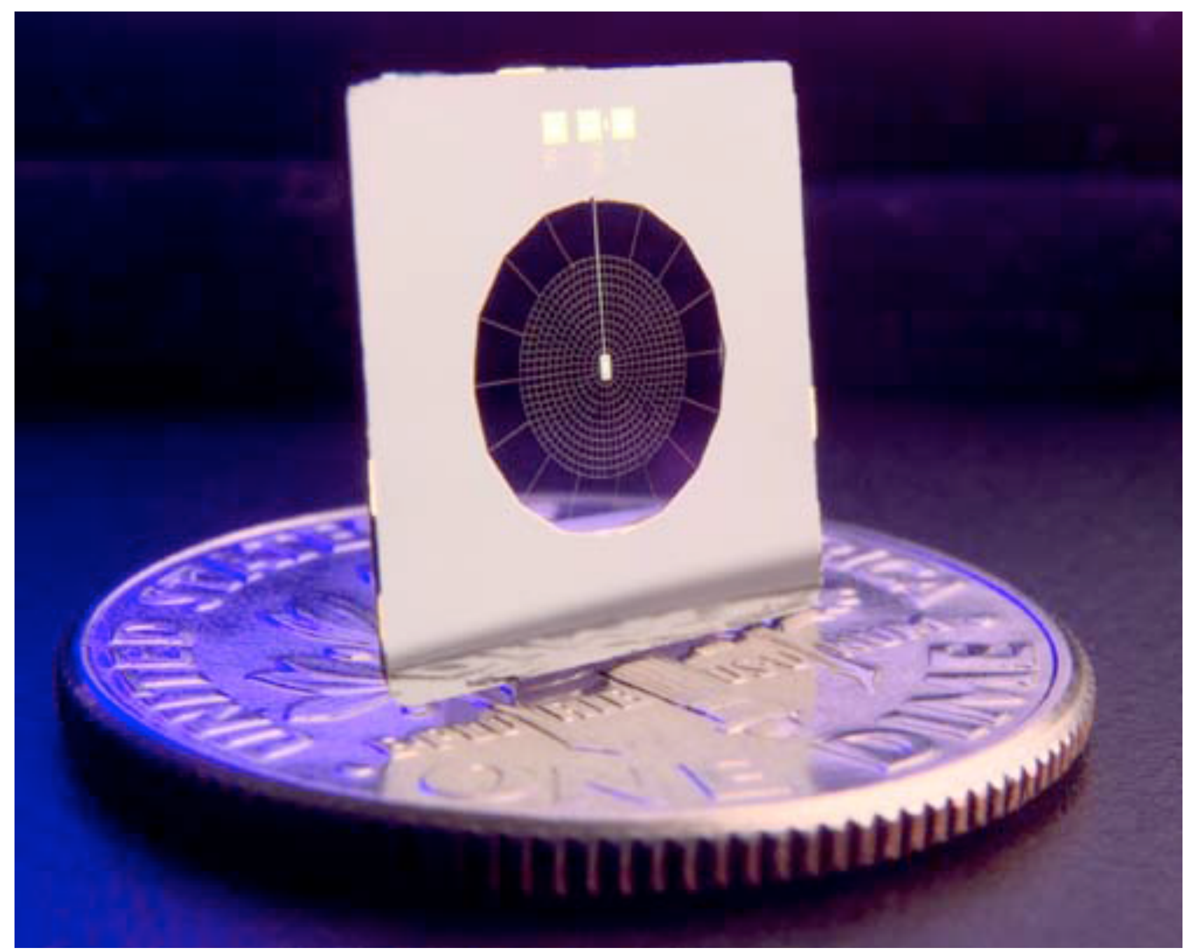

Planck Focal Plane Unit with polarization sensitive bolometers (spiderweb bolometers). Here one has two bolometers back-to-back with orthogonal grids.

Low multipole “anomaly”

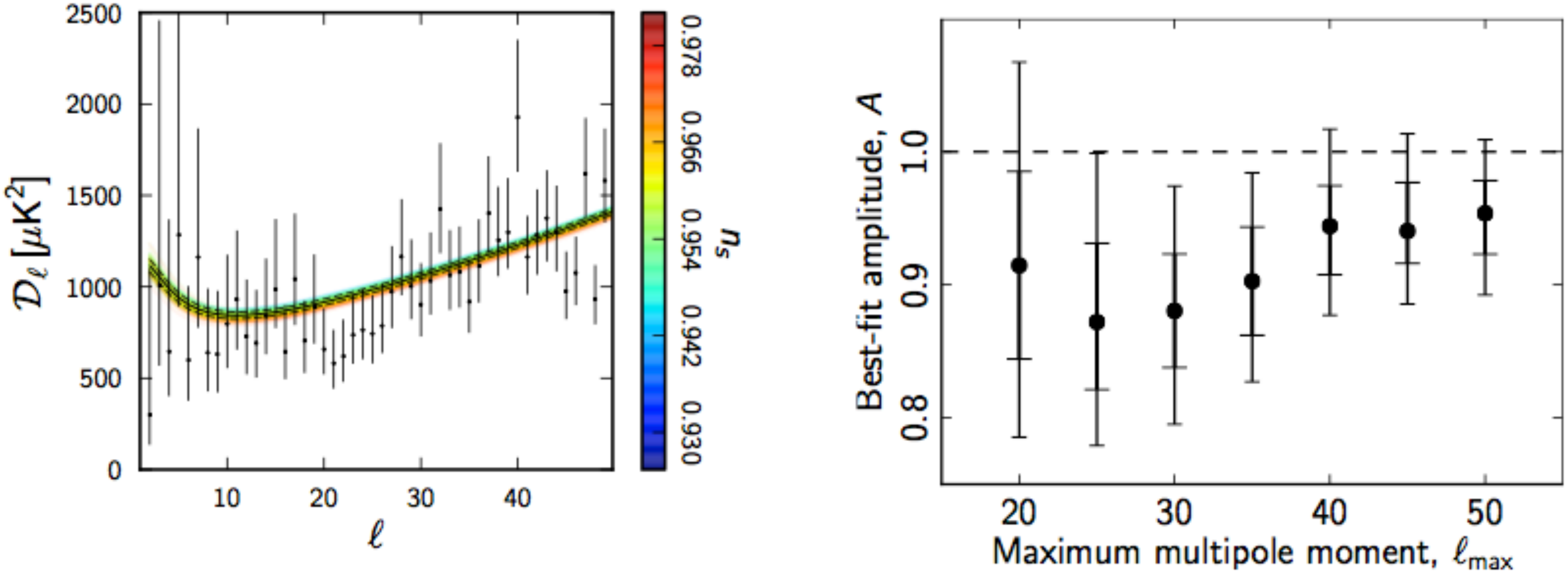

Planck collaboration (2013)

Fig. 39. *Left*: *Planck TT* spectrum at low multipoles with 68% ranges on the posteriors. The “rainbow” band show the best fits to the entire *Planck*+WP likelihood for the base ΛCDM cosmology, colour-coded according to the value of the scalar spectral index n_s. *Right*: Limits (68% and 95%) on the relative amplitude of the base ΛCDM fits to the *Planck*+WP likelihood *fitted only to the Planck TT likelihood* over the multipole range $2 \leq \ell \leq \ell_{max}$.

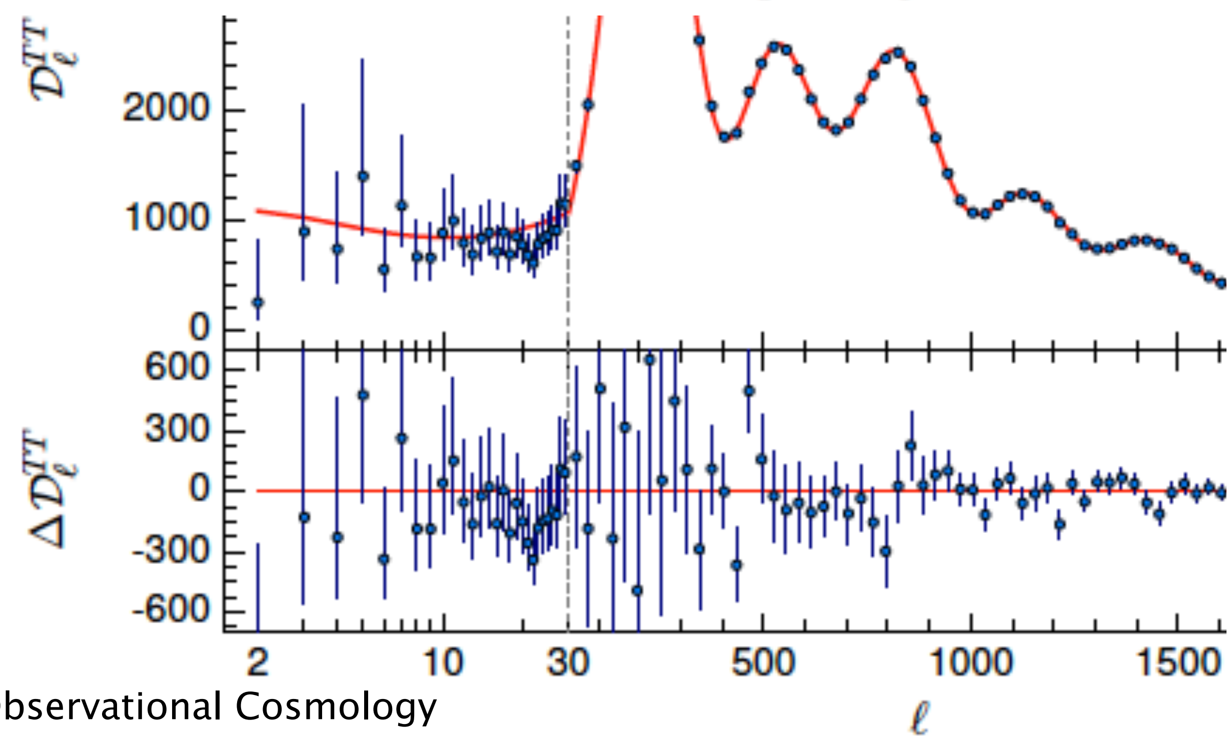

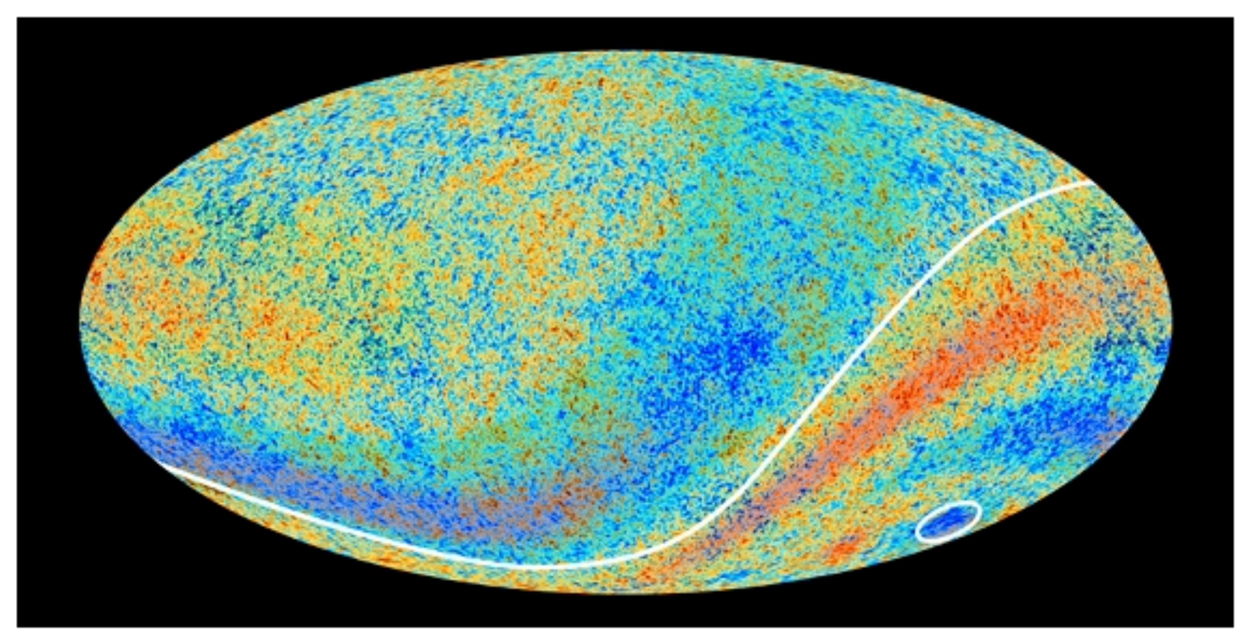

Planck’s anomalous sky: the hemispheric asymmetry and the cold spot. *Credit: ESA and the Planck Collaboration*

Low multipole “anomaly”

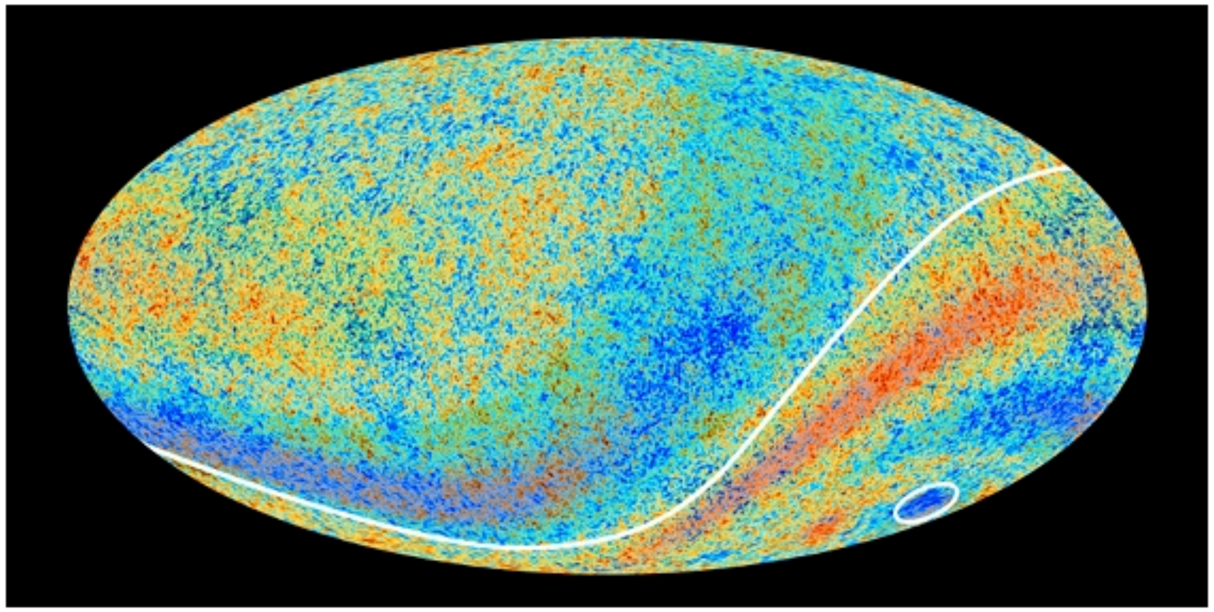

Planck’s anomalous sky: the hemispheric asymmetry and the cold spot. *Credit: ESA and the Planck Collaboration*

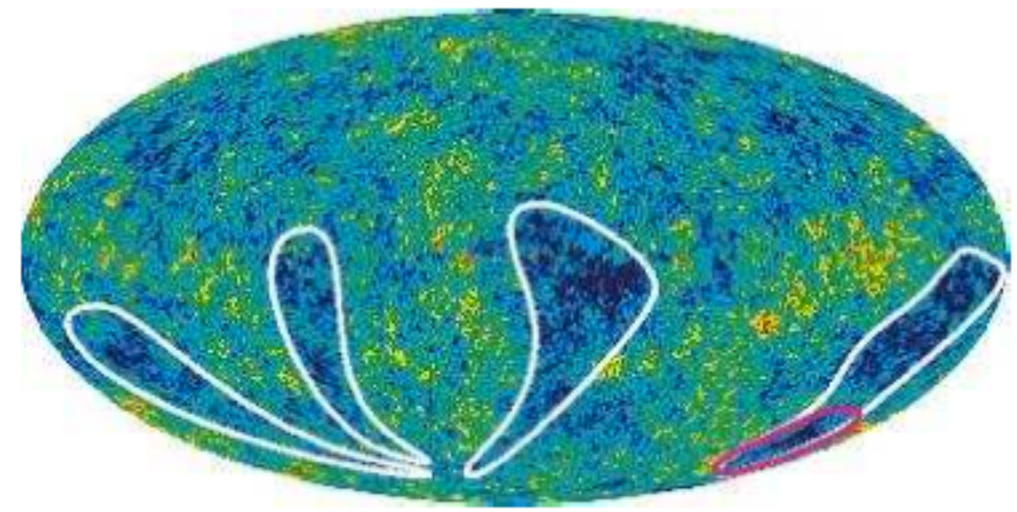

WMAP “fingers”

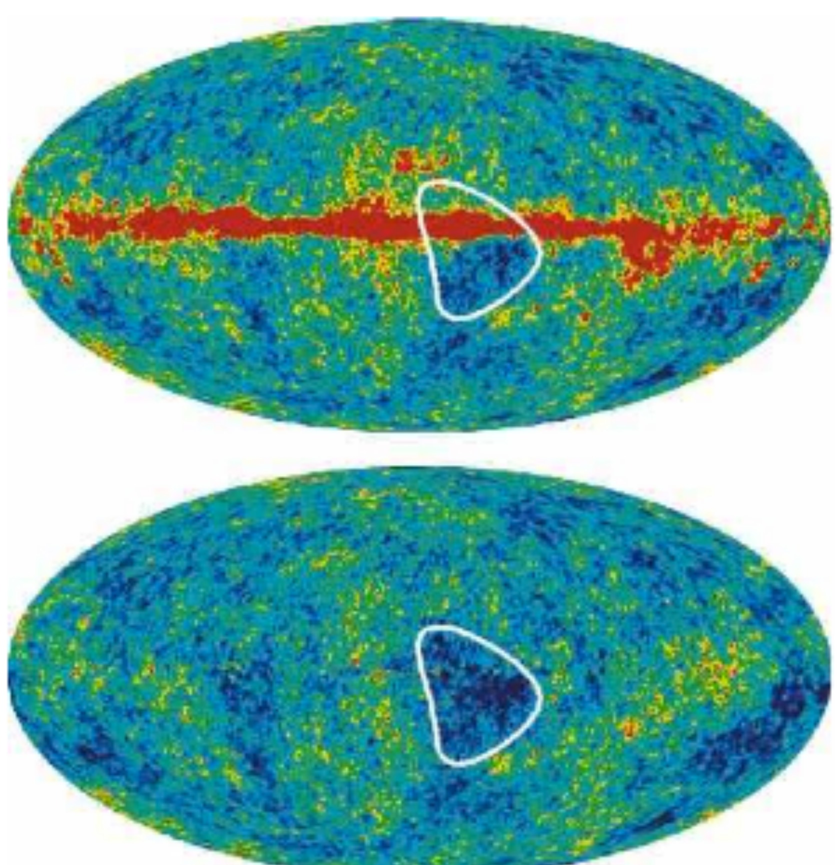

WMAP cold spot

Bennett et al. (2011)

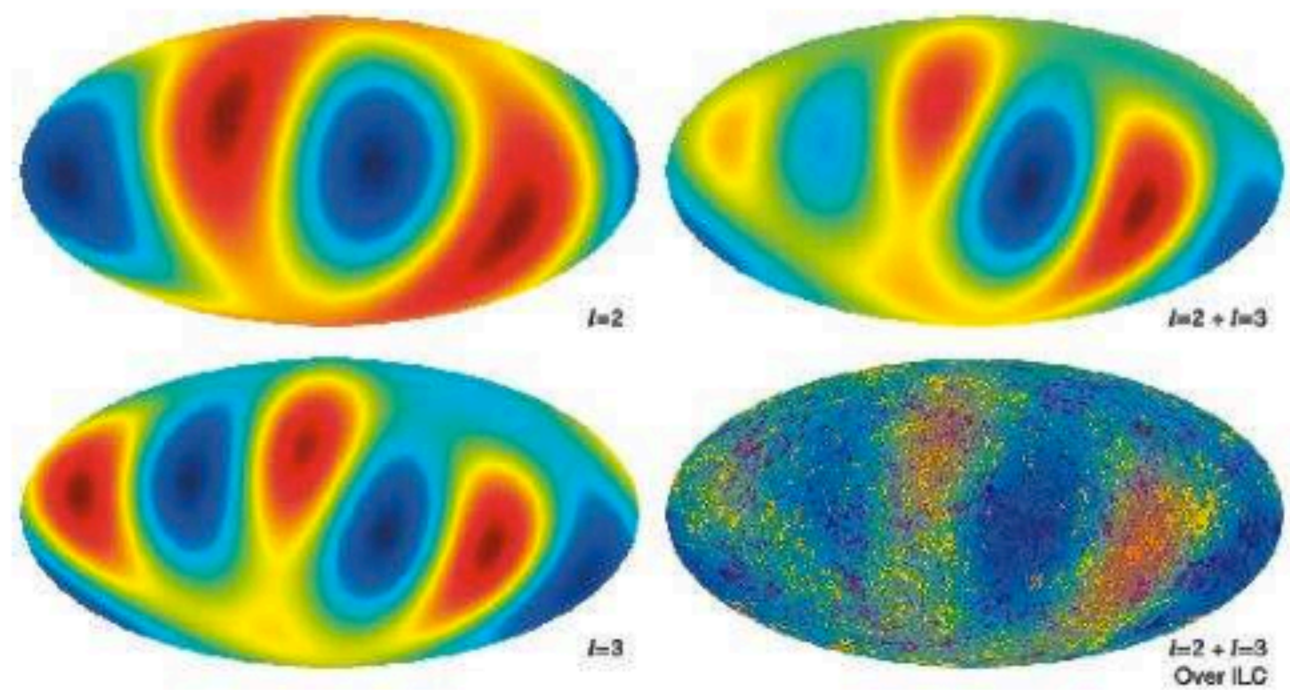

Figure 14. $l = 2$ quadrupole and $l = 3$ octupole maps are added. The combined map is then shown superposed on the ILC map from Figure 2. Note that the quadrupole and octupole components arrange themselves to match the cool fingers and the warm regions in between. The fingers and the alignment of the $l = 2$ and $l = 3$ multipoles are intimately connected.

CMB "anomalies"

WMAP 7 yr result
Bennett et al. (2011)

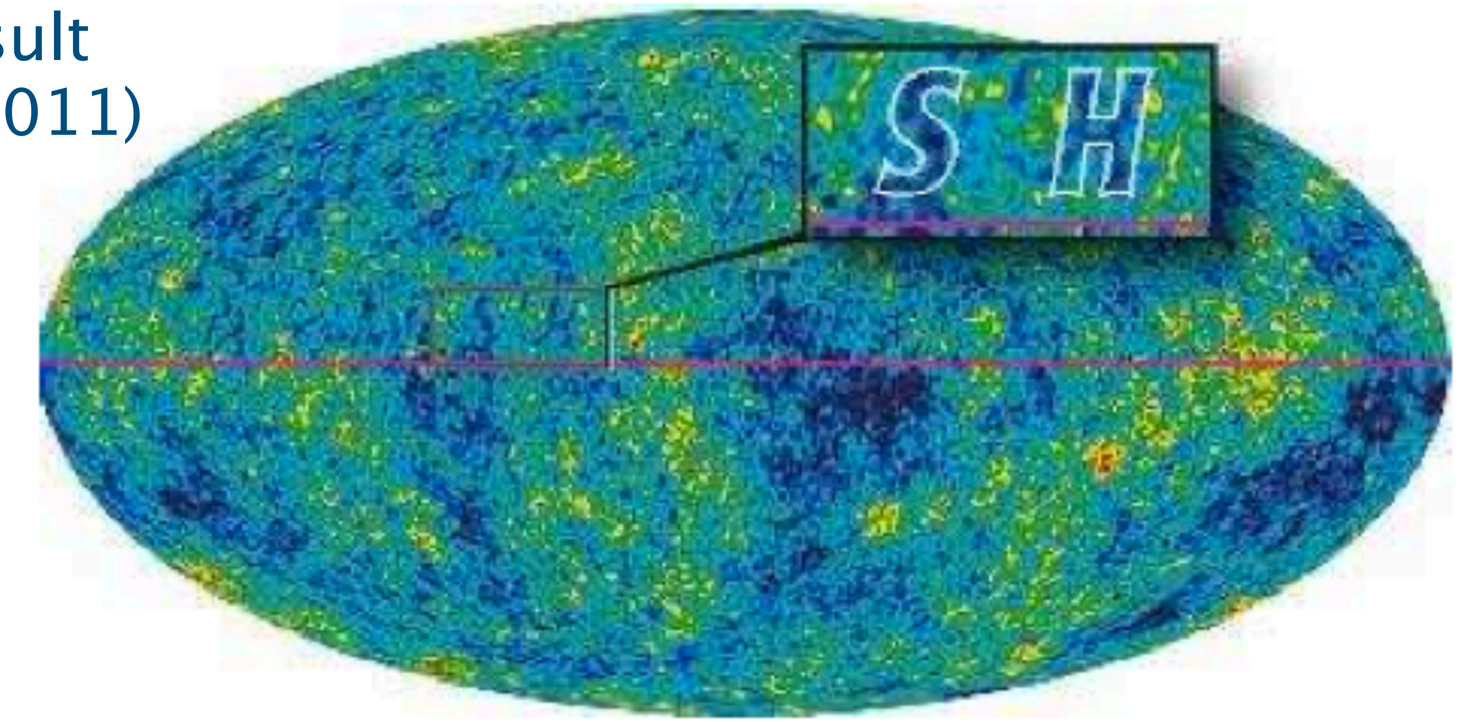

Figure 17. "SH" initials of Stephen Hawking are shown in the ILC sky map. The "S" and "H" are in roughly the same font size and style, and both letters are aligned neatly along a line of fixed

A large fraction of simulated CMB skies will have some kind of anomaly or oddity. The key is whether the oddity is specified in advance.

timized" for maximum effect by analysis choices, does not result in a fair unbiased assessment. This is a recurrent issue with CMB data analysis and is often a tricky issue and one that is difficult to overcome.

“pi” in the sky

Ali Frolop & Douglas Scott, arXiv:1603.09703

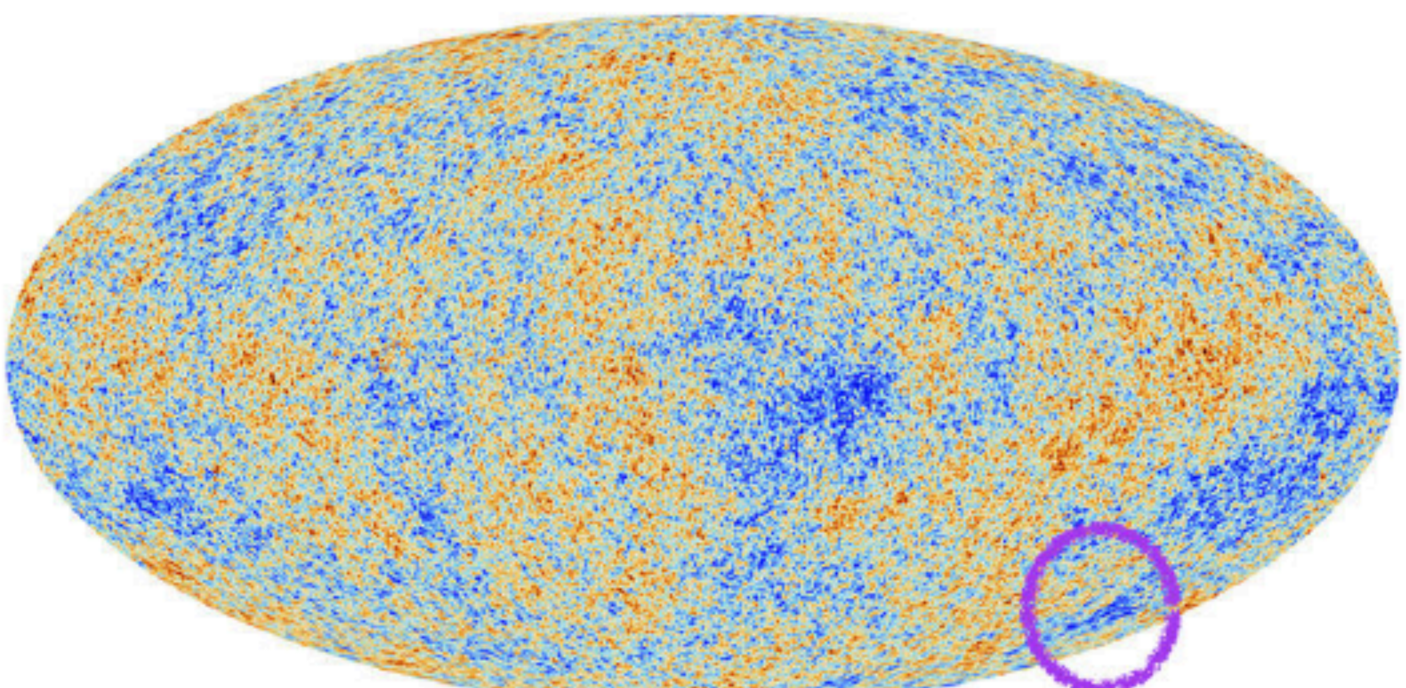

(a)

3141592653589793238462643383279502884197169399375105
8209749445923078164062862089986280348253421170679
8214808651328230664709384460955058223172535940812848
1117450284102701938521105559644622948954930381964428
8109756659334461284756482337867831652712019091
4564856692346034861045432664821339360726024914127372
4587006606315588174881520920962829254091715364367892
5903600113305305488204665213841469519415116094330572
7036575959195309218611738193261179310511854807446237
9962749567351885752724891227938183011949129833673362
4406566430860213949463952247371907021798
6094370277053921717629317675238467481846766940513200
0568127145263560827785771342757789609173637178721468
4409012249534301465495853710507922796892589235420199
5611212902196086403441815981362977477130996051870721
1349999998372978049951059731732816096318595024459455
3469083026425223082533446850352619311881710100031378
387528865875332083814206171776691473035

(b)

Part 3:

Secondary CMB Anisotropies

SECONDARY temperature anisotropies

Table 1. Sources of temperature fluctuations.

PRIMARY	Gravity	
	Doppler	
	Density fluctuations	
	Damping	
	Defects	Strings
		Textures
SECONDARY	Gravity	Early ISW
		Late ISW
		Rees-Sciama
		Lensing
	Local reionization	Thermal SZ
		Kinematic SZ
	Global reionization	Suppression
		New Doppler
		Vishniac
"TERTIARY" (foregrounds & headaches)	Extragalactic	Radio point sources
		IR point sources
	Galactic	Dust
		Free-free
		Synchrotron
	Local	Solar system
		Atmosphere
		Noise, *etc.*

CMB photons on their way to us

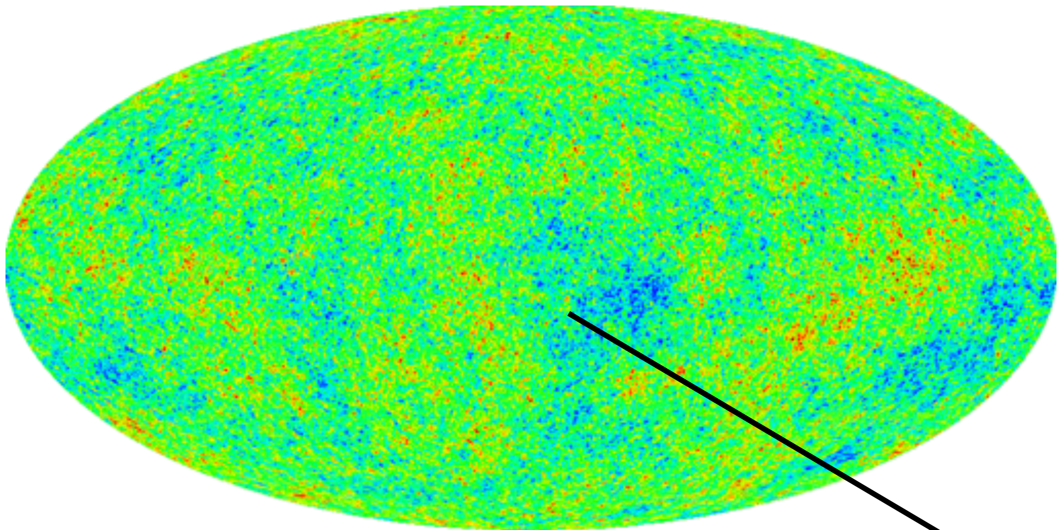

Last scattering surface

Two things can happen to the CMB photons:

1. *they are deflected by gravitational potentials*
2. *they get scattered off electrons*

Observer

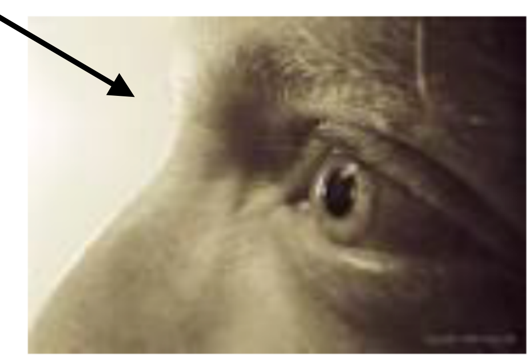

CMB power at small angular scales

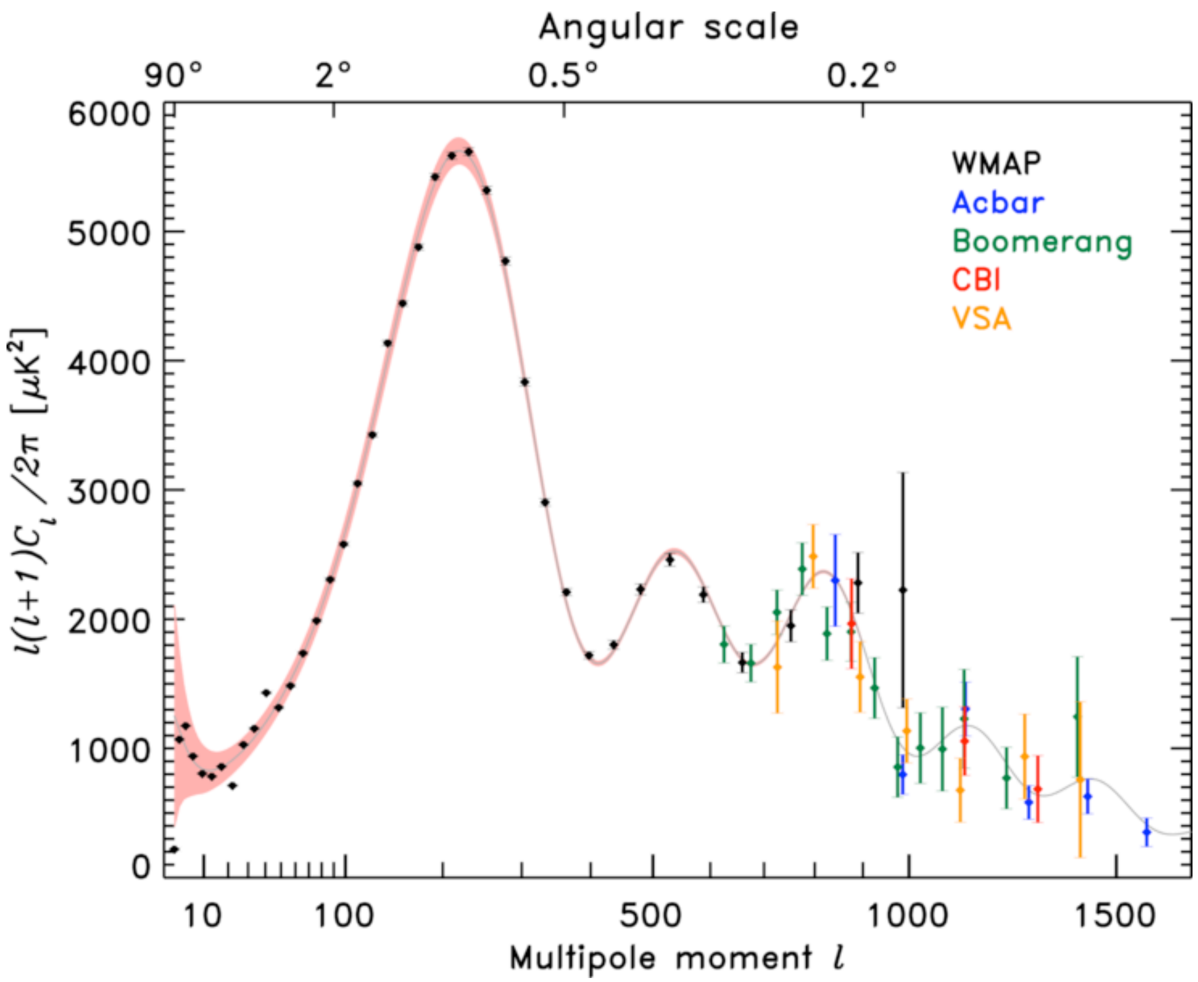

~2006

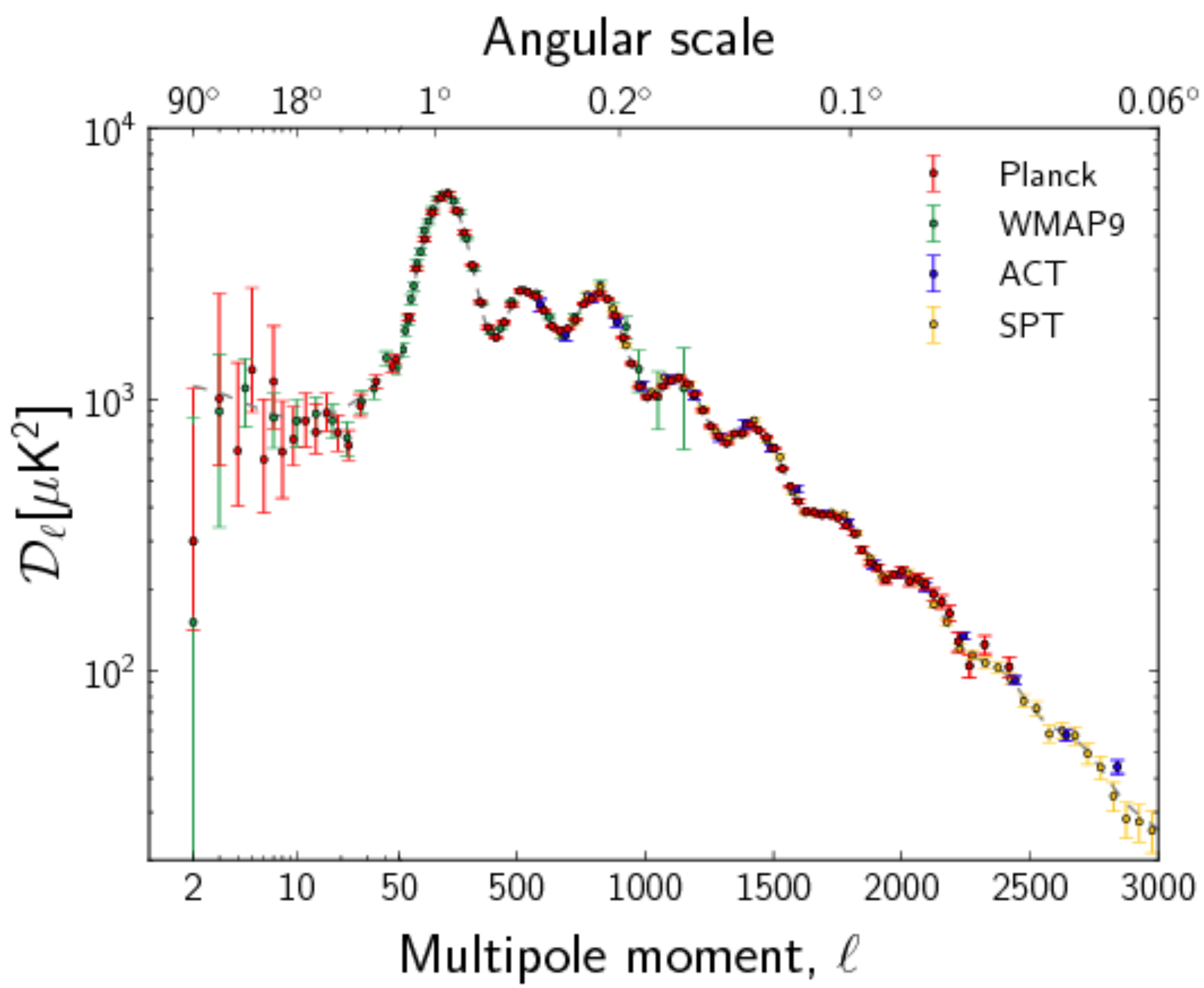

~2015

Power at small angles

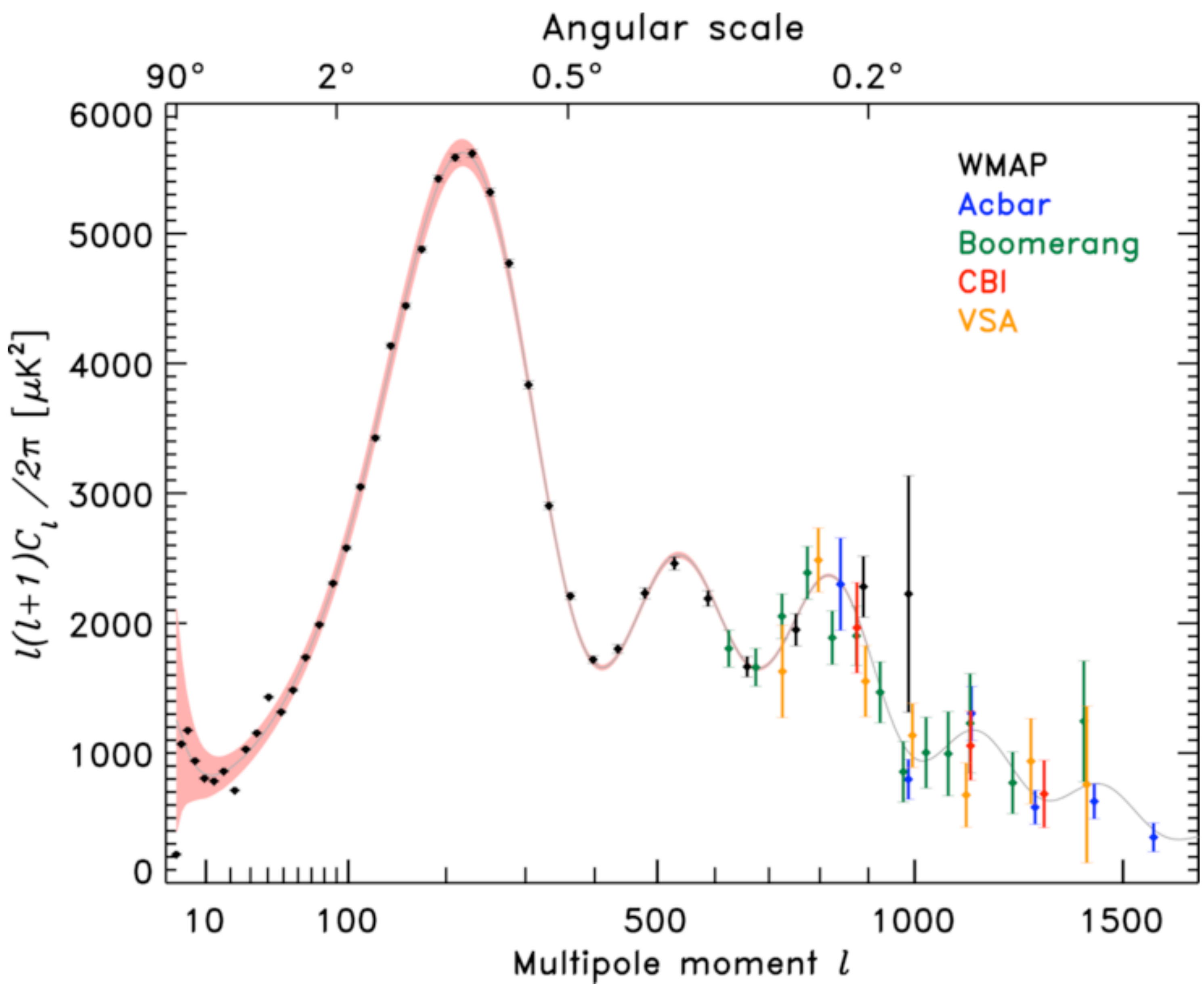

The signal is actually C_l - our power spectrum plots boost the apparent variance at large l by a factor l^2 . Observations at high-l therefore requires far greater sensitivity over the same angular beam.

Lensing of the CMB photons

Slide from A. Lewis

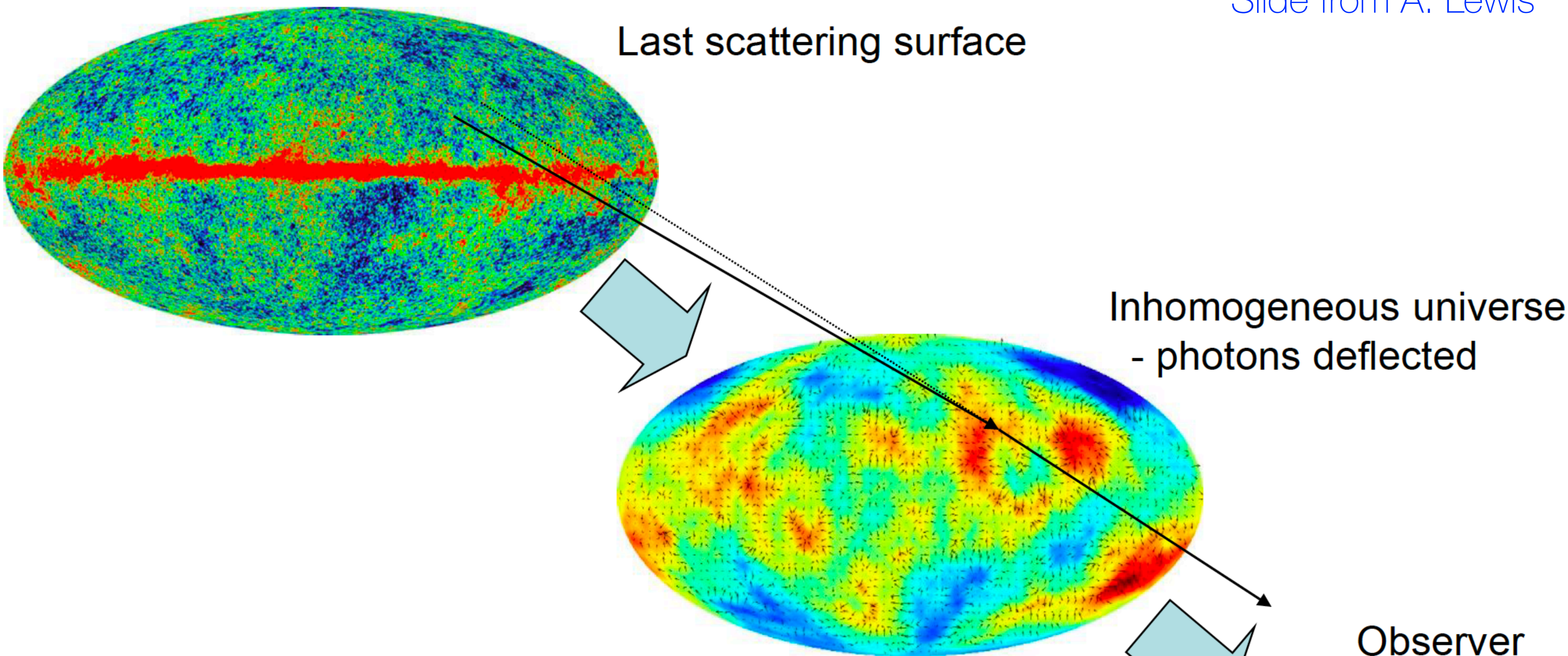

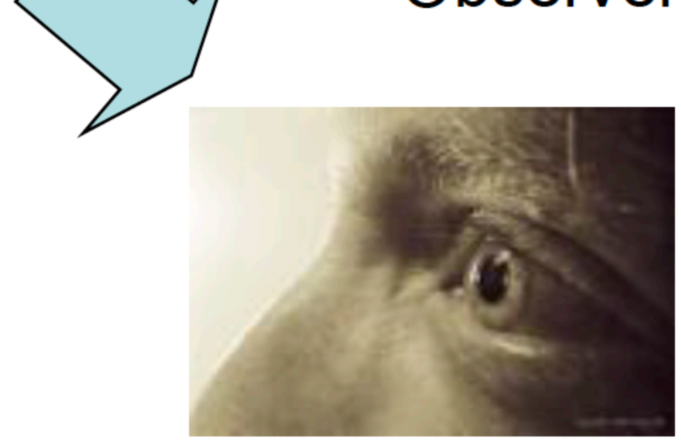

$$\tilde{T}(\hat{\mathbf{n}}) = T(\hat{\mathbf{n}}') = T(\hat{\mathbf{n}} + \boldsymbol{\alpha})$$

$$\boldsymbol{\alpha} = \nabla\psi$$

$$\psi(\hat{\mathbf{n}}) = -2\int_0^{\chi_*} \mathrm{d}\chi\, \Psi(\chi\hat{\mathbf{n}}; \eta_0 - \chi)\, \frac{f_K(\chi^* - \chi)}{f_K(\chi^*) f_K(\chi)}$$

CMB lensing formalism – I

Slide from A. Lewis

Calculating the deflection angles

$$\frac{de}{d\eta} = -\nabla_\perp(\Phi + \Psi)$$

Weyl Potential:
$\Psi_W \equiv (\Phi + \Psi)/2$
determines scalar
part of the Weyl tensor
Conformally invariant

$$\delta\beta = -2\delta\chi\nabla_\perp\Psi$$

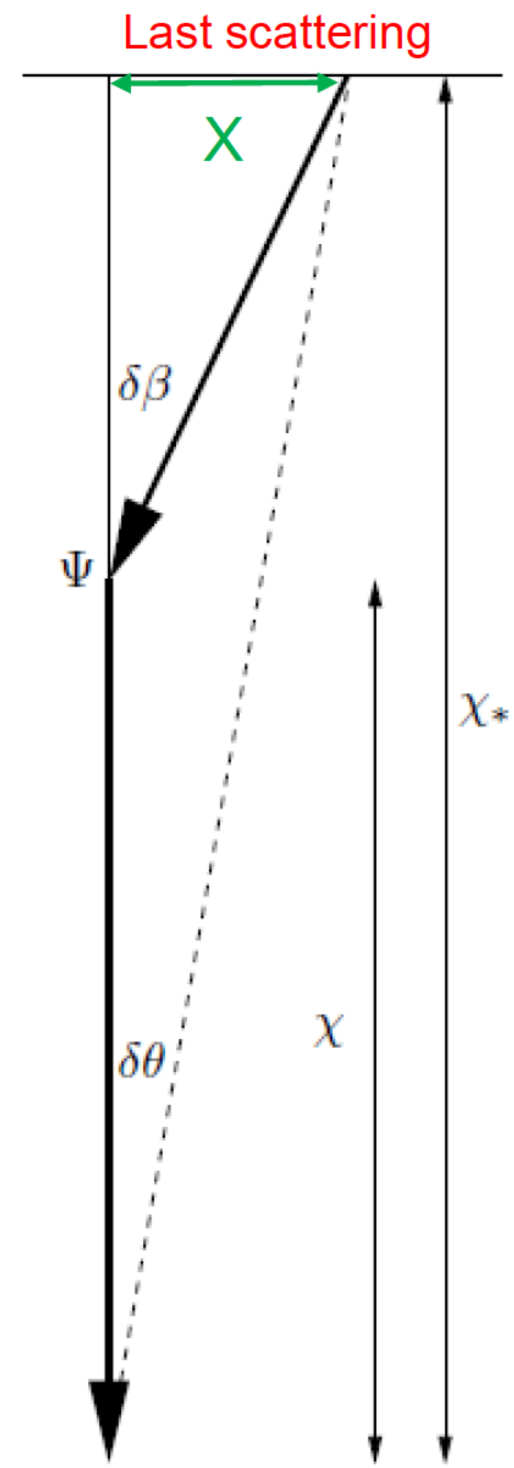

FRW background: comoving angular diameter distance

$$f_K(\chi) = \begin{cases} K^{-1/2}\sin(K^{1/2}\chi) & \text{for } K > 0, \text{ closed,} \\ \chi & \text{for } K = 0, \text{ flat,} \\ |K|^{-1/2}\sinh(|K|^{1/2}\chi) & \text{for } K < 0, \text{ open.} \end{cases}$$

Write X, in two ways $f_K(\chi_* - \chi)\delta\beta = f_K(\chi_*)\delta\theta$

$$\delta\theta_\chi = \frac{f_K(\chi_* - \chi)\delta\beta}{f_K(\chi_*)} = -\frac{f_K(\chi_* - \chi)}{f_K(\chi_*)}2\delta\chi\nabla_\perp\Psi$$

Observed deflection

CMB lensing formalism – II

Slide from A. Lewis

Lensed temperature depends on deflection angle

$$\tilde{T}(\hat{\mathbf{n}}) = T(\hat{\mathbf{n}}') = T(\hat{\mathbf{n}} + \boldsymbol{\alpha})$$

Newtonian (Weyl) potential

$$\boldsymbol{\alpha} = \delta\theta = -2\int_0^{\chi^*} \mathrm{d}\chi \frac{f_K(\chi^* - \chi)}{f_K(\chi^*)} \nabla_\perp \Psi(\chi\hat{\mathbf{n}}; \eta_0 - \chi)$$

co-moving distance to last scattering

See lensing review for more rigorous spherical derivation

Lensing Potential

Deflection angle on sky given in terms of angular gradient of lensing potential $\boldsymbol{\alpha} = \nabla\psi$

$$\boldsymbol{\nabla}_\perp \Psi = (\nabla_{\hat{\mathbf{n}}} \Psi)/f_K(\chi)$$

$$\Rightarrow \quad \psi(\hat{\mathbf{n}}) = -2\int_0^{\chi_*} \mathrm{d}\chi\, \Psi(\chi\hat{\mathbf{n}}; \eta_0 - \chi) \frac{f_K(\chi^* - \chi)}{f_K(\chi^*) f_K(\chi)}$$

$$\tilde{X}(\mathbf{n}) = X(\mathbf{n}') = X(\ \mathbf{n} + \nabla\psi(\mathbf{n})\ )$$

Lensing of the CMB photons

CMB photons get deflected by the intervening large scale structure. This is quantified by the deflection angle $\boldsymbol{\alpha} = \nabla\psi$

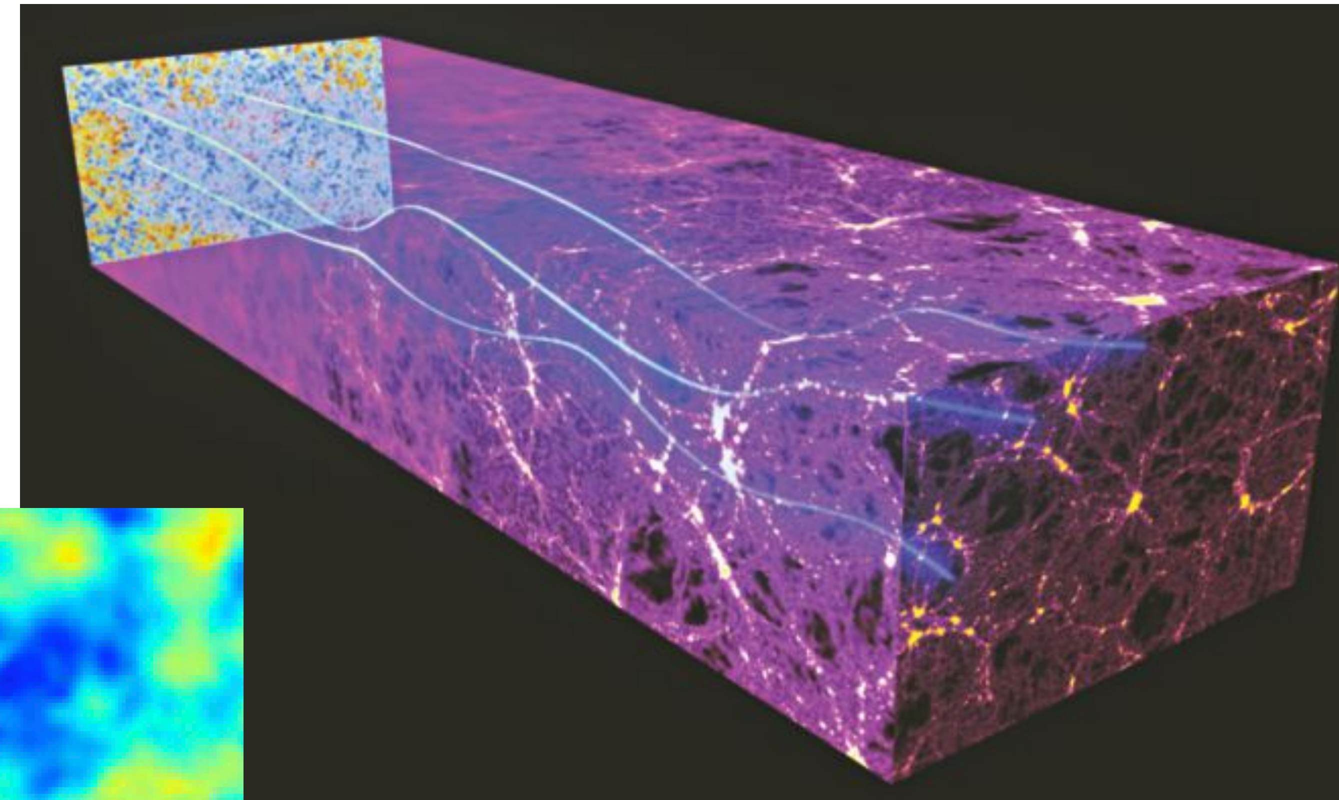

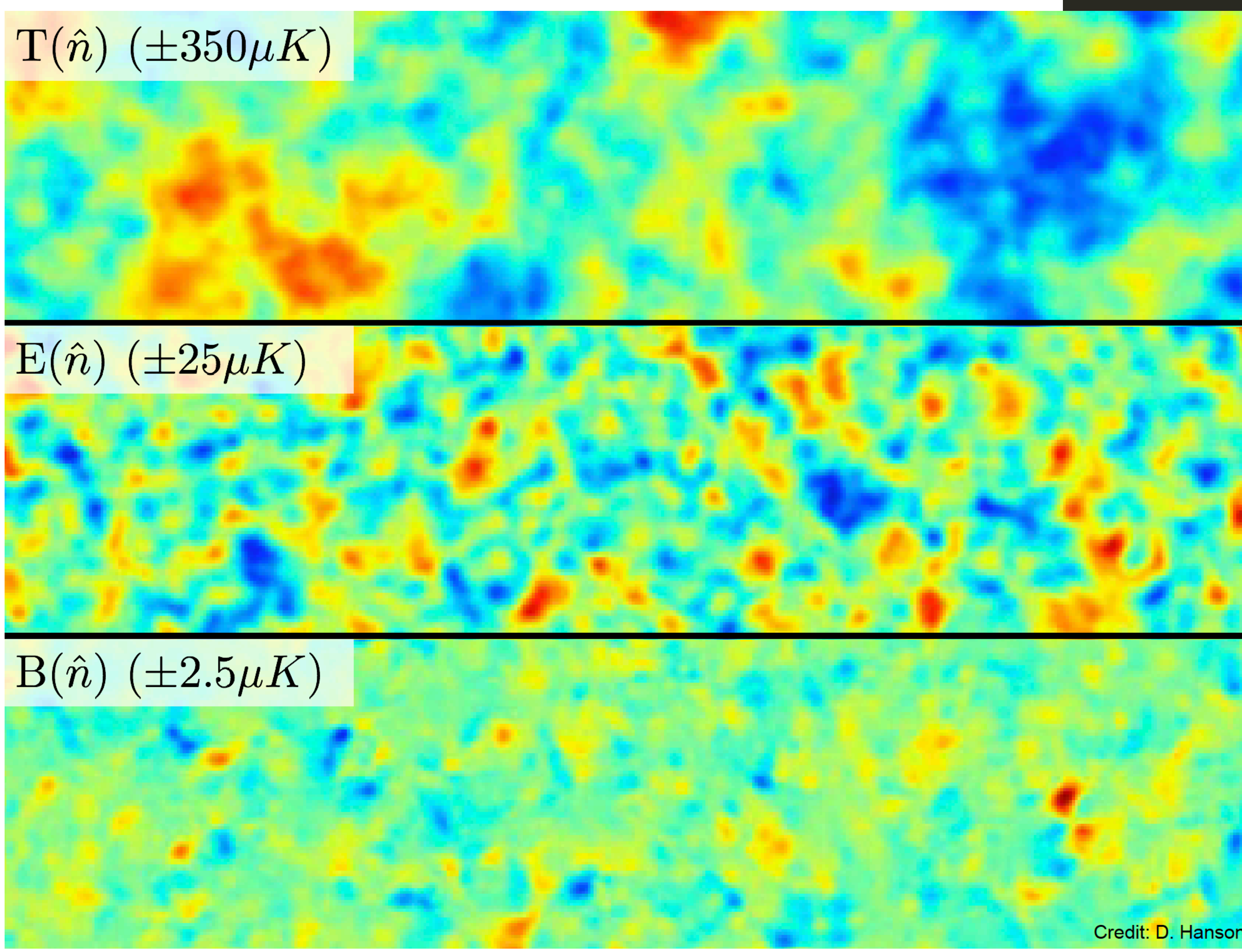

One result of CMB lensing is blurring of temperature and E-mode polarization anisotropies, as the angular scales associated with the peaks are smeared.

Another result is the creation of B-mode polarization from E-mode (by mixing Stokes Q and U params).

Temperature & polarization after lensing

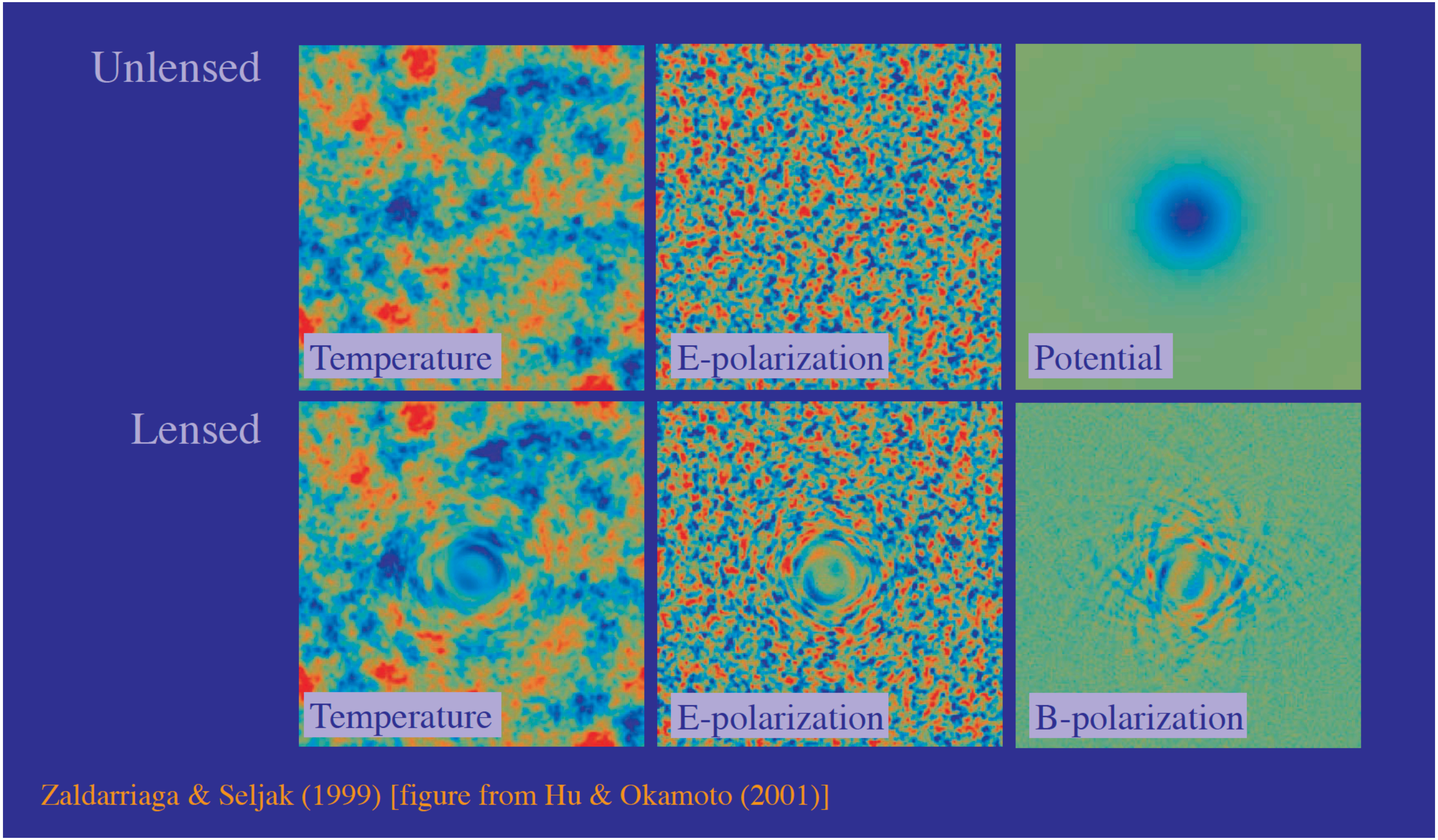

Unlensed CMB

CMB Temp.

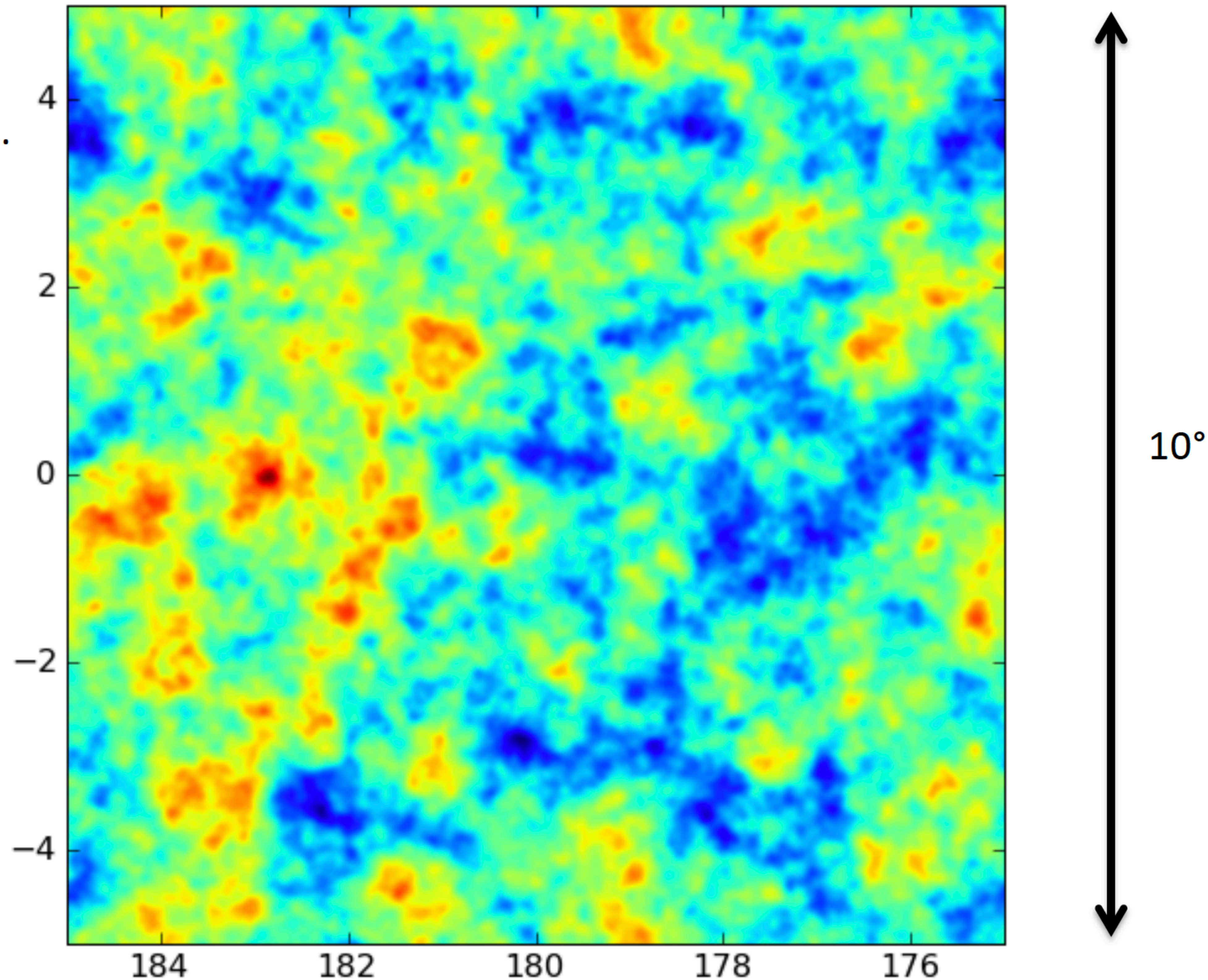

$T(\hat{\mathbf{n}})_{\mathrm{unlensed}}$

Lensed CMB

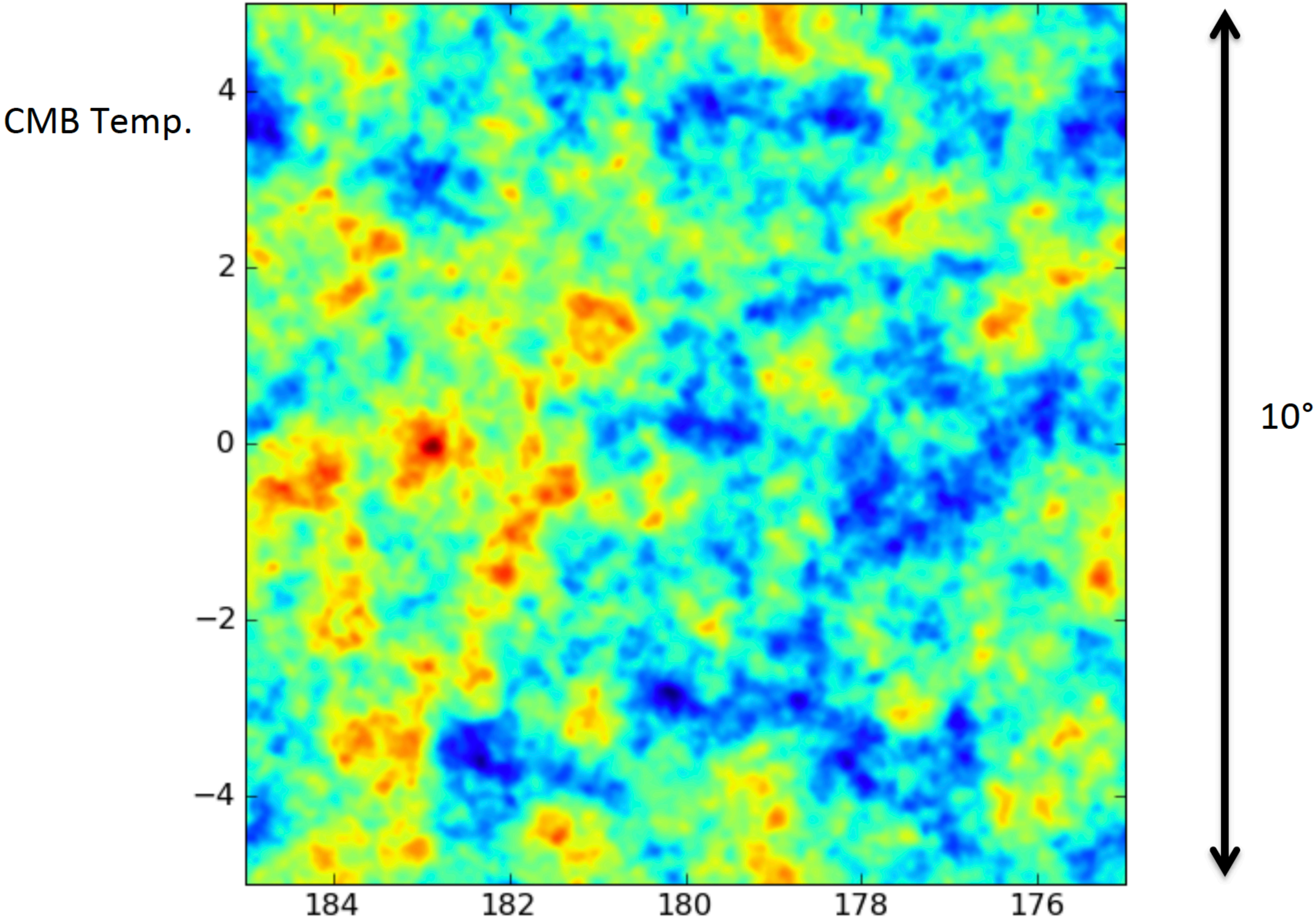

$$T(\hat{\mathbf{n}})_{\text{lensed}} = T(\hat{\mathbf{n}} + \mathbf{d}(\hat{\mathbf{n}}))_{\text{unlensed}}$$

Lensing of the CMB photons

- Lensing is a surface brightness conserving remapping of source to image planes by the gradient of the projected potential

$$\phi(\hat{\mathbf{n}}) = 2 \int \frac{dz}{H(z)} \frac{D_A(D_s - D)}{D_A(D)\, D_A(D_s)} \Phi(D_A \hat{\mathbf{n}}, D)\,,$$

such that the fields are remapped as

$$x(\hat{\mathbf{n}}) \to x(\hat{\mathbf{n}} + \nabla\phi)\,,$$

where $x \in \{T, Q, U\}$ temperature and polarization.

- Taylor expansion leads to product of fields and Fourier mode-coupling
- Appears in the power spectrum as a convolution kernel for T and E and an $E \to B$.

Beware!
Different notation!

Slide from Wayne Hu

Lensing effect on the power spectrum

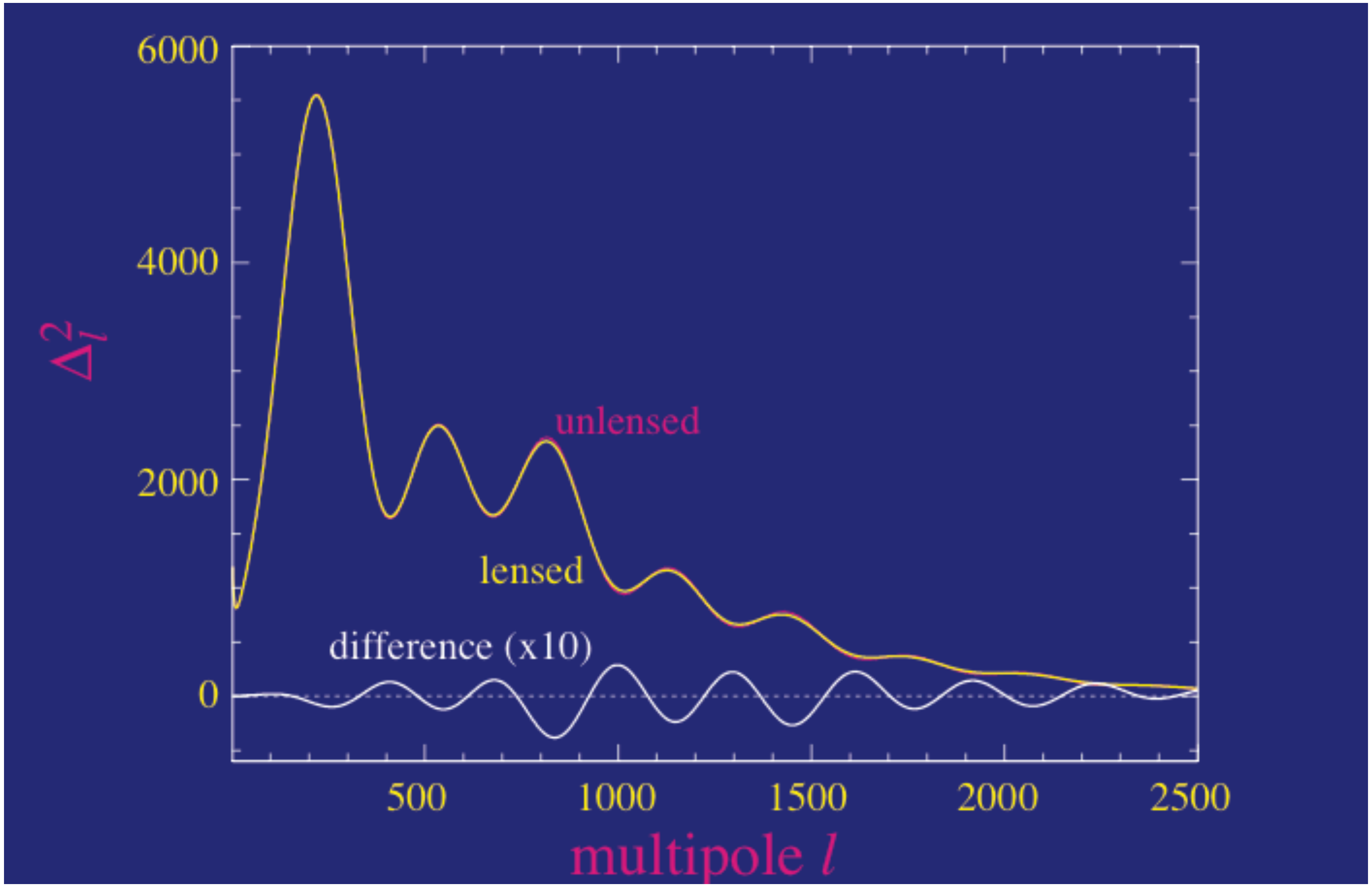

Lensing smooths the temperature power spectrum (and E mode polarization) with a width `Δl~60` This is a small, subtle effect, but reaches up to ~20% at `l~3000`.

Lensed TT and EE power

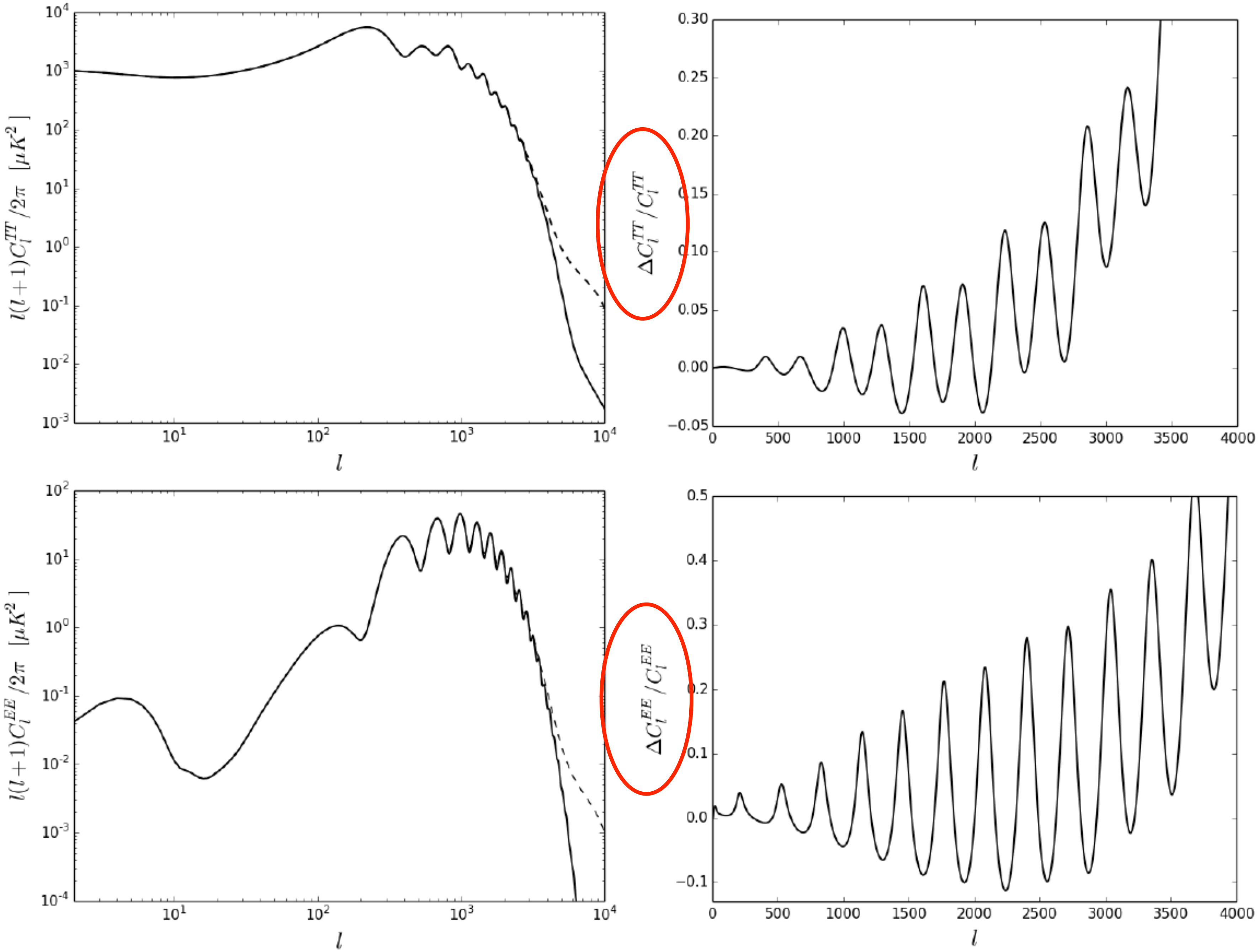

The left panels show the unlensed (solid) and lensed (dashed) power spectra of the CMB temperature (top) and E mode polarisation (bottom). Lensing spreads out the peaks very slightly while transferring power to large l. The right panels show the fractional change in the power spectrum caused by lensing.

CMB lensing measurements

Statistically detectable at high-significance with Planck because low foregrounds and other secondaries at large angular scales.

$$\phi(\hat{\mathbf{n}}) = 2\int \frac{dz}{H(z)} \frac{D_A(D_s - D)}{D_A(D)\, D_A(D_s)} \Phi(D_A\hat{\mathbf{n}}, D)$$

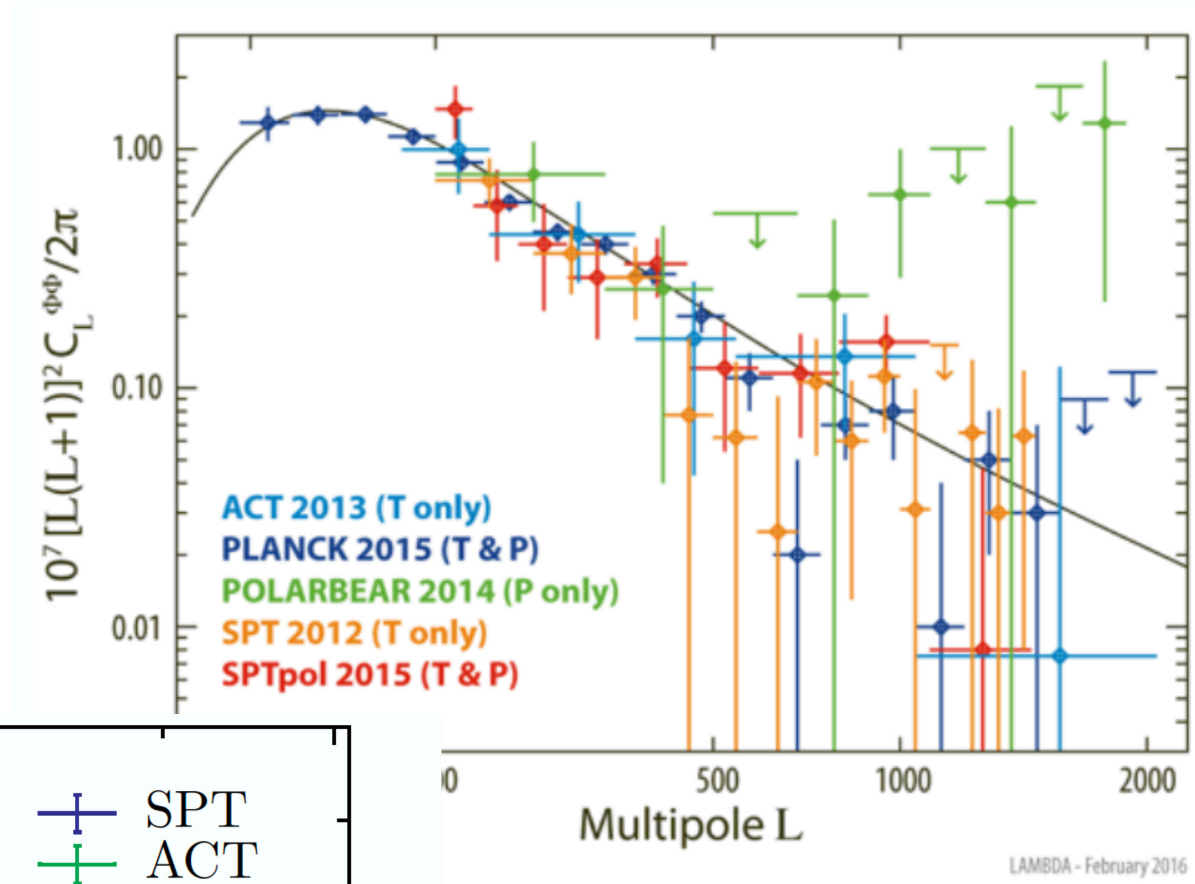

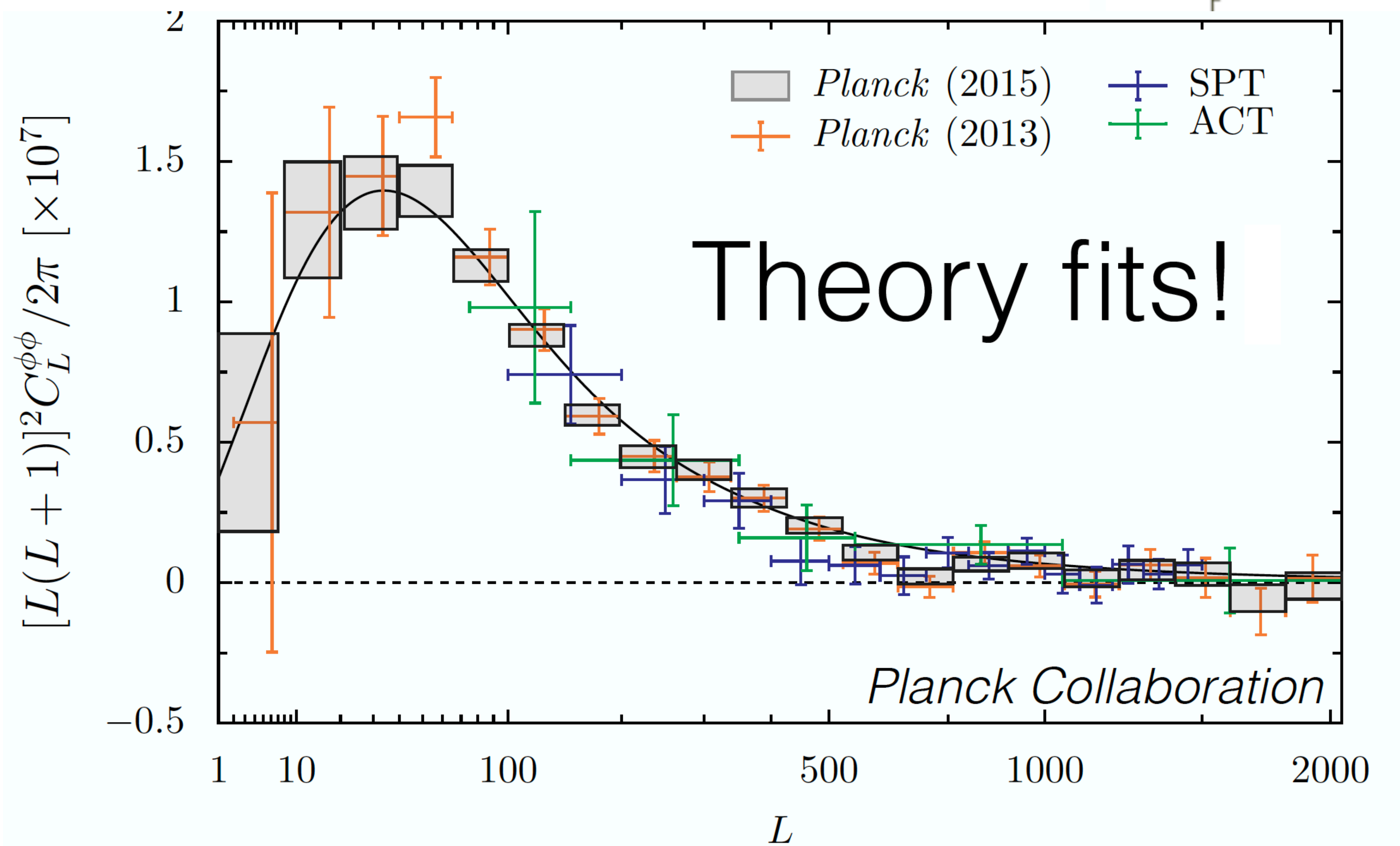

Planck 2015 results

Matter distribution from CMB lensing

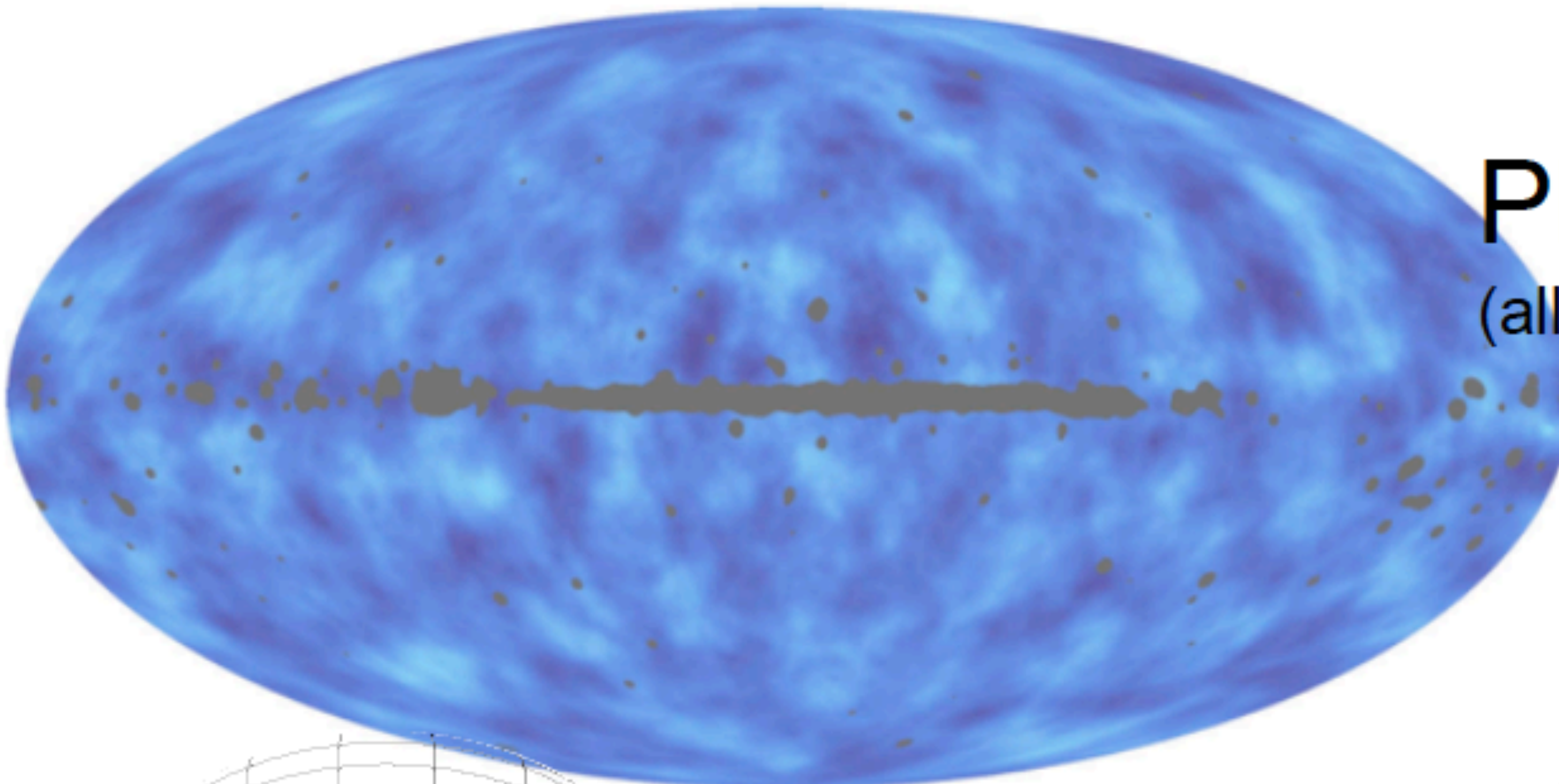

Planck
(all-sky)

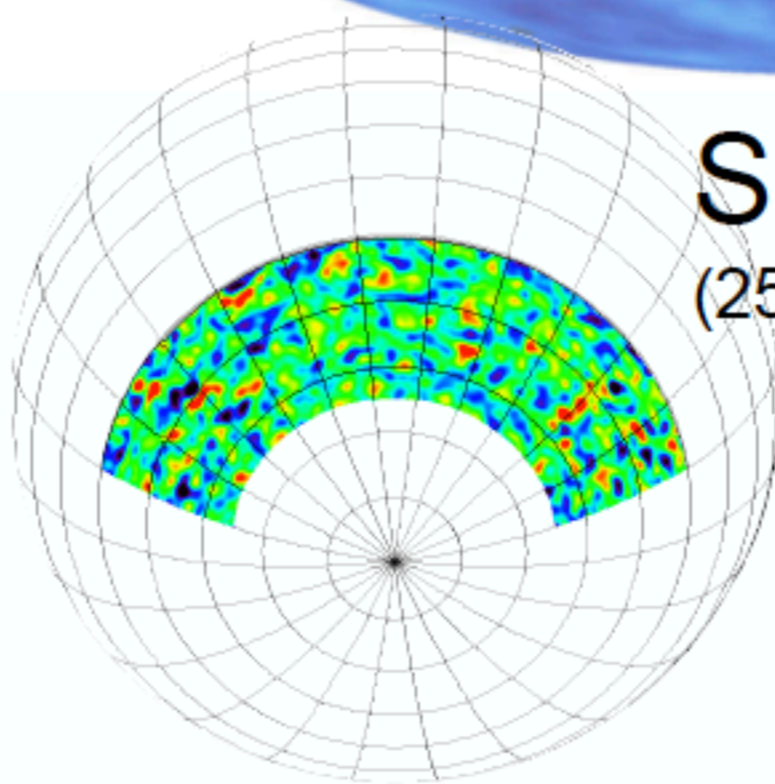

SPT
(2500 sq deg)

SPT-Pol
(100 sq deg)

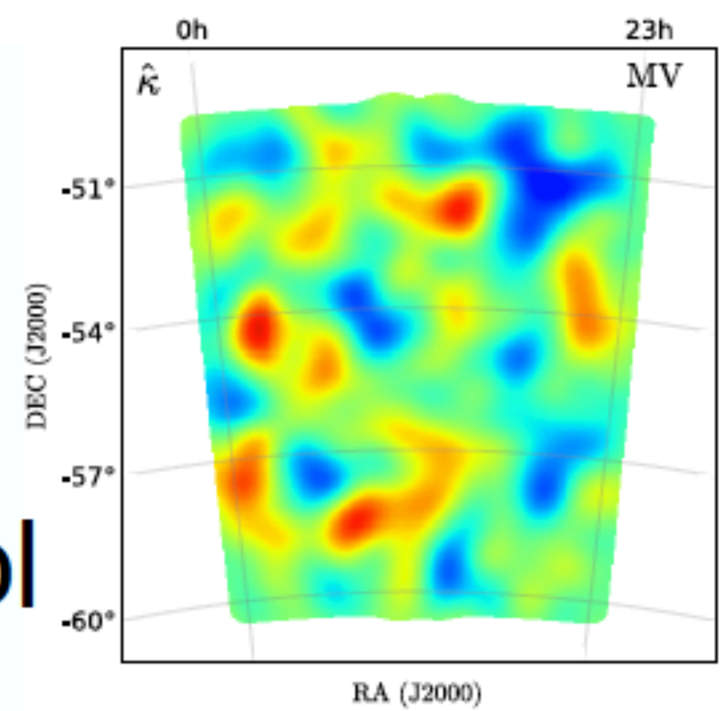

Cosmology with CMB lensing

CMB lensing currently competitive with galaxy lensing

Probes higher redshift ⇒ constrains $\Omega_m \sigma_8^{0.25}$ vs. galaxy $\Omega_m \sigma_8^{0.5}$

DES 1YR +Planck lensing only LCDM forecast

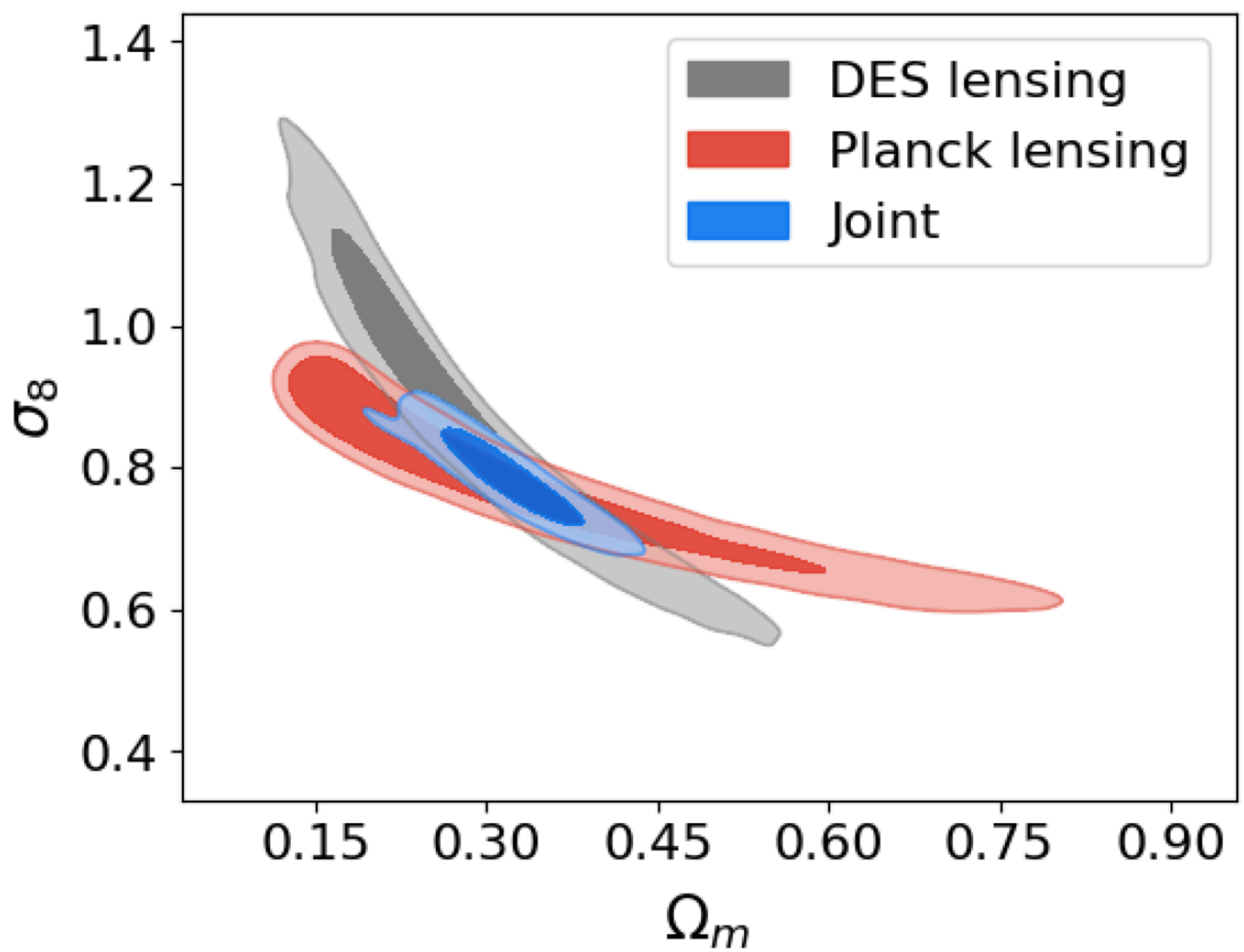

DES 1Yr has 10 nuisance parameters, conservative cuts: limited by modelling not statistics
CMB lensing currently limited by low S/N (and only one source redshift plane)

CMB lensing by galaxy clusters

Slide from Anthony Lewis

CMB very smooth on small scales: approximately a gradient

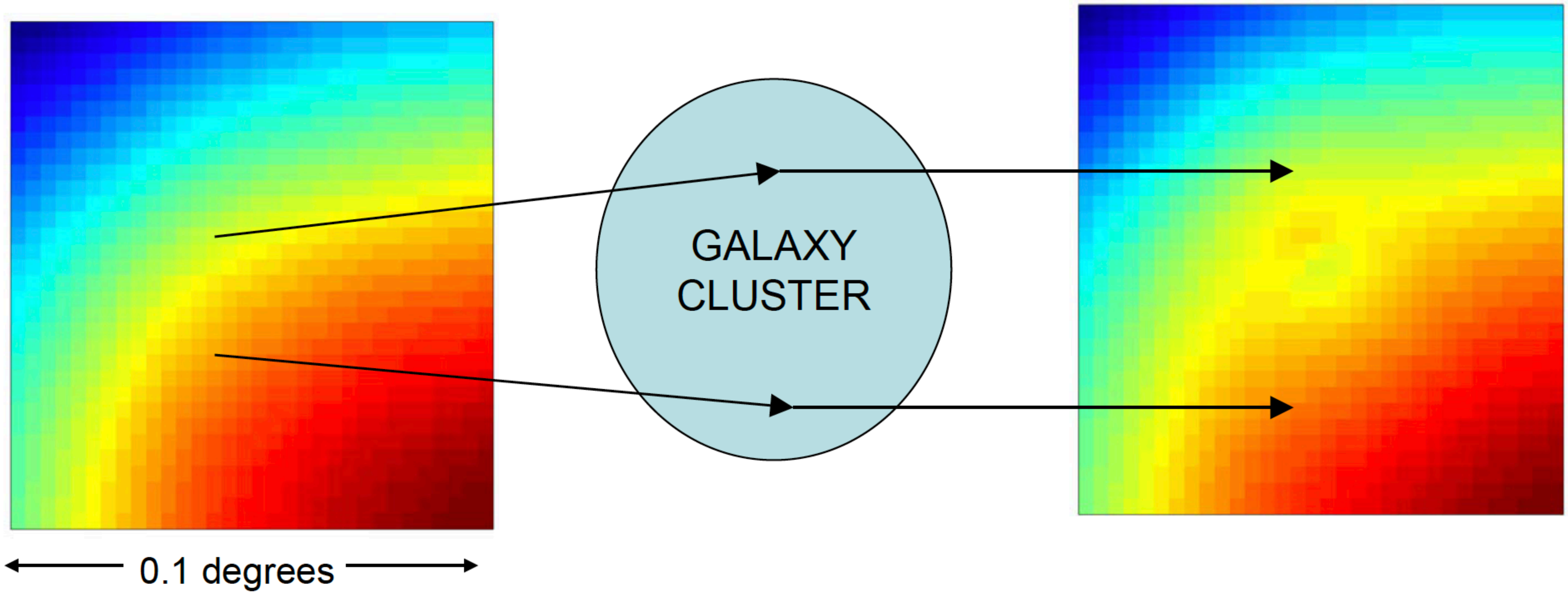

Need sensitive ~ arcminute resolution observations

CMB lensing by galaxy clusters

Slide from Anthony Lewis

RMS gradient ~ 13 μK / arcmin
deflection from cluster ~ 1 arcmin

Lensing signal ~ 10 μK

BUT: depends on CMB gradient behind a given cluster

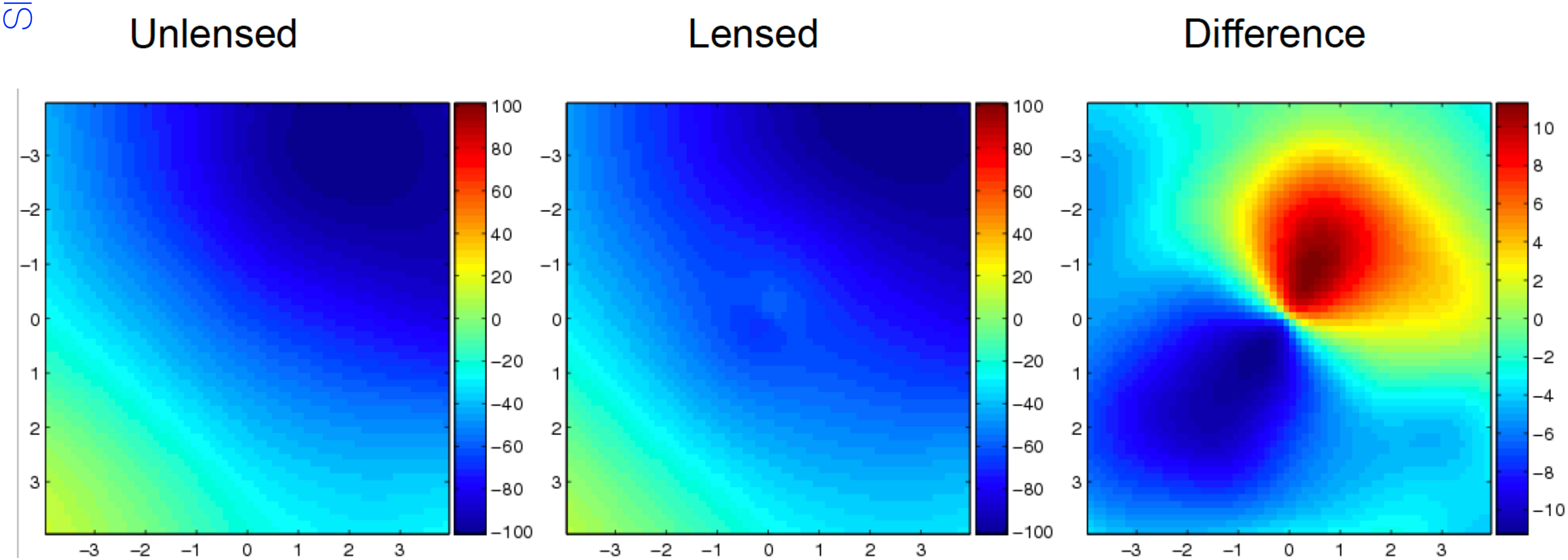

Unlensed CMB unknown, but statistics well understood (background CMB Gaussian) :

can compute likelihood of given lens (e.g. NFW parameters) essentially exactly

Cluster lensing state-of-the-art

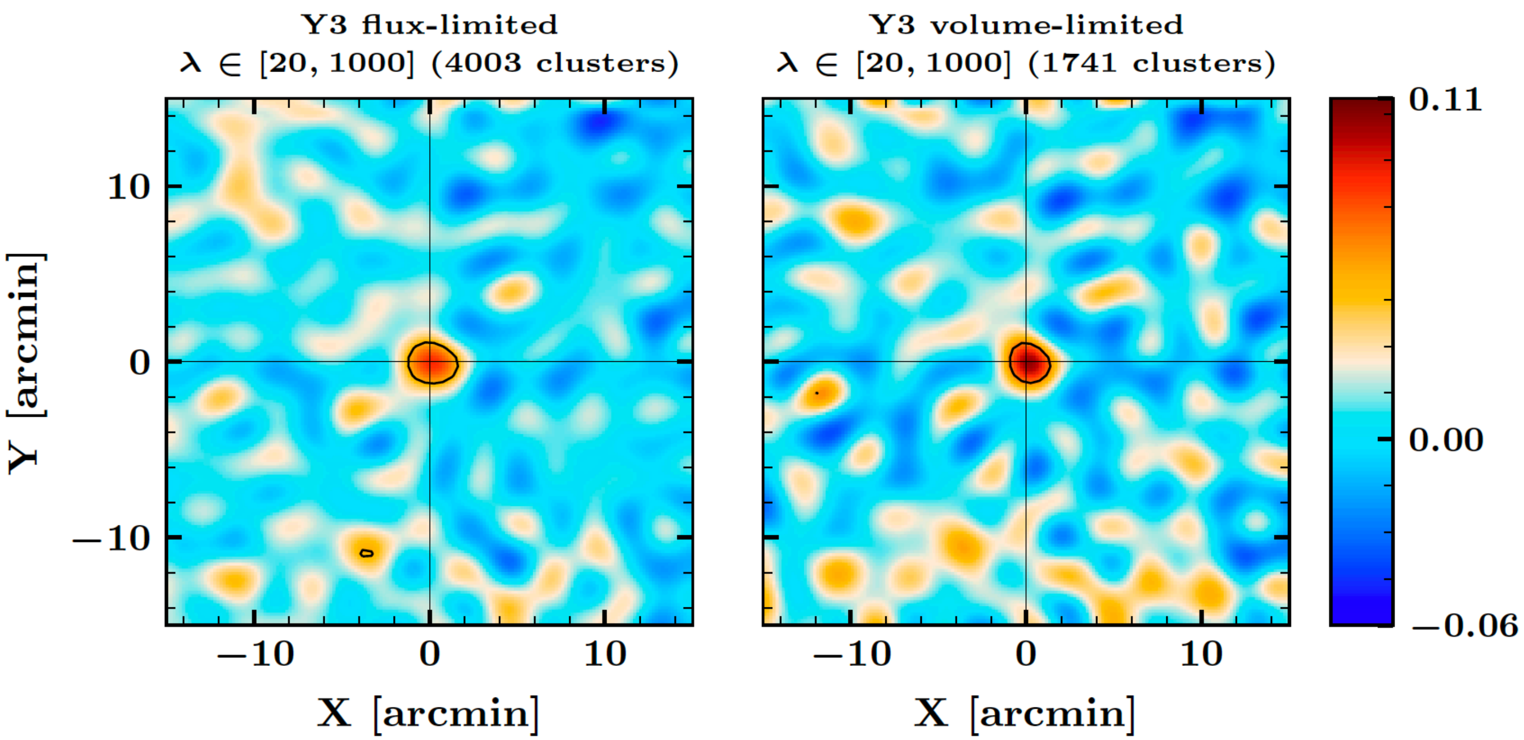

Raghunathan et al. (2019): DES and SPTpol

Current ground-based CMB experiments (SPT and ACT) are able to measure the lensing convergence from galaxy clusters by stacking 1000s of objects. This precision is expected to improve dramatically in the coming years.

High-sensitivity, high resolution CMB can calibrate mass of 1000 stacked clusters to a few percent

S4 Science Book

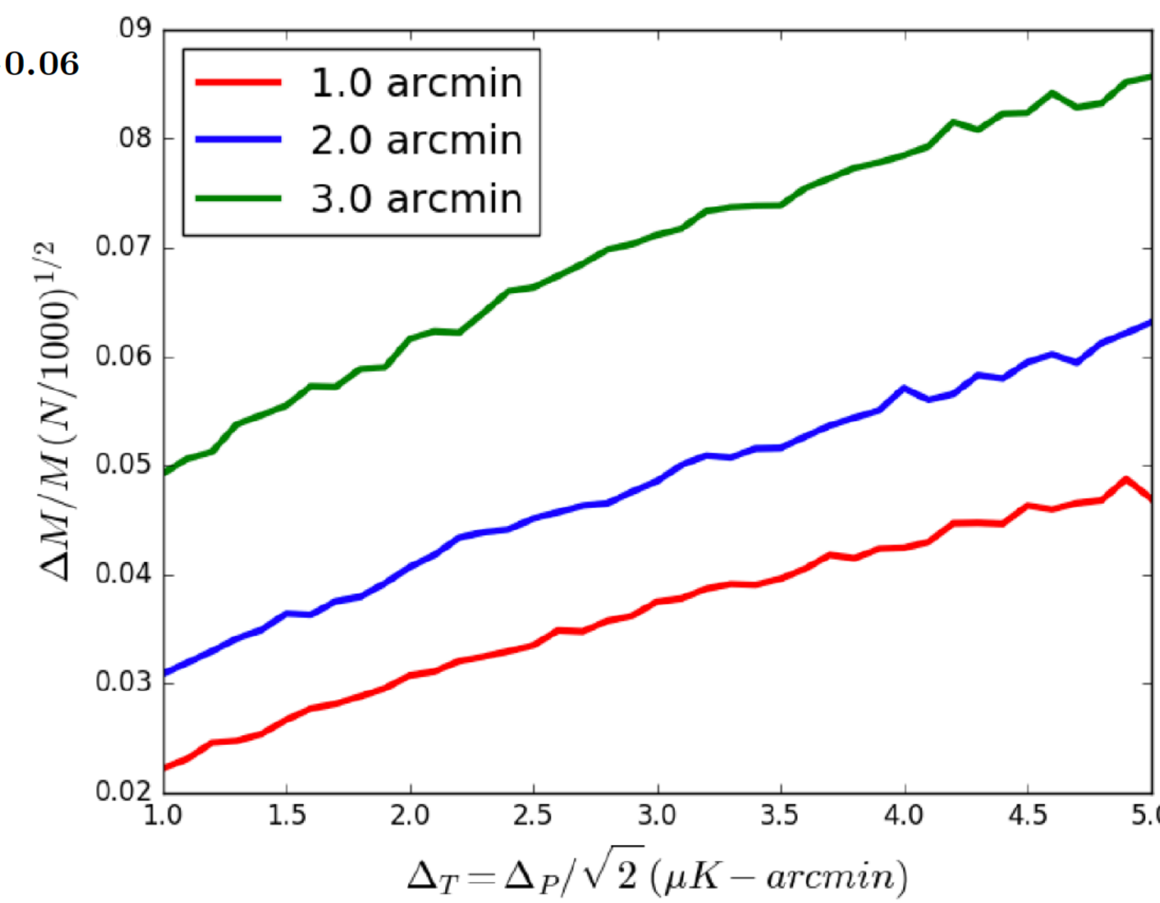

Other lensing effects: Moving lens

Birkinshaw & Gull (1983)

$$\frac{\Delta T(\hat{\mathbf{n}})}{T_{\rm CMB}} = \mathbf{v}_\perp \cdot \nabla\psi$$

Yasini et al. (2018)
Hotinli et al. (2018)

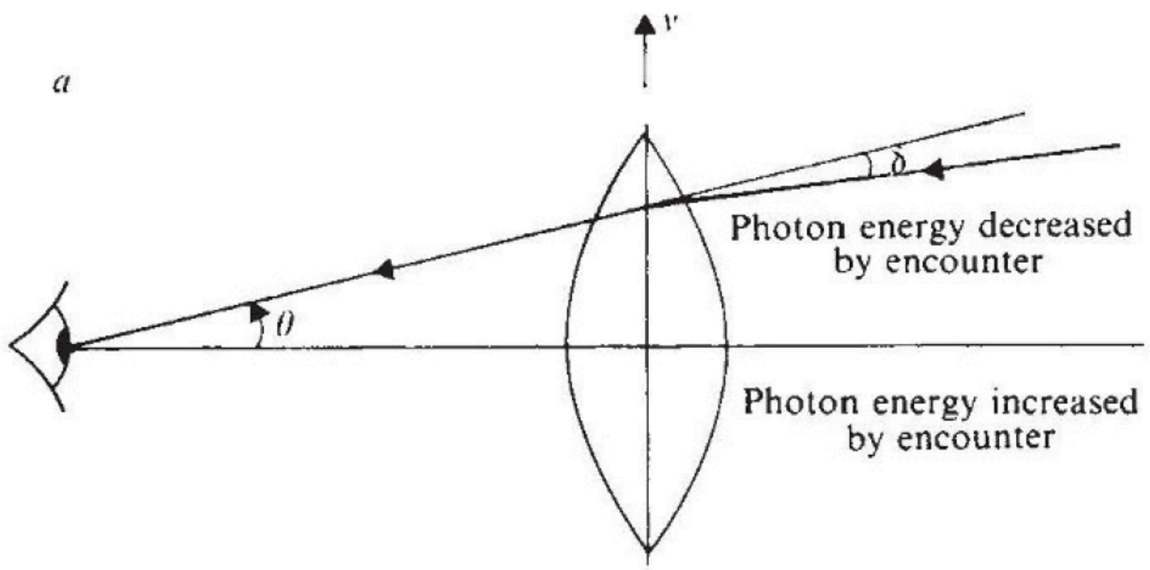

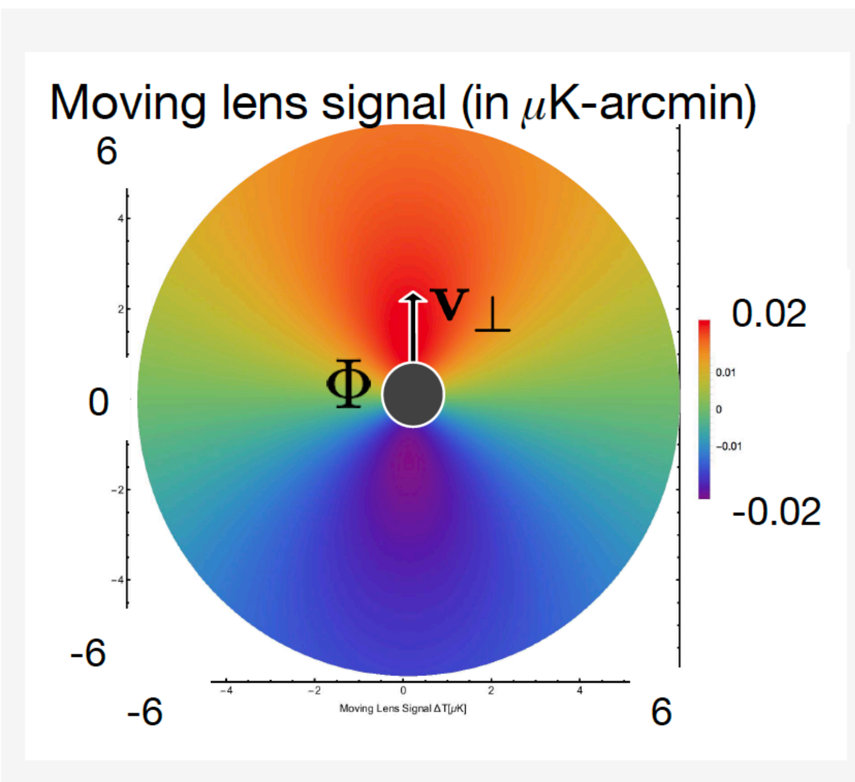

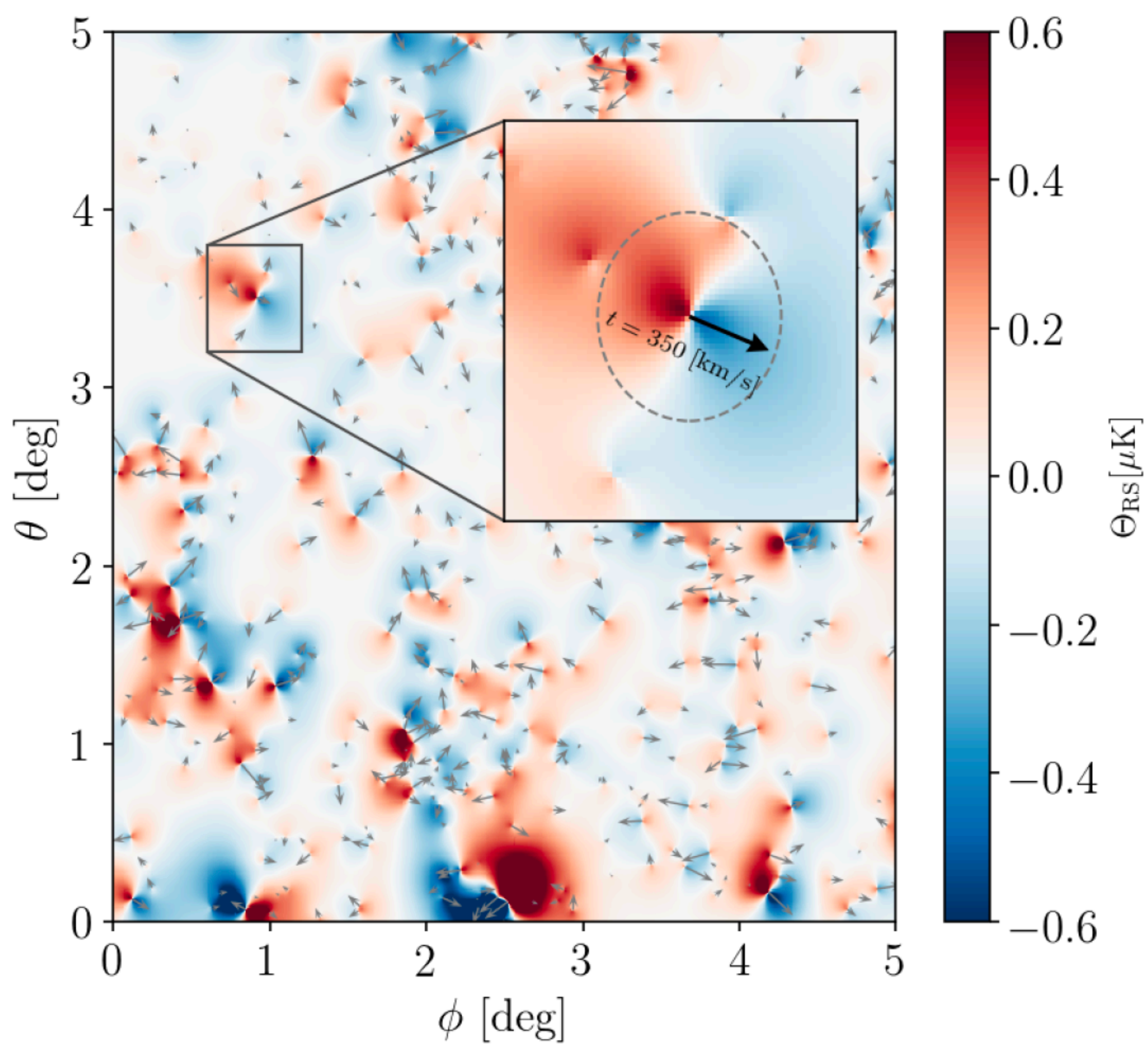

Scattering of CMB after recombination

The main impact of cosmic reionization at redshift z ~ 6-10 is to dampen the temperature anisotropies, and create new E-mode anisotropies at very large angles.

τ degenerate with other cosmological parameters, especially A_s and related parameters n_s, σ_8, and foregrounds.

$$C_\ell^{TT} \propto A_s e^{-2\tau}$$

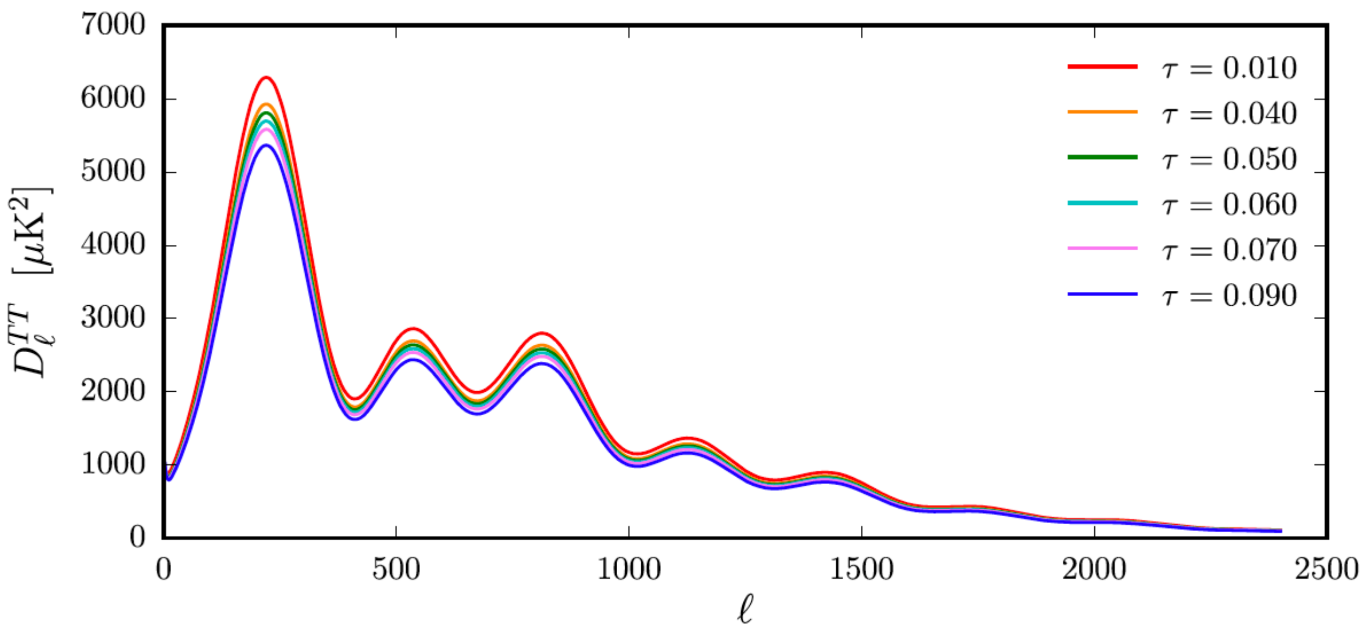

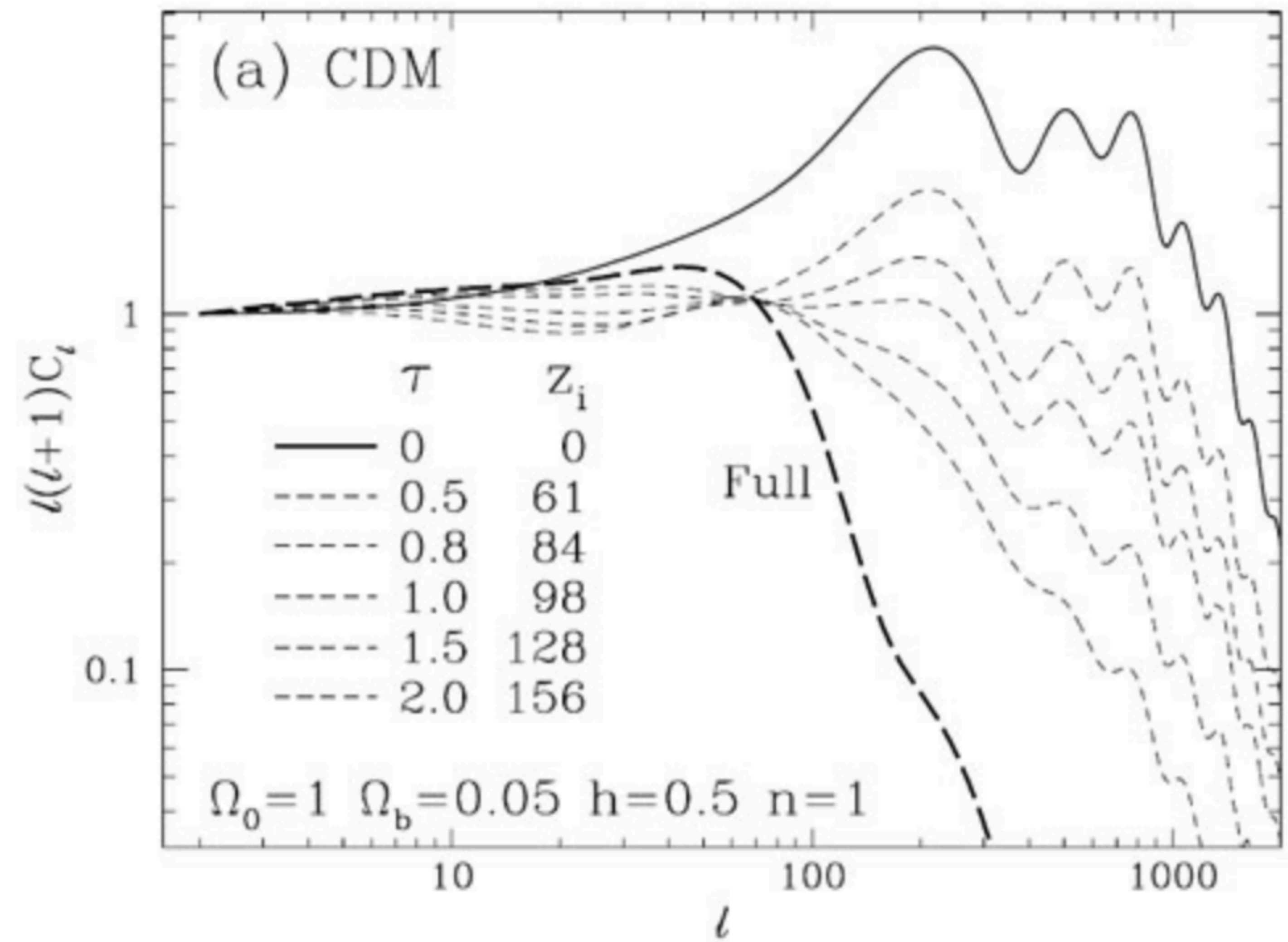

Current constraint from Planck (2018):

τ = 0.054 ± 0.007

$$\tau(z) = \int_{t(z)}^{t_0} n_e \sigma_T c\, dt'$$

ΔT/T from reionization

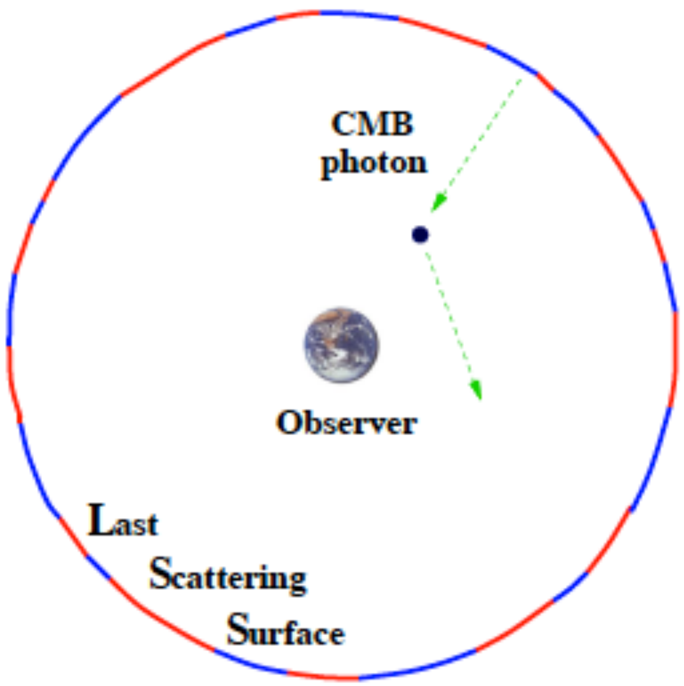

$$\frac{\Delta T}{T_0}(\theta) = e^{-\tau}\,\frac{\Delta T}{T_0}(\theta)\Big|_{orig.} + \frac{\Delta T}{T_0}(\theta)\Big|_{new}$$

"suppression (blurring)" & "generation"

Re-scattering of CMB photons damps anisotropy power (ΔT^2) as $e^{-2\tau}$, with τ the optical depth to Thomson scattering.

For $\tau = 0.095$, this means a 20% reduction from initial power.

New perturbations are generated on small scales due to the bulk motion of electrons in over-dense regions (Ostriker-Vishniac effect) → also called **kSZ from reionization**

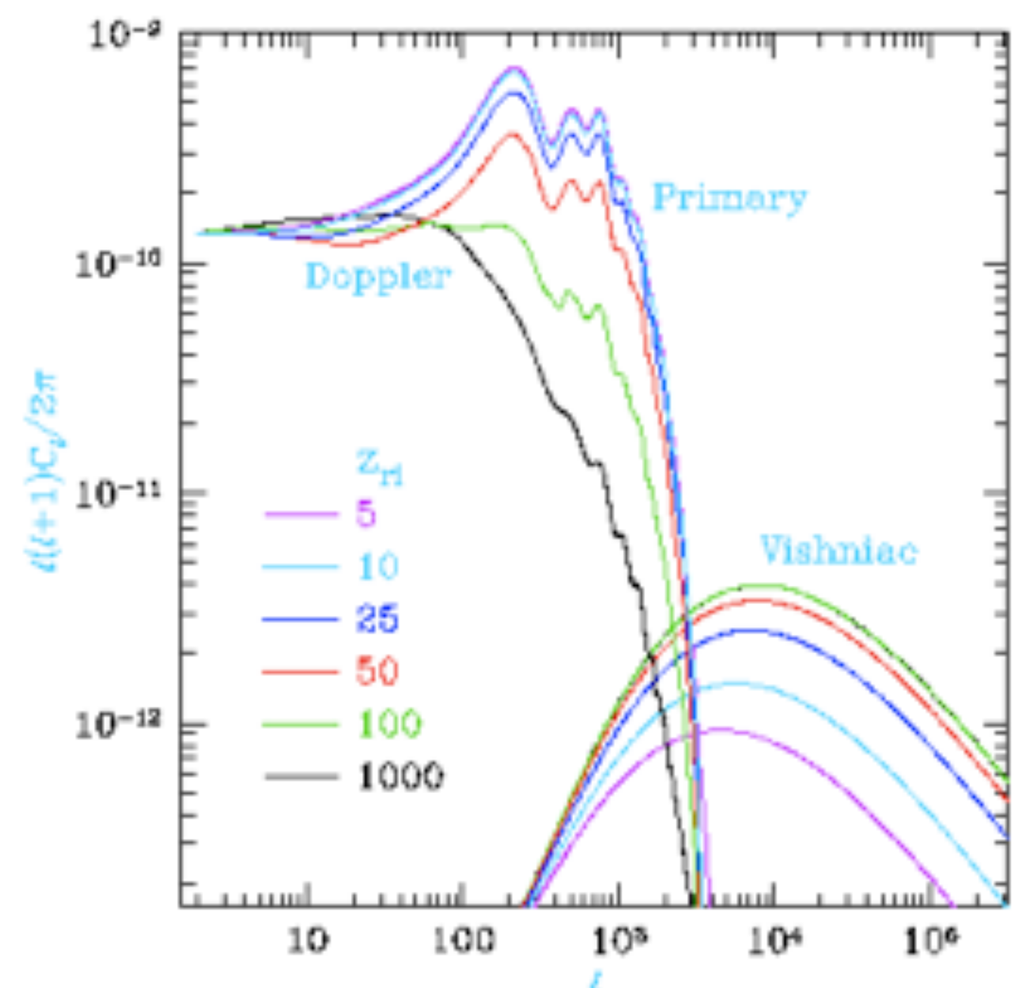

Additional small effects

Resonant scattering by atoms and molecules (CMB spectroscopy!)

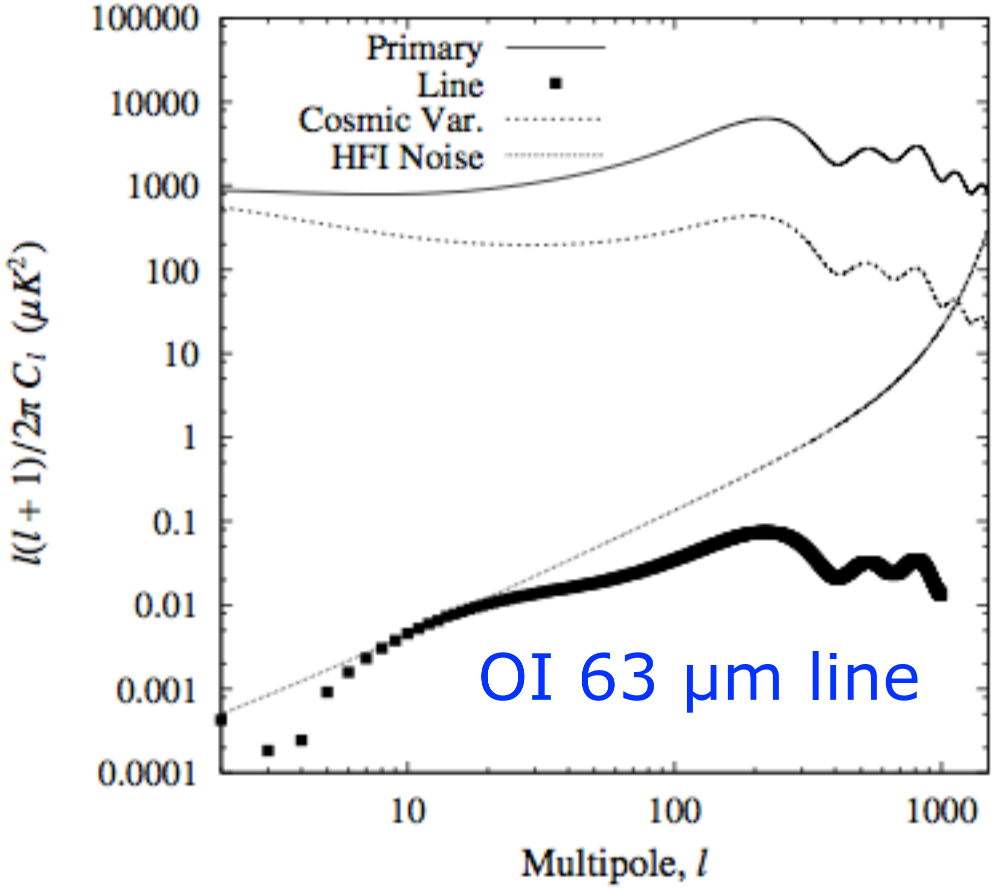

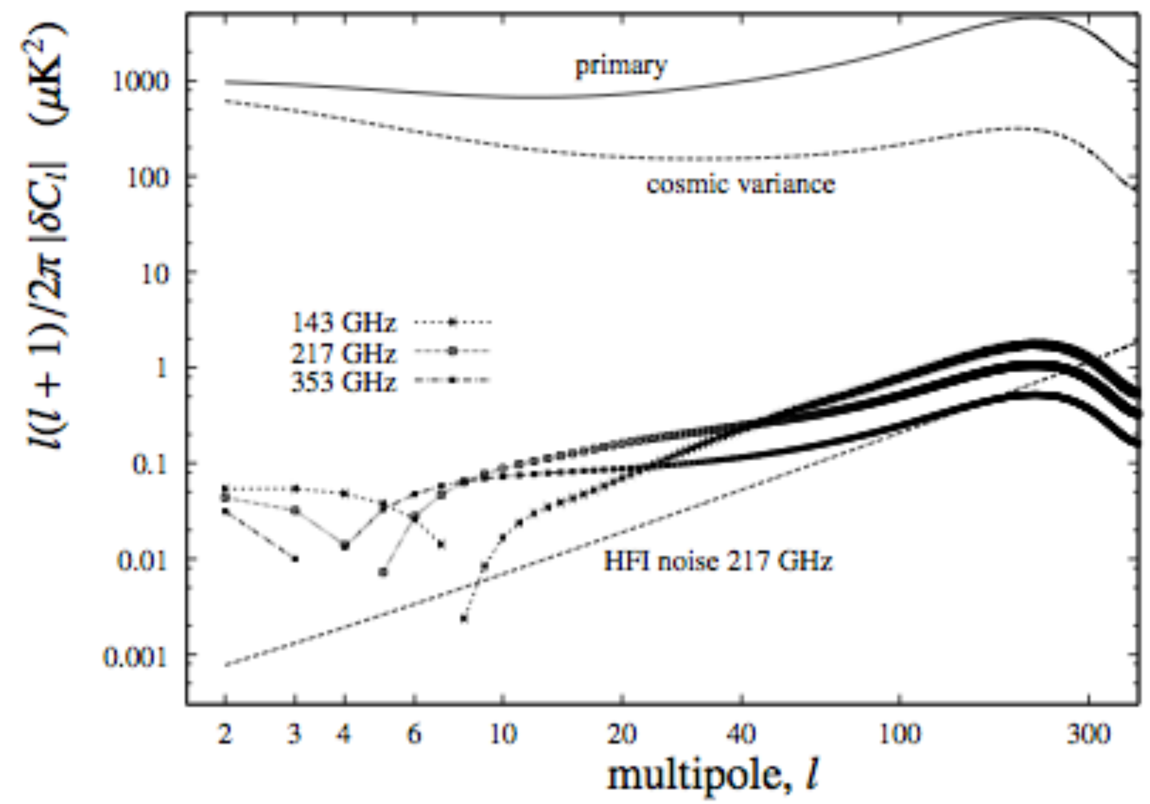

Basu, Hernandez-Monteagudo & Sunyaev 2004

$$\frac{\delta T}{T_0}(\boldsymbol{n}, z=0) = (1-\tau_{X_i})\,\frac{\delta T}{T_0}(\boldsymbol{n}, z_{X_i}) + \tau_{X_i}\,\frac{\delta T}{T_0}\bigg|_{\rm new}^{\rm lin}(\boldsymbol{n}, z_{X_i}) + O\left[\tau_{X_i}^2\right].$$

$$\Rightarrow$$

$$\delta C_l \equiv C_l^{X_i} - C_l = \tau_{X_i}\cdot C_1 + \tau_{X_i}^2\cdot C_2 + O\left(\tau_{X_i}^3\right).$$

Local y-distortion: Sunyaev-Zeldovich effect(s)

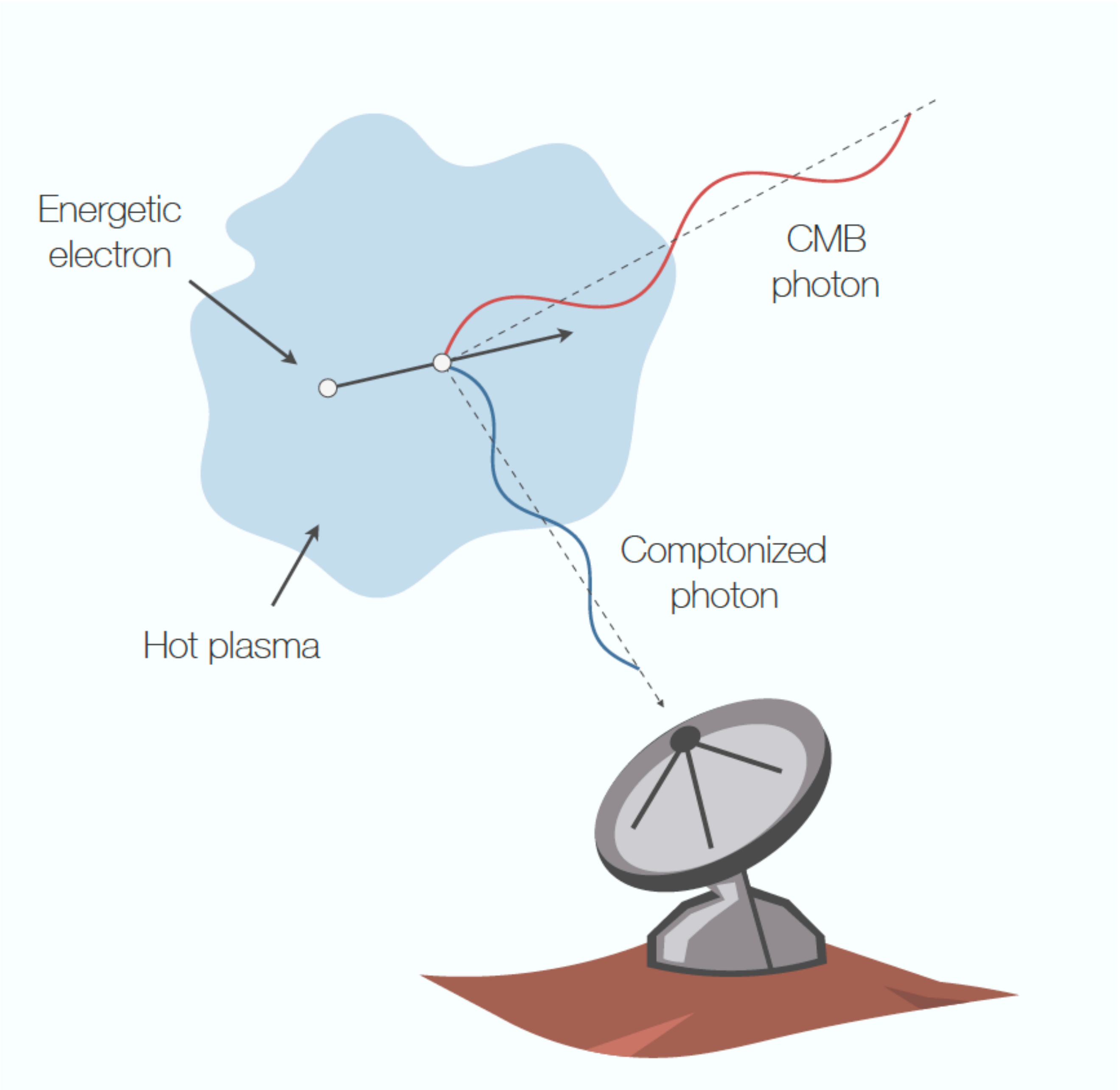

See recent review: arXiv:1811.02310

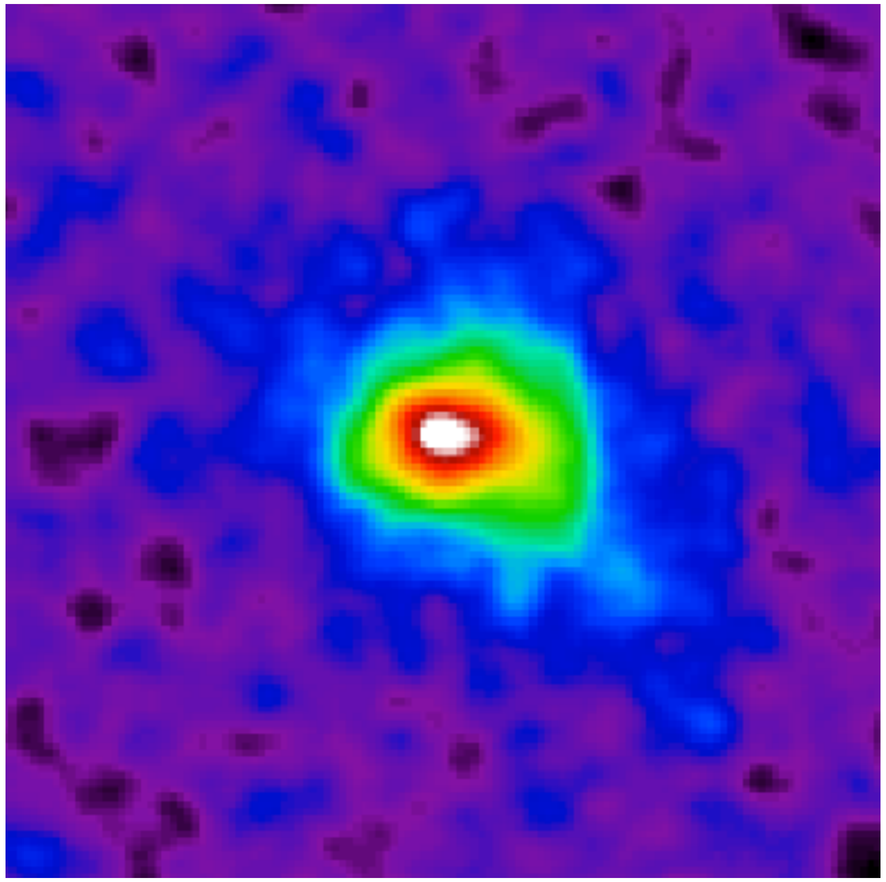

Coma cluster from Jens Erler's master's thesis, created using ILC method and Planck data

Single IC scattering of CMB photons

The physics of the SZ effect is very simple. Moving electrons transfer some of their kinetic energy to the low-energy CMB photons, via Doppler effect. This is the well-known energy ratio of photons after Compton scattering when $h\nu \ll \gamma m_e c^2$

$$\frac{\nu'}{\nu} = \frac{1 - \beta\mu}{1 - \beta\mu' + \frac{h\nu}{\gamma m_e c^2}(1 - \mu_{sc})} \approx \frac{1 - \beta\mu}{1 - \beta\mu'}.$$

Here $\beta = v/c$ is the speed of the scattering electron with Lorentz factor $\gamma = 1/\sqrt{1 - \beta^2}$ in units of the speed of light, c; m_e is the electron mass; h is the Planck constant; μ and μ' are respectively the direction cosines of the incoming and scattered photon with respect to the incoming electron; and μ_{sc} is the corresponding direction cosine between the incoming and scattered photons.

In single-scattering events with electrons at speed drawn from an isotropic velocity distribution there is no net effect, as the gains and losses average out to leading order, leaving a second order term. The average energy gained by a CMB photon in each scattering is determined by $\Delta\nu/\nu = (4/3)\,\beta^2 = 4k_B T_e / m_e c^2$.

This is referred to a Compton y-type distortion, first derived for the case of galaxy clusters by Sunyaev & Zeldovich (1969).

Single IC scattering of CMB photons

The **scattering probability function** P(s;β) from a single electron with velocity β (β = 0.01, 0.02, 0.05, 0.10, 0.20, and 0.50)

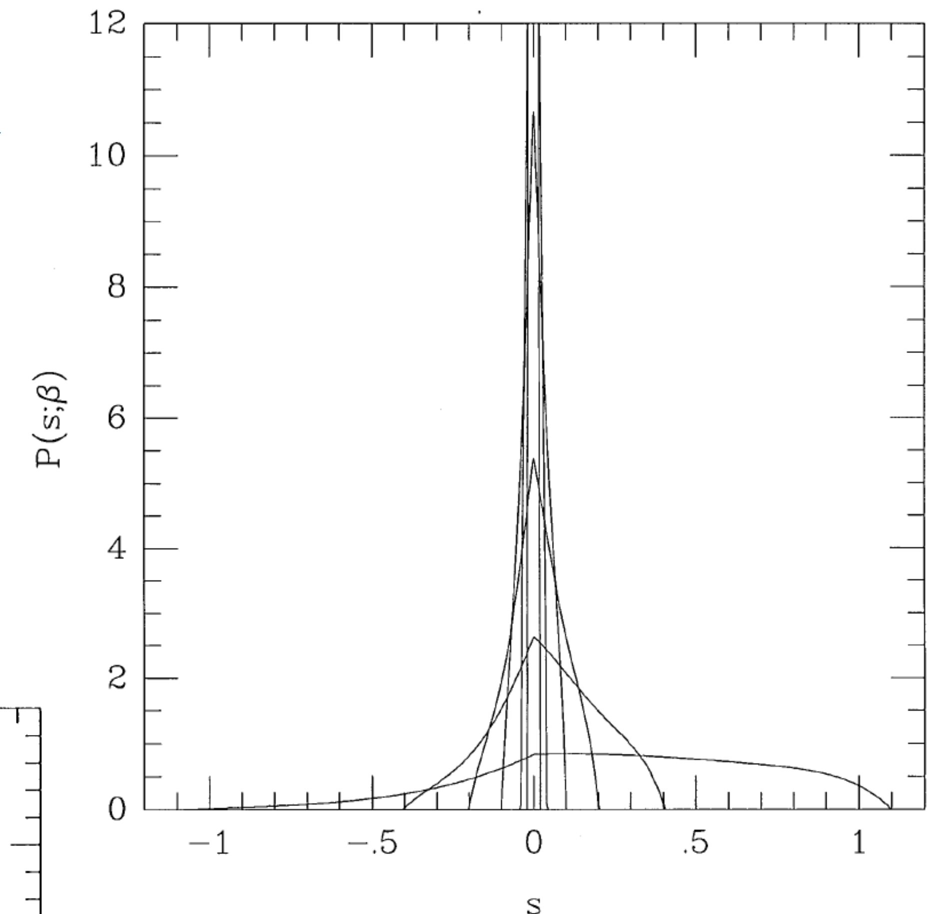

s = logarithmic frequency shift due to scattering

$$s = \log(\nu'/\nu)$$

This function needs to be integrated over the velocity distribution of electrons.

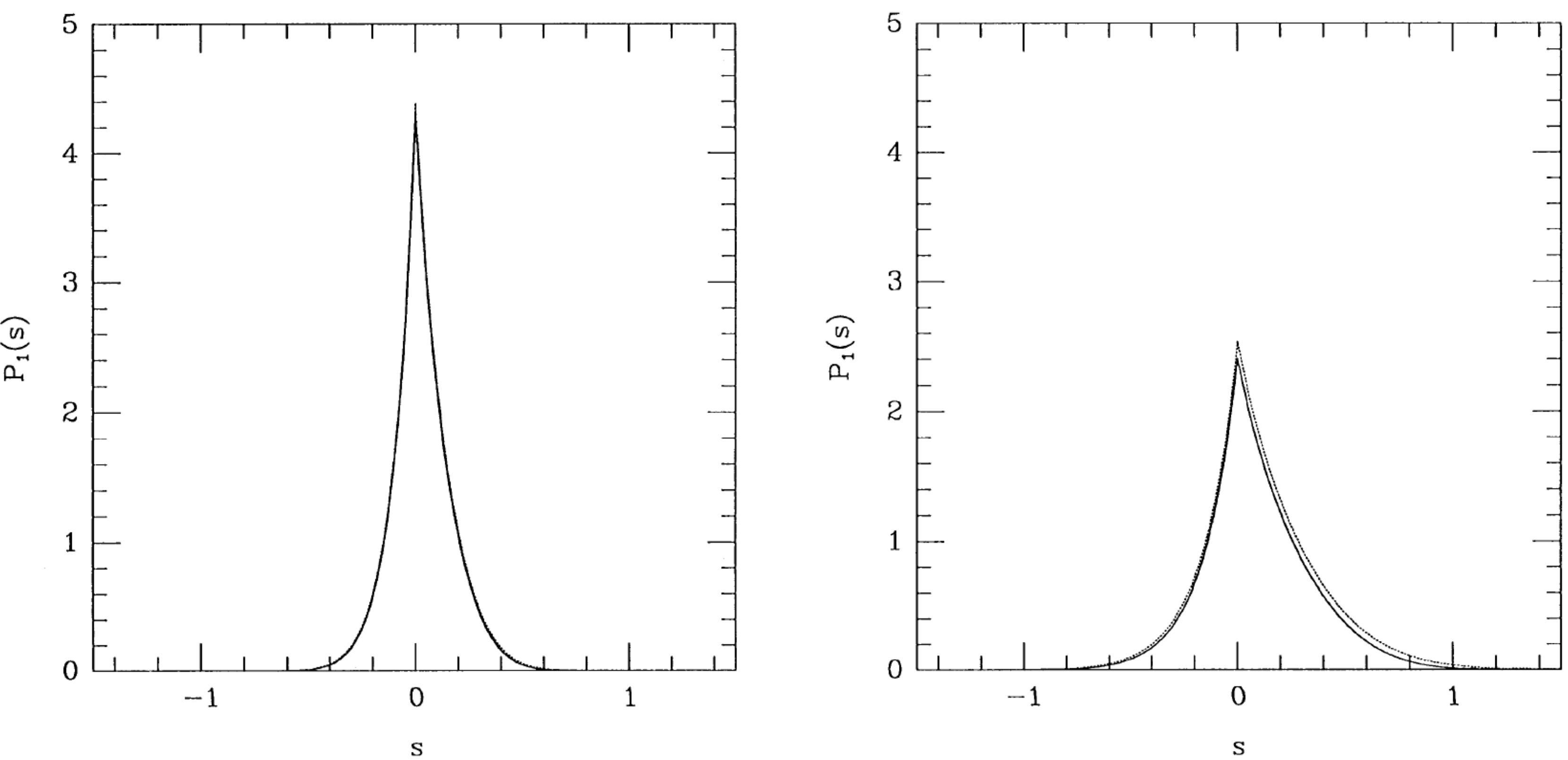

Scattering kernel for **5 keV and 15 keV thermal plasma** (taken from Birkinshaw 1999)

It can be seen that the distribution of scattered photon frequencies is asymmetric, with a stronger upscattering tail than a downscattering tail.

This is the origin of the SZ effect!

Spectrum of the SZ effect

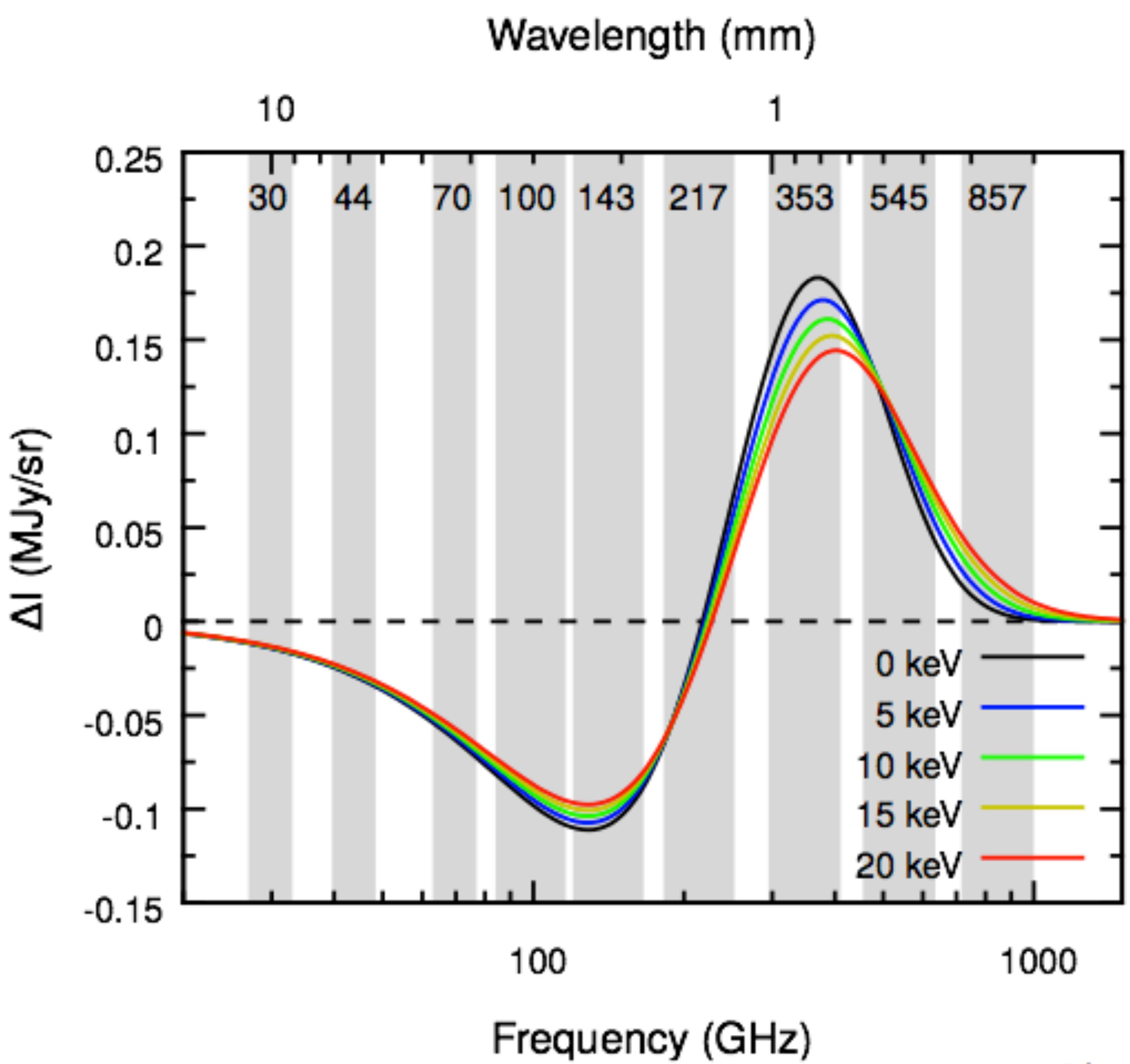

$$\frac{\Delta I_{\rm SZ}}{I_0} = h(x)\left[\underbrace{f(x, T_{\rm e})\, y}_{\rm tSZ} - \underbrace{\tau_{\rm e}\left(\frac{v_{\rm pec}}{c}\right)}_{\rm kSZ}\right]$$

The y-parameter is the line-of-sight integral of pressure:

$$y = \frac{\sigma_{\rm T}}{m_{\rm e}c^2}\int_{\rm l.o.s.} n_{\rm e}k_{\rm B}T_{\rm e}\,{\rm d}l,$$

The following definitions are used:

$$x \equiv h\nu/(k_{\rm B}T_{\rm CMB})$$

$$I_0 = 2(k_{\rm B}T_{\rm CMB})^3/(hc)^2,$$

$$h(x) = x^4\exp(x)/(\exp(x)-1)^2$$

and

$$f(x, T_{\rm e}) = \left(x\frac{\exp(x)+1}{\exp(x)-1} - 4\right)(1+\delta_{\rm SZE}(x, T_{\rm e}))$$

Magnitude of the SZ effect

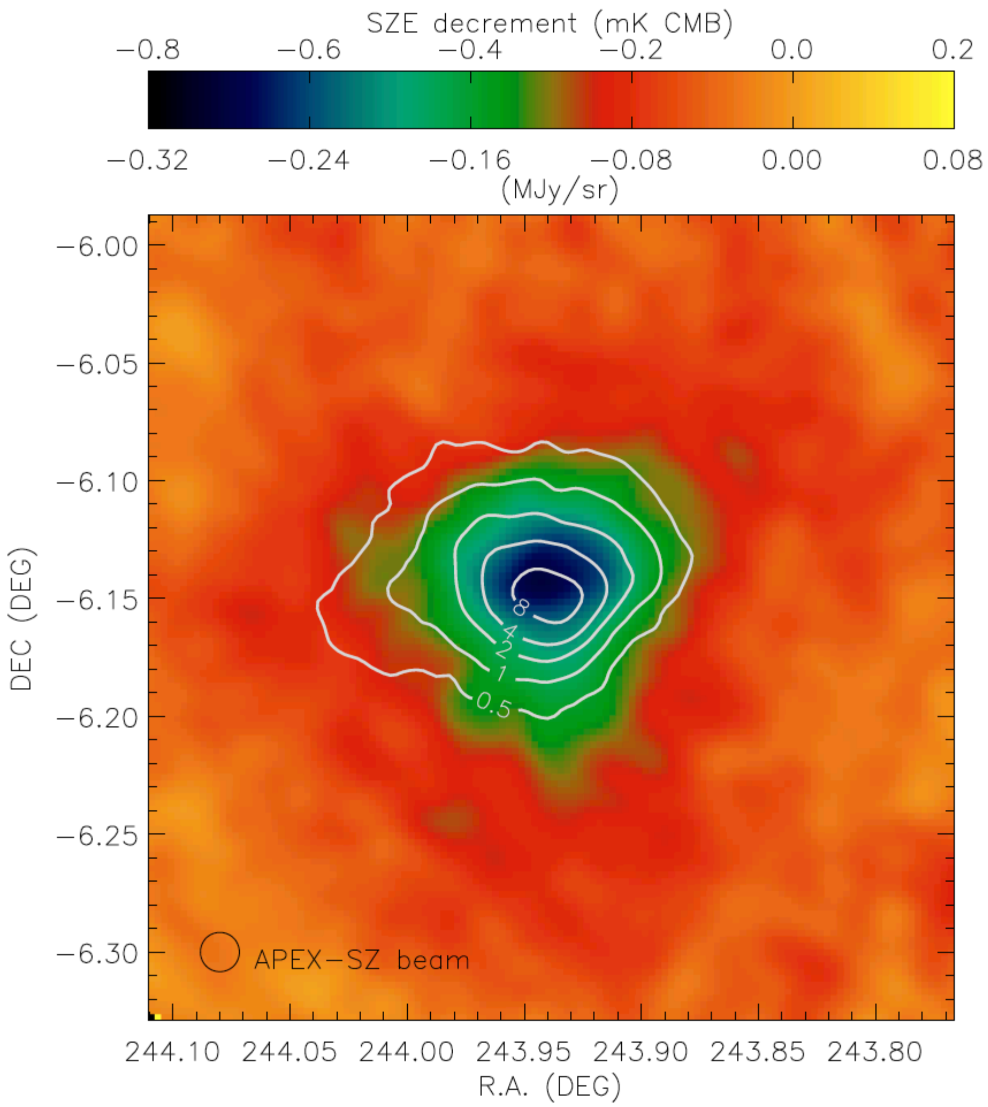

Actual SZ measurement (APEX-SZ 150 GHz) for the galaxy cluster Abell 2163

In this example, $y_0 = 3.4x10^{-4}$

$y<<1 \ \Rightarrow \ \Delta I/I_{CMB} = g(\nu)\ y <<1$

$g(\nu)$ is the frequency spectrum

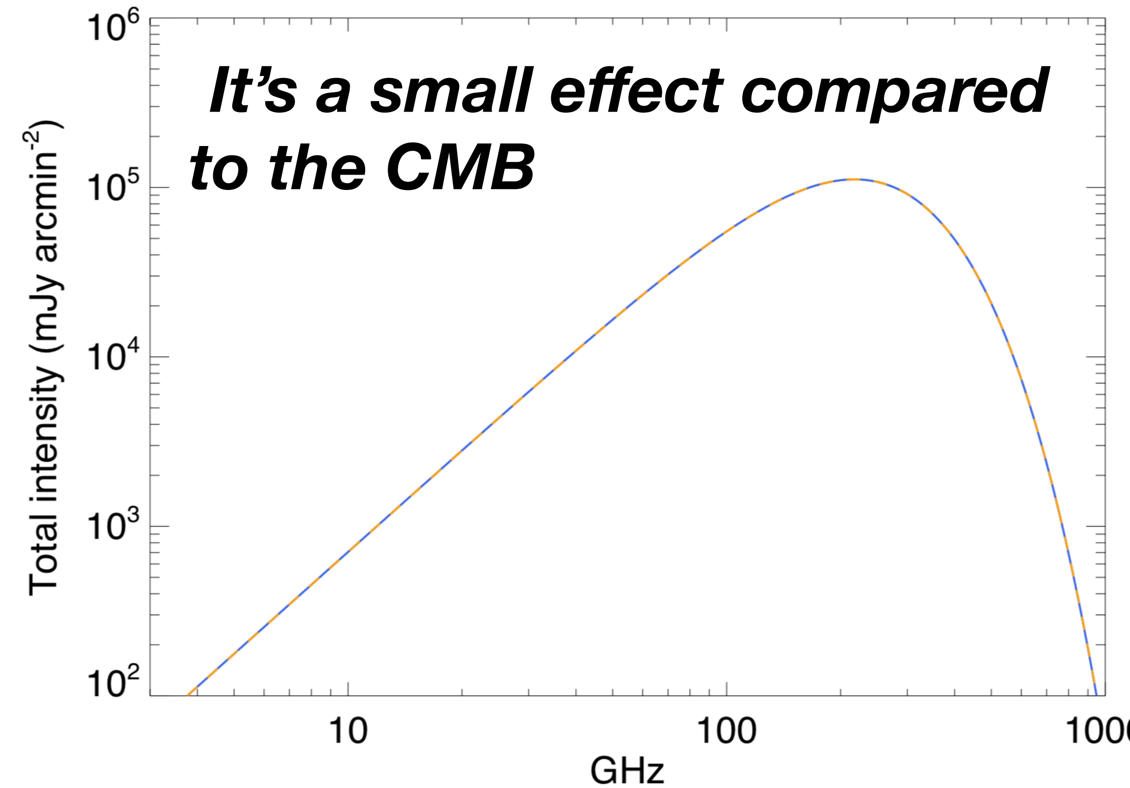

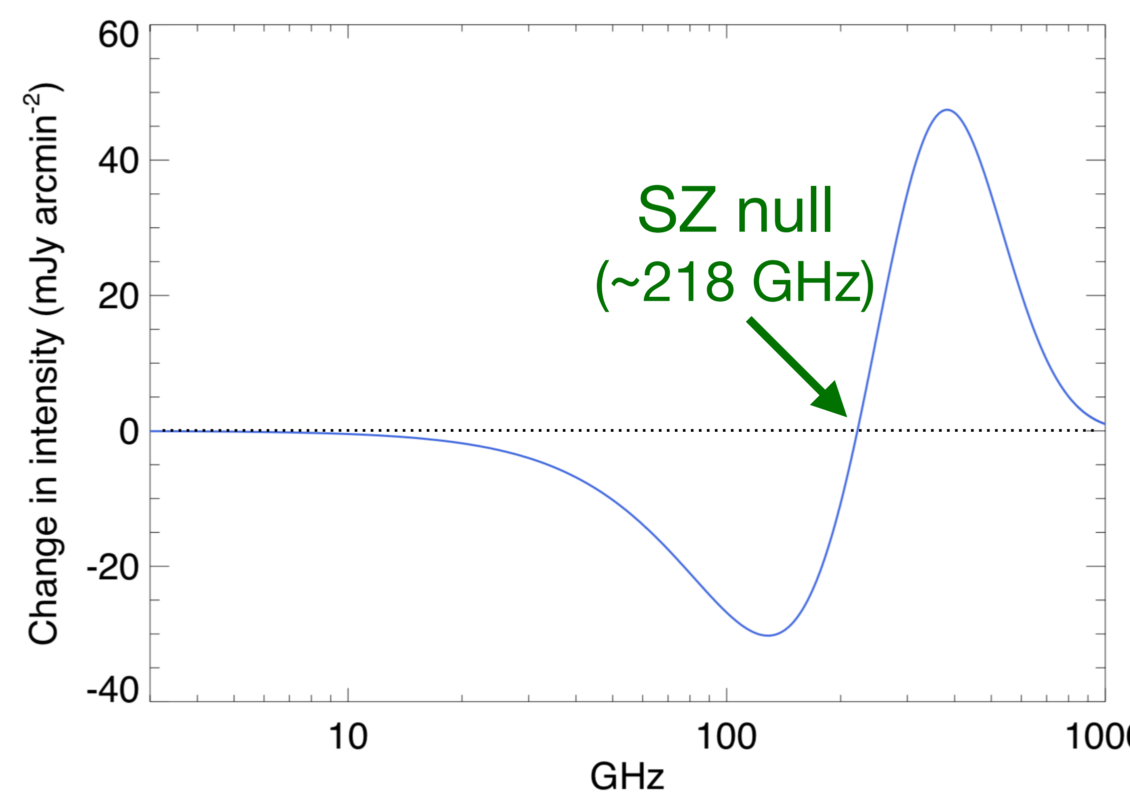

K. Basu: CMB theory and experiments

tSZ spectral distortion: the rSZ effect

For very high energy electrons, the Komaneets approximation breaks down (scattering can no longer be considered elastic). This is often the case for hot galaxy clusters, where average temperature can exceed 10 keV, so there are enough relativistic ($\gamma \gtrsim 100$) electrons in the thermal tail (sometimes called the Maxwell-Jüttner distribution).

This spectral departure from the classical non-relativistic calculation is termed as the **relativistic SZ, or rSZ, effect**. Just like measuring the X-ray Bremsstrahlung spectrum in the high-energy part, this is an effective tool to measure cluster temperatures directly.

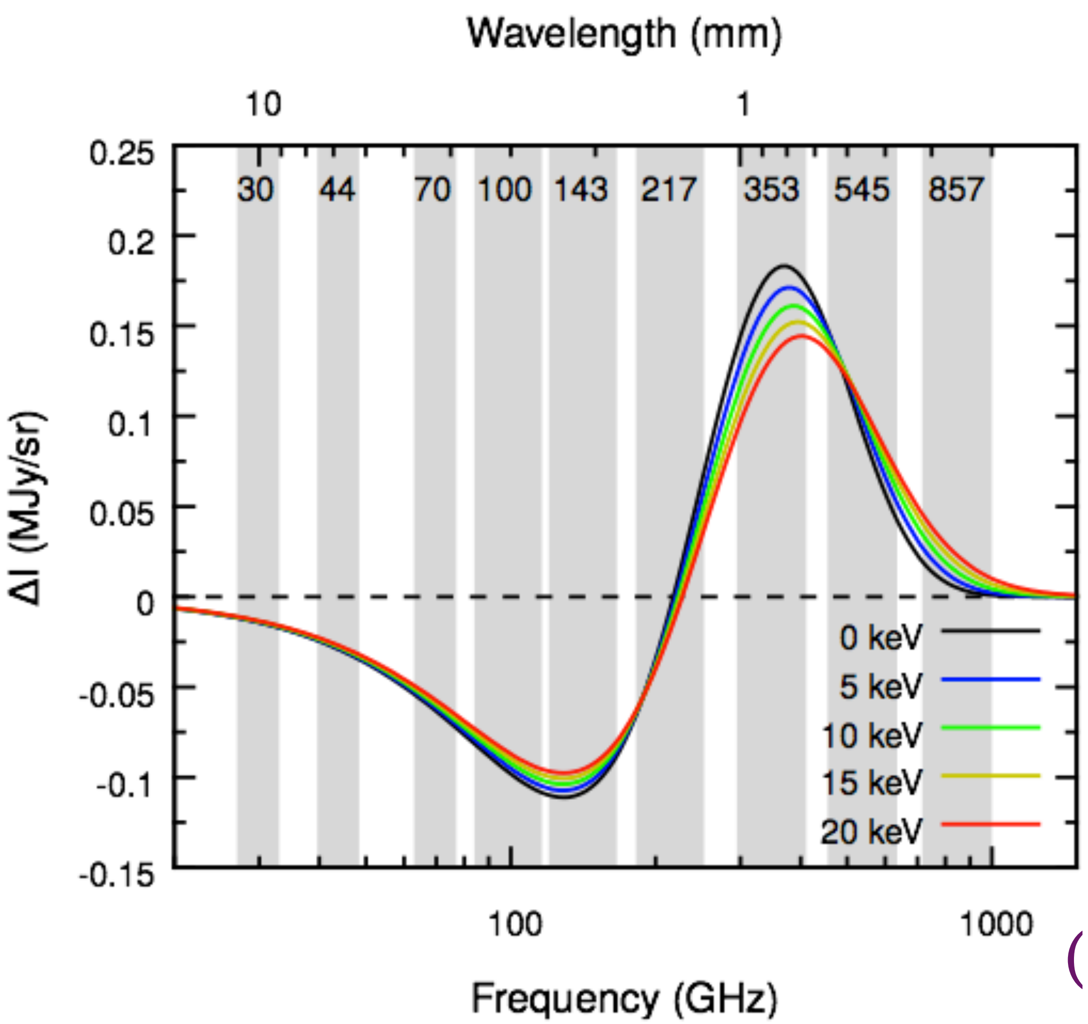

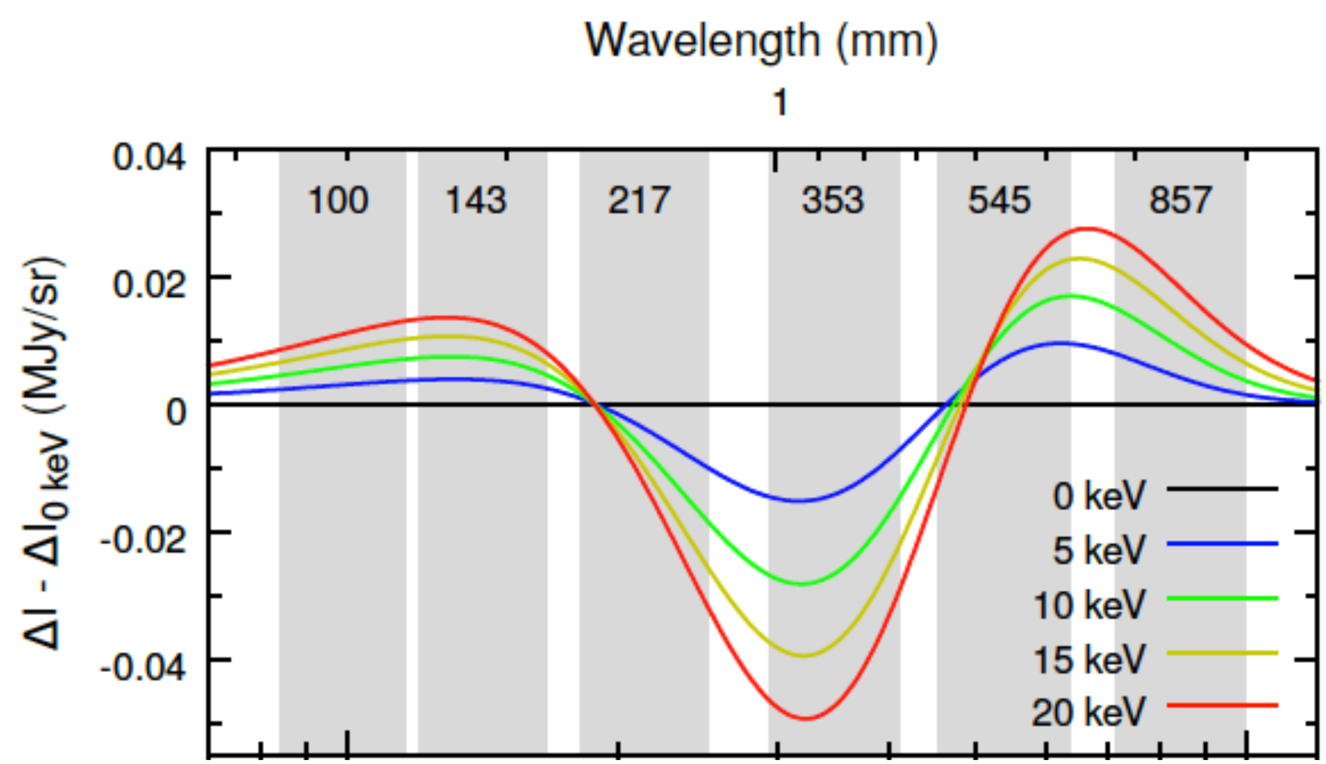

(difference from 0 keV)

The five different SZ effects

tSZ

kSZ

rSZ

pSZ

ntSZ

The thermal SZ (tSZ) effect is the main effect, caused by inverse Compton scattering from the hot electrons in the intracluster plasma. For a typical massive cluster, its amplitude can be ~few 100 μK_{CMB}.

The second most important is the kinematic SZ (kSZ) effect, which arises if there is a strong bulk motion of the scattering gas along the line of sight. This gives a Doppler boost (or decrease) to the CMB temperature without changing its spectrum. Since typical velocities are ~100 km/s, the kSZ signal is roughly 10 times smaller than the tSZ, of the order 10 μK_{CMB}.

When the electron temperature is high ($\gtrsim$5 keV), then the higher-order relativistic corrections to both the tSZ and kSZ spectra can be noticeable. Generally, one refers to the relativistic correction to the tSZ effect, calling it relativistic SZ (rSZ) effect. Typical signal ~1 μK_{CMB}, depending strongly on the frequency.

There can be also scattering from electron populations other than thermal, most notably, power-law energy distributions (e.g. created by shock acceleration). This is the same effect that creates inverse Compton emission at hard X-ray band. It has a different spectrum than the tSZ, hence is called nonthermal SZ (ntSZ) effect. Depending upon the energy density, signal is ~0.01–0.1 μK_{CMB}.

Lastly, SZ effect can be polarized. The two main contributors are (a) scattering of the intrinsic CMB quadrupole, and (b) a quadrupole generated by the clusters own motion. This is labelled polarized SZ (pSZ) effect. Signal is ~0.001 μK_{CMB}.

Kinematic SZ effect

Caused by Doppler shift of photon energy. In the electron's rest frame there is a CMB dipole, which the IC scattering partially isotropize. Then, transferred to the observer's frame, there is a net anisotropic signal.

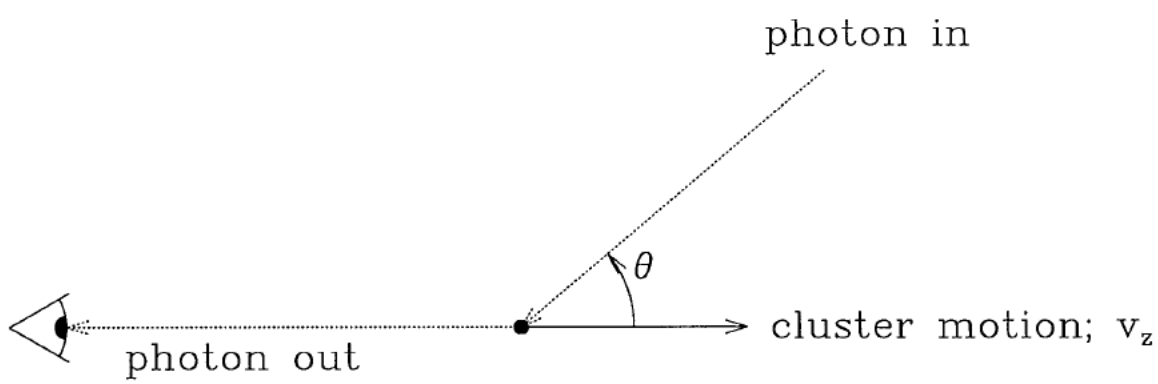

The signal is simply proportional to the line-of-sight velocity of the clusters multiplied by its optical depth

$$\frac{\Delta T}{T} = -\frac{v_r}{c}\tau \equiv -\frac{v_r}{c}\int \sigma_T n dl$$

Note that kSZ can be either positive or negative!

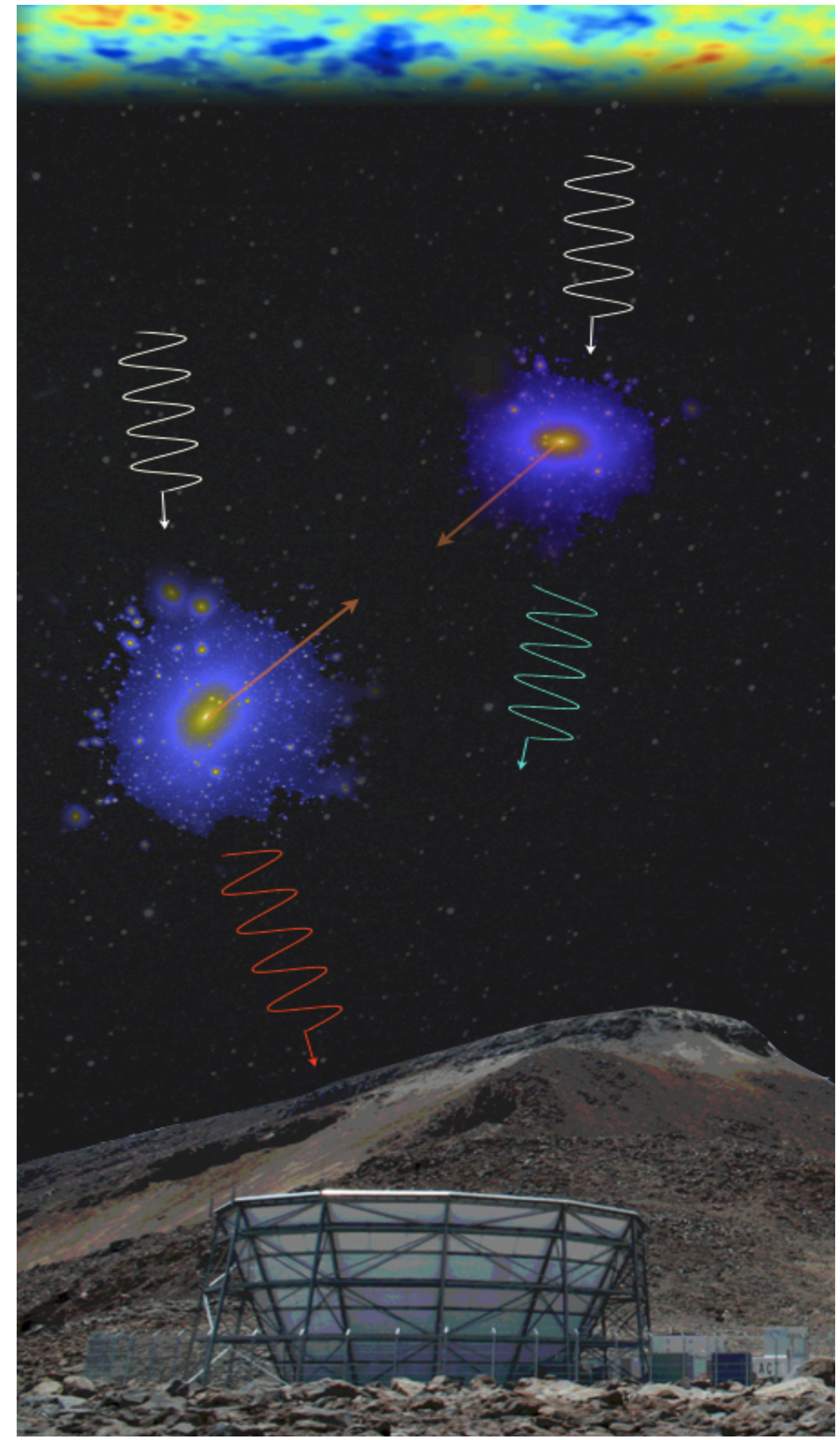

Credit: Hand et al. ACT collaboration

Kinematic SZ effect

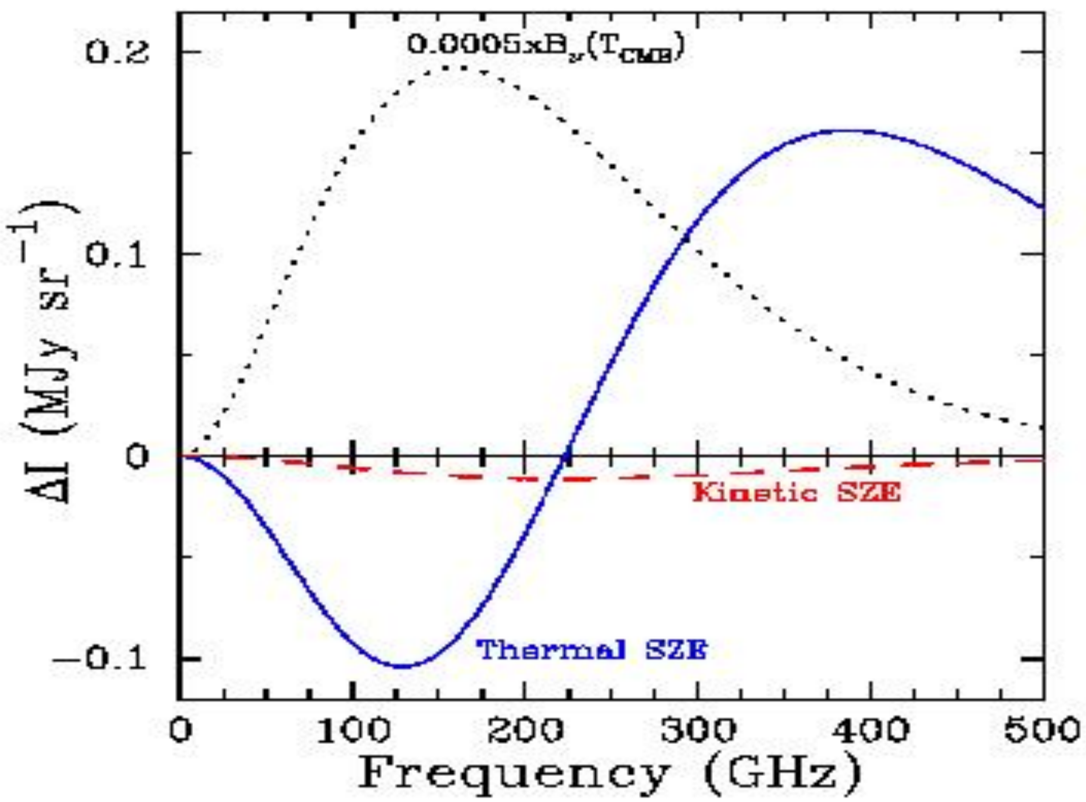

Note that a kSZ signal is indistinuishable from a CMB hot or cold spot.

$$\frac{\Delta J_\nu}{B_\nu} = \frac{\mathrm{d}\ \ln B_\nu}{\mathrm{d}\ \ln T}\left(\frac{\Delta T}{T}\right) = \frac{x e^x}{e^x - 1}\left(\frac{\Delta T}{T}\right)$$

This is because we are not considering any energy distribution of the electrons, but rather the case when *all* electrons have the same bulk kinetic energy.

Here is the *first measurement* of the kSZ effect from internal gas motions in a cluster (MACS J0717.5; Mroczkowski et al. 2012, Adam et al. 2017)

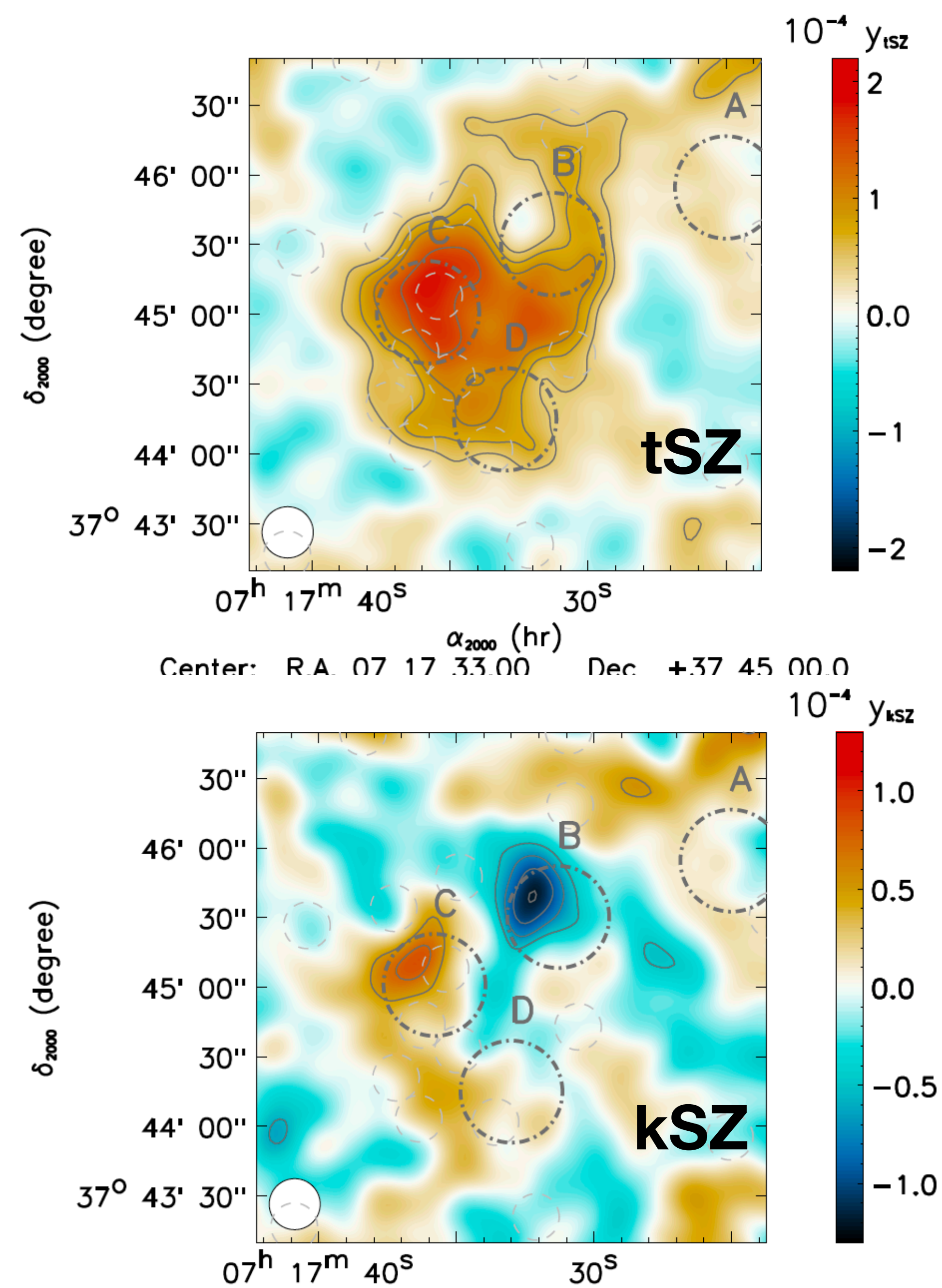

kSZ effect for cosmology

kSZ effect is one of the most promising tool to map the cosmic velocity field in the linear regime. This has huge potential for cosmology, since the amplitude of the velocity field is directly proportional to the growth rate of structure and the matter density.

$$\boxed{\vec{v}(\vec{k}) = i\,\frac{d\ln D}{d\ln a}\,\frac{aH\,\delta(\vec{k})\vec{k}}{k^2}}$$

Predictions for the CCAT-prime telescope cosmology survey

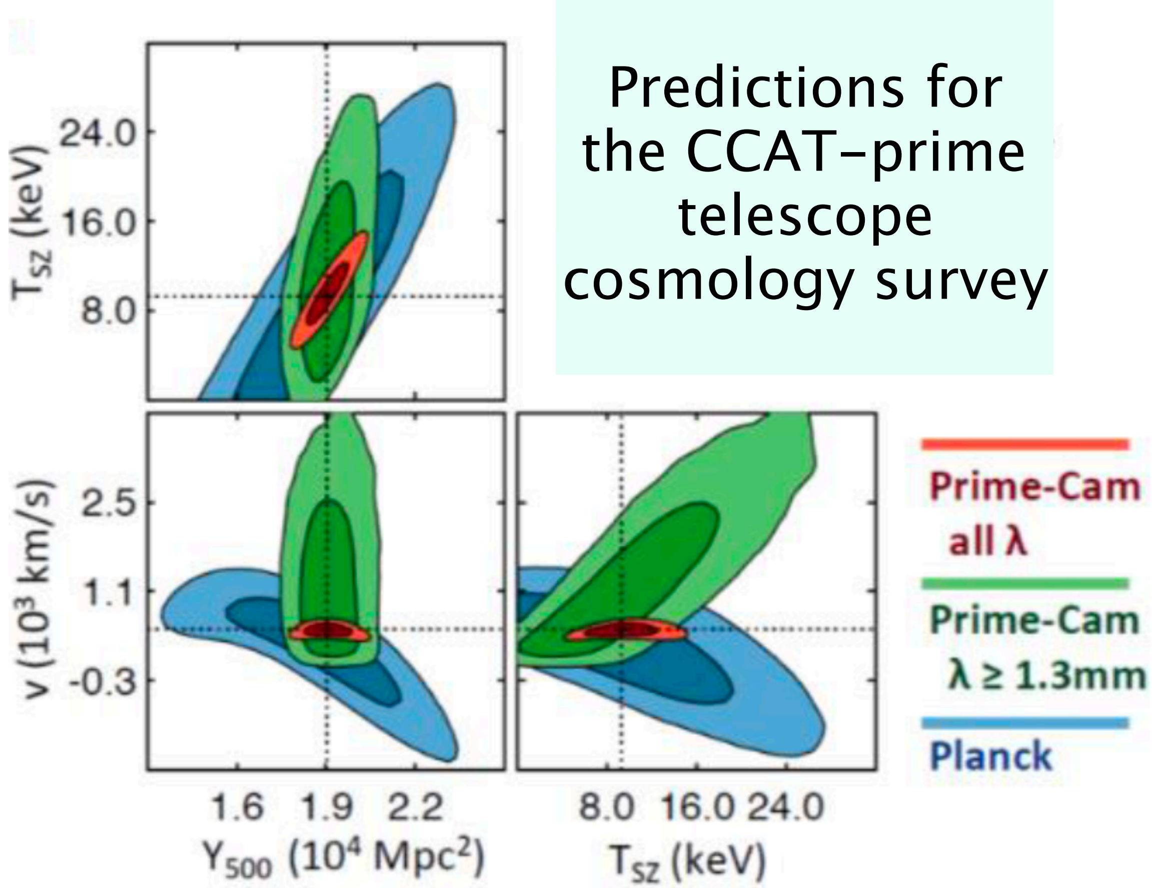

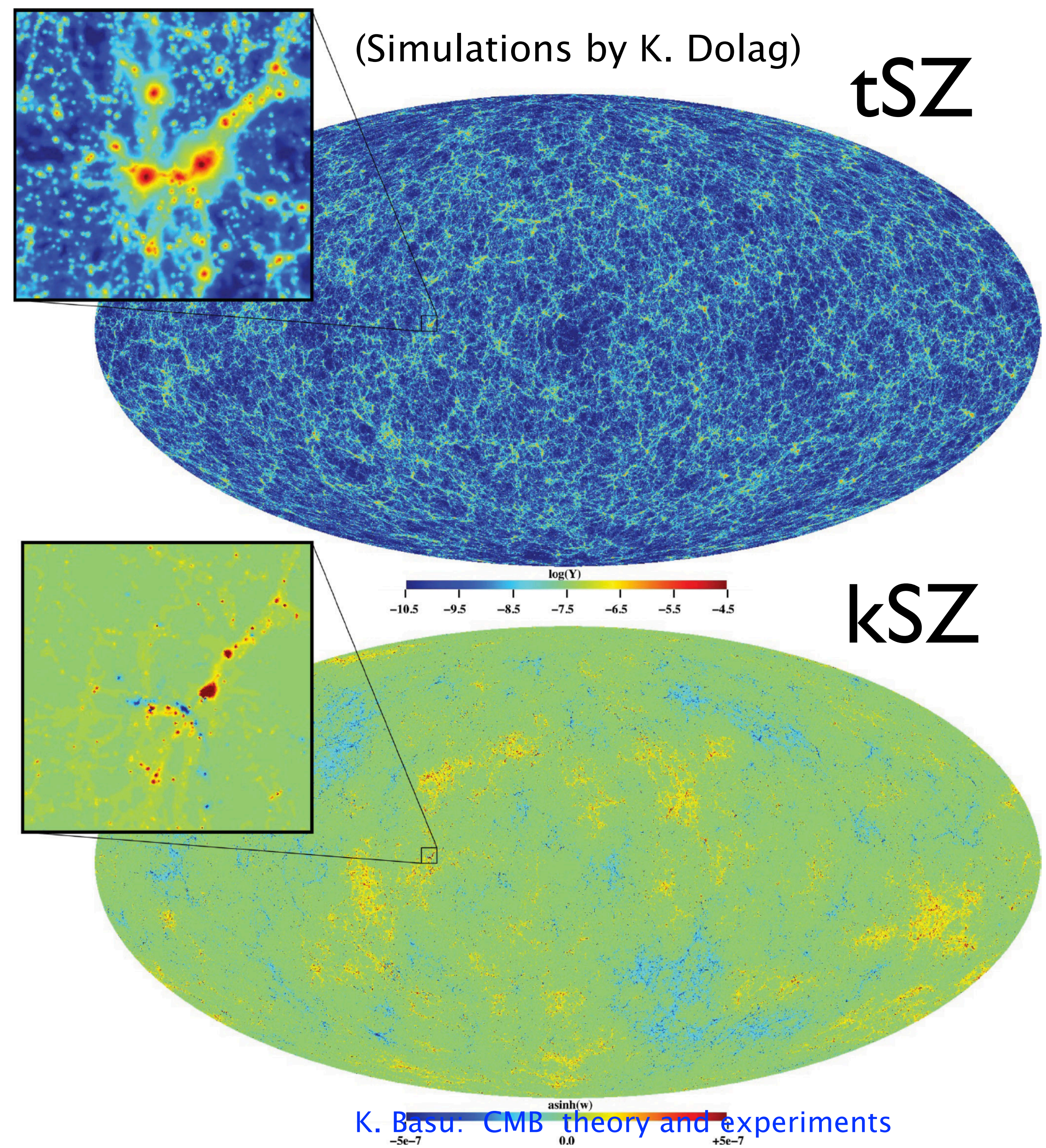

Non-thermal SZ effect

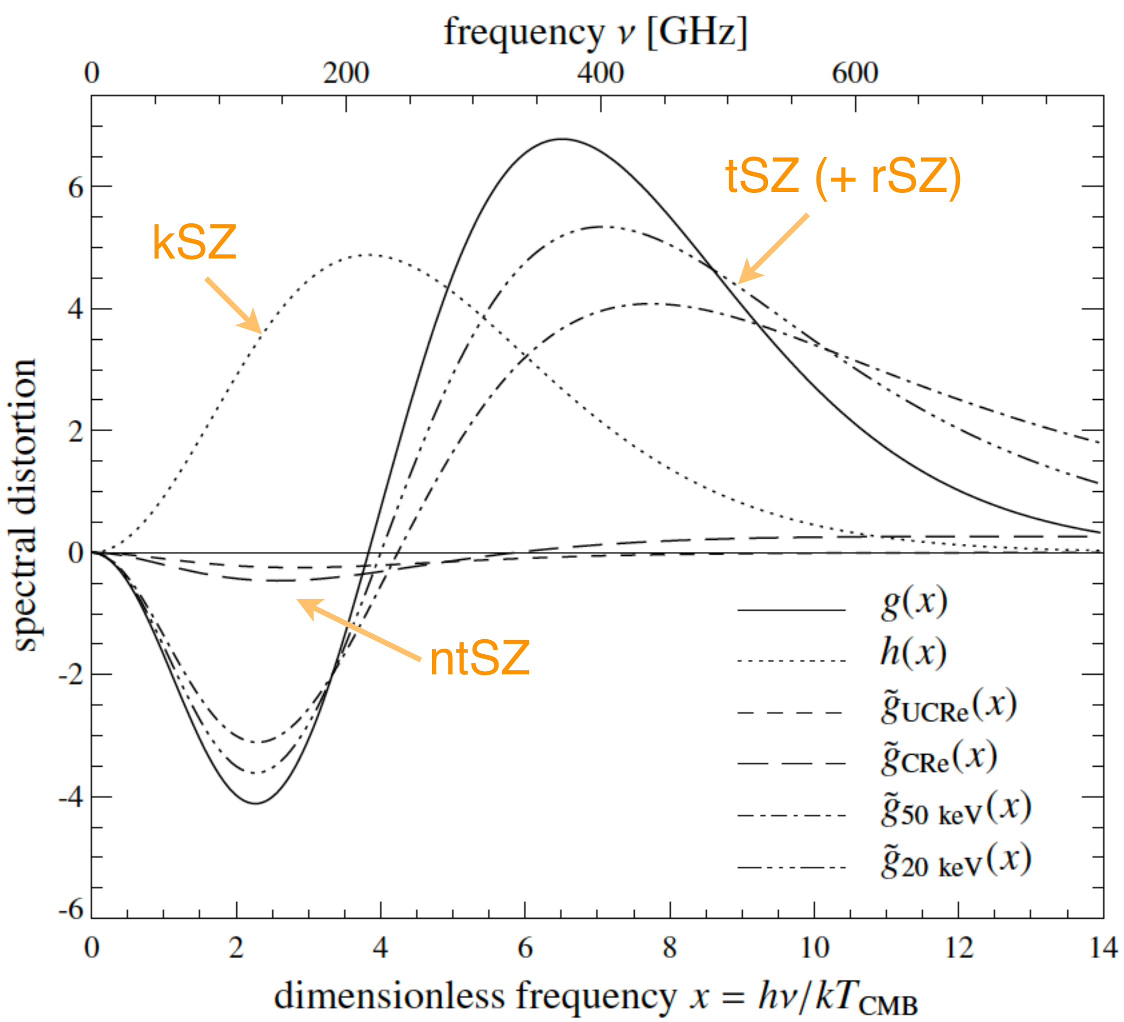

Pfrommer et al. (2005)

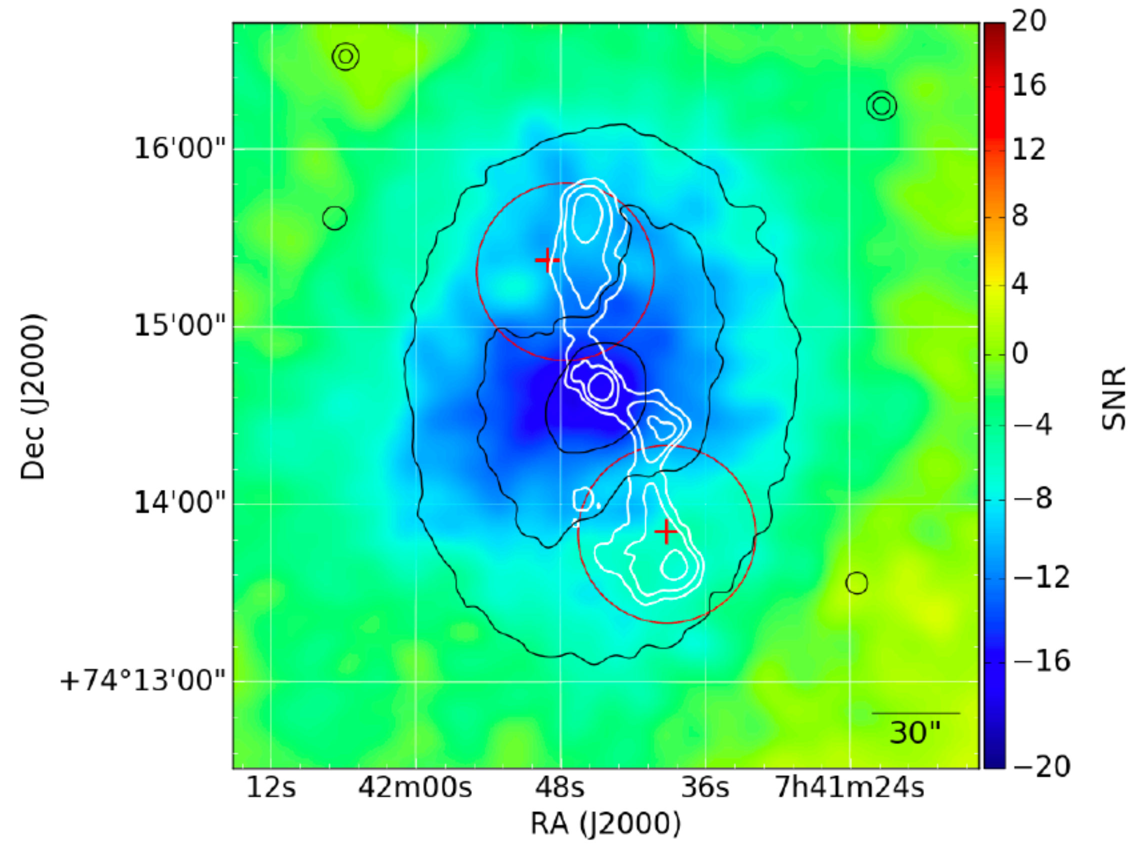

Abdulla et al. (2018)

arXiv:1806.05050

tSZ

kSZ

rSZ

pSZ

ntSZ

Non-thermal SZ is the spectral distortion from ultra-high energy electrons with power-law energy distribution (i.e. cosmic ray electrons) or any other non-Maxwellian distribution.

A very recent observation has provided strong evidence for this signal inside AGN bubbles on galaxy clusters.

Non-thermal SZ effect — in the X-ray!

This is the same effect that causes the Inverse Compton (IC) emission in the hard X-ray band. There we are observing the effect from the very high-energy tail of the power-law electrons, typically at 10-100 keV (10^{18}—10^{20} Hz).

X-ray IC emission from radio AGN lobes are now routinely detected.
ntSZ is yet undetected.

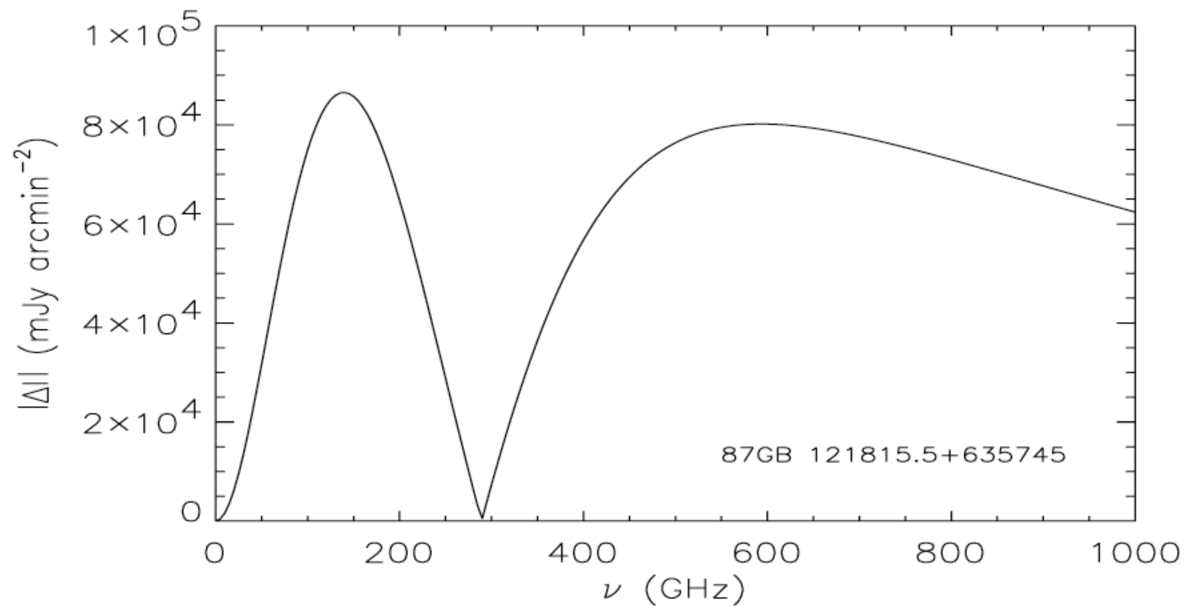

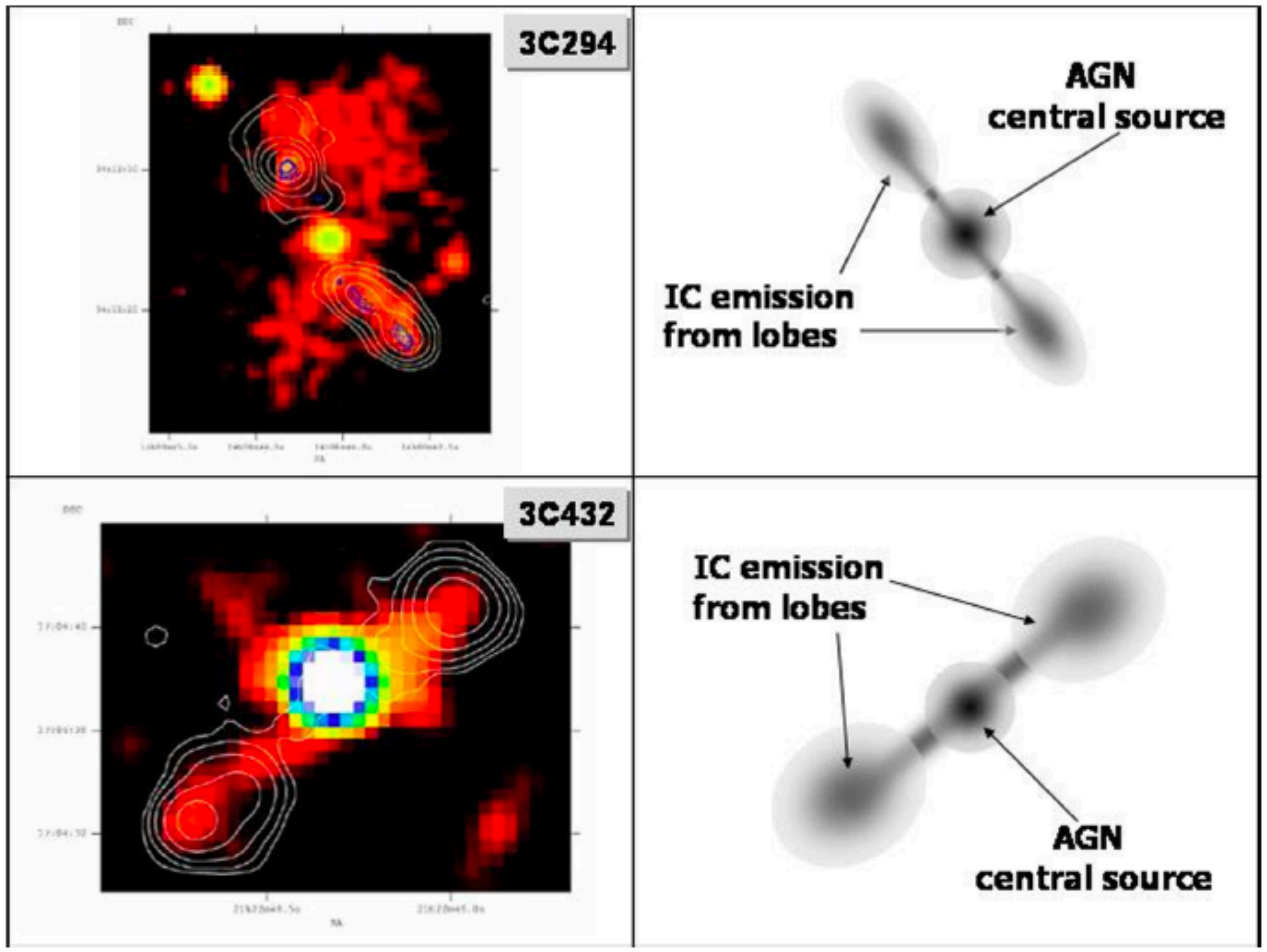

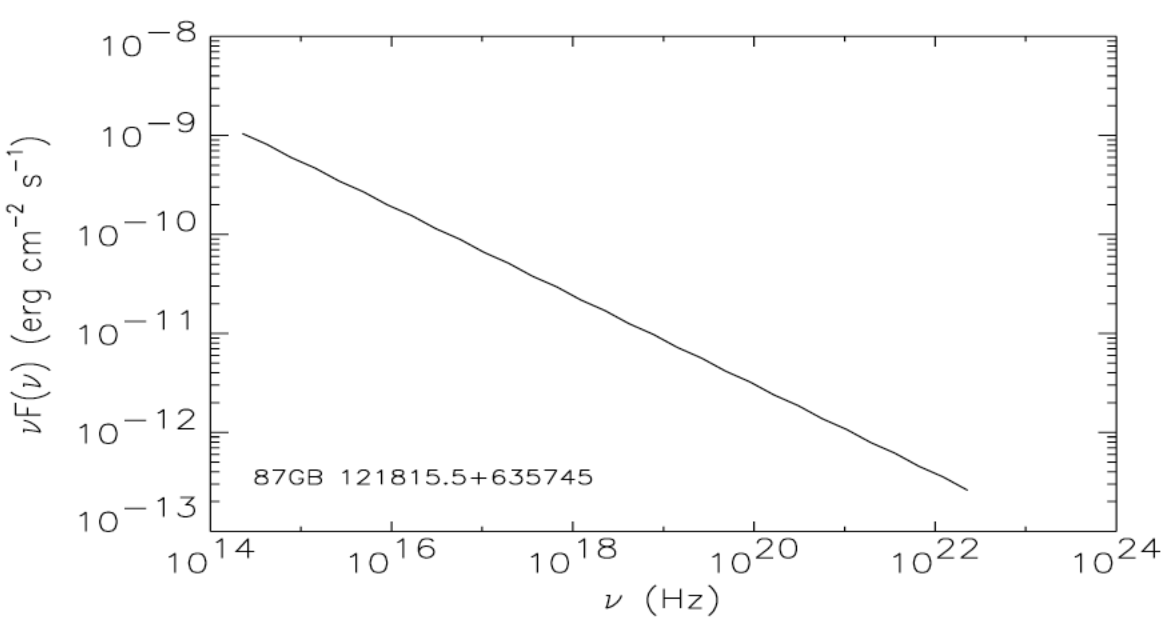

Thermal SZ effect summary

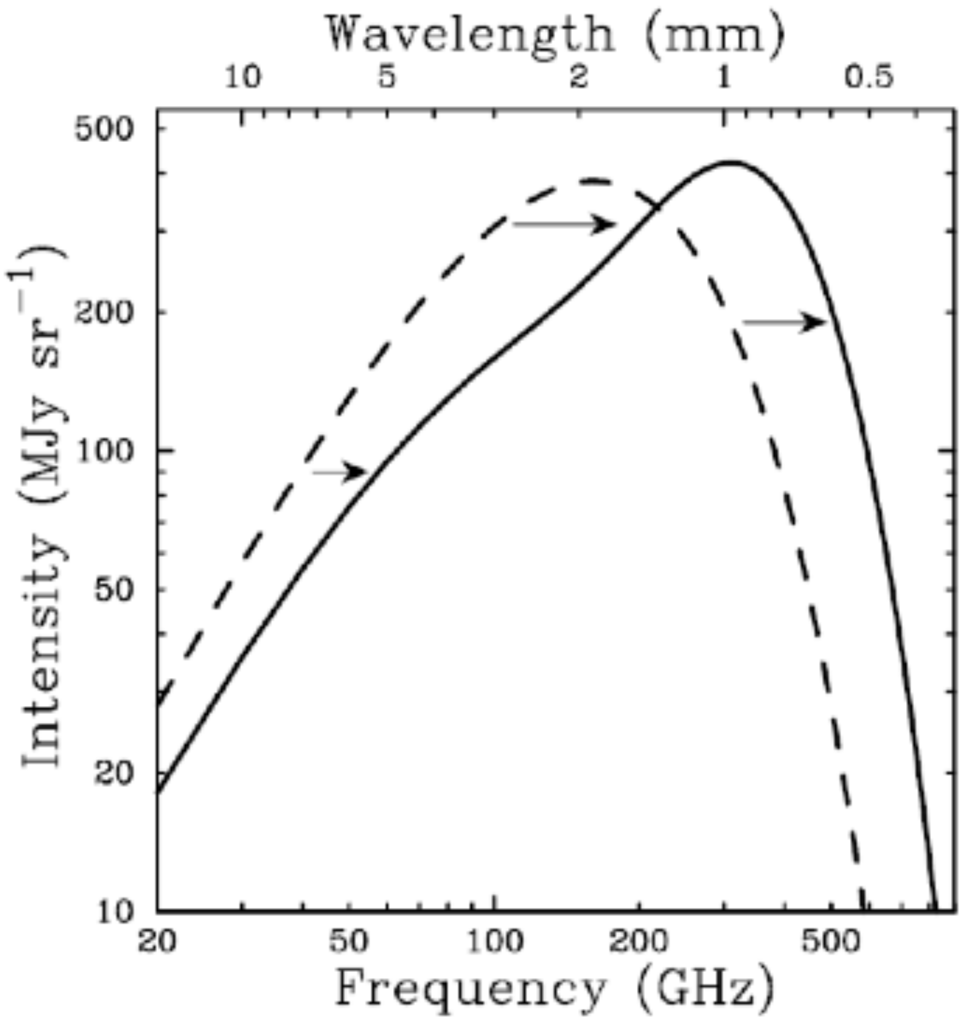

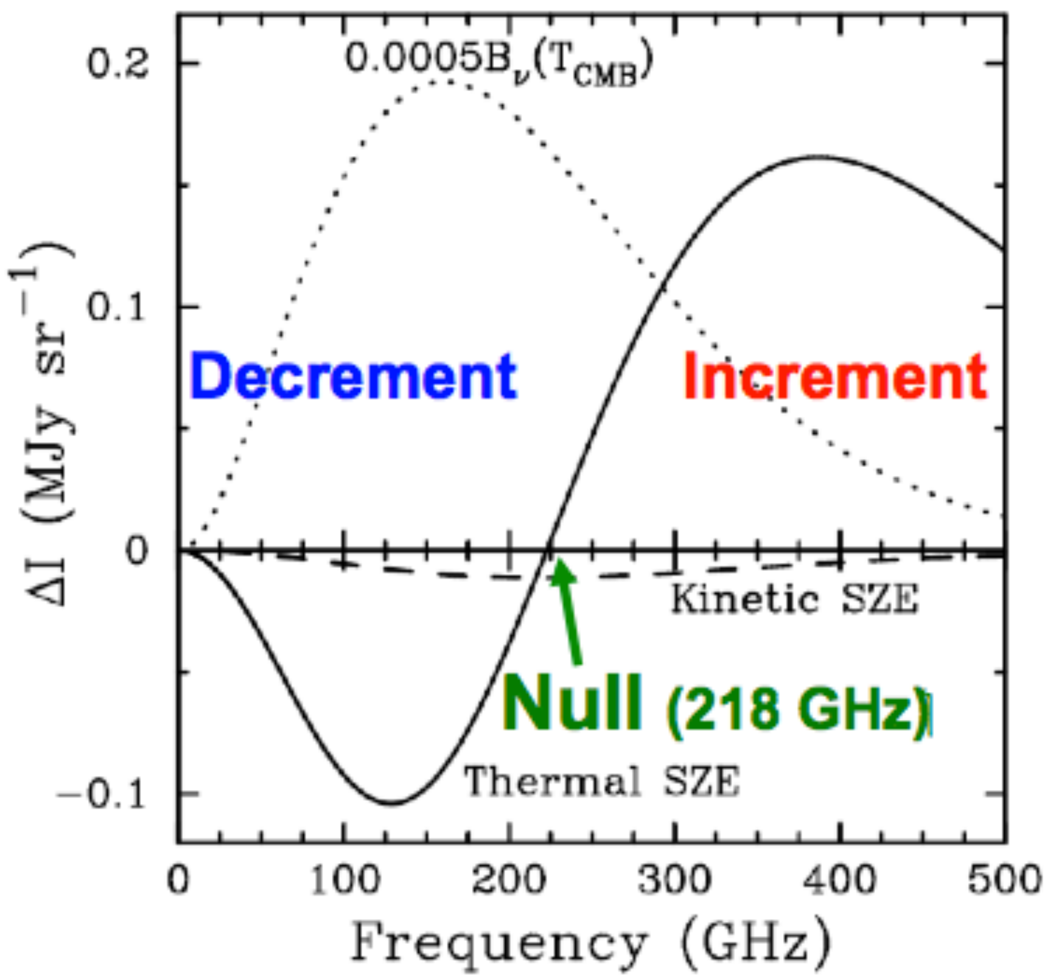

$$y \equiv \int \frac{k_B T_e}{m_e c^2} d\tau_e = \int \frac{k_B T_e}{m_e c^2} n_e \sigma_T dl = \frac{\sigma_T}{m_e c^2} \int P_e \, dl.$$

$$\Delta I_\nu \approx I_0 \, y \frac{x^4 e^x}{(e^x - 1)^2} \left(x \frac{e^x + 1}{e^x - 1} - 4 \right) \equiv I_0 \, y \, g(x) \qquad \frac{\Delta T_{\mathrm{CMB}}}{T_{\mathrm{CMB}}} \approx y \left(x \frac{e^x + 1}{e^x - 1} - 4 \right) = y \, f(x).$$

Kinematic SZ effect summary

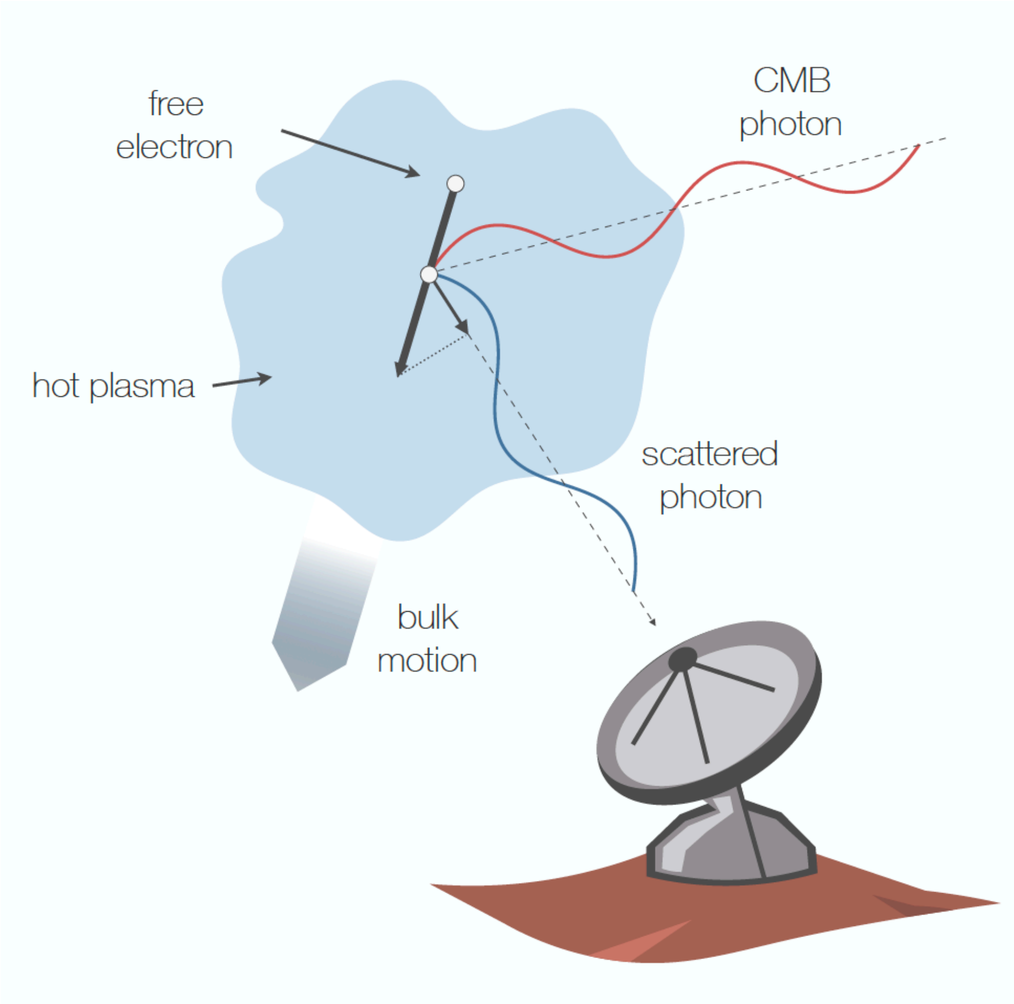

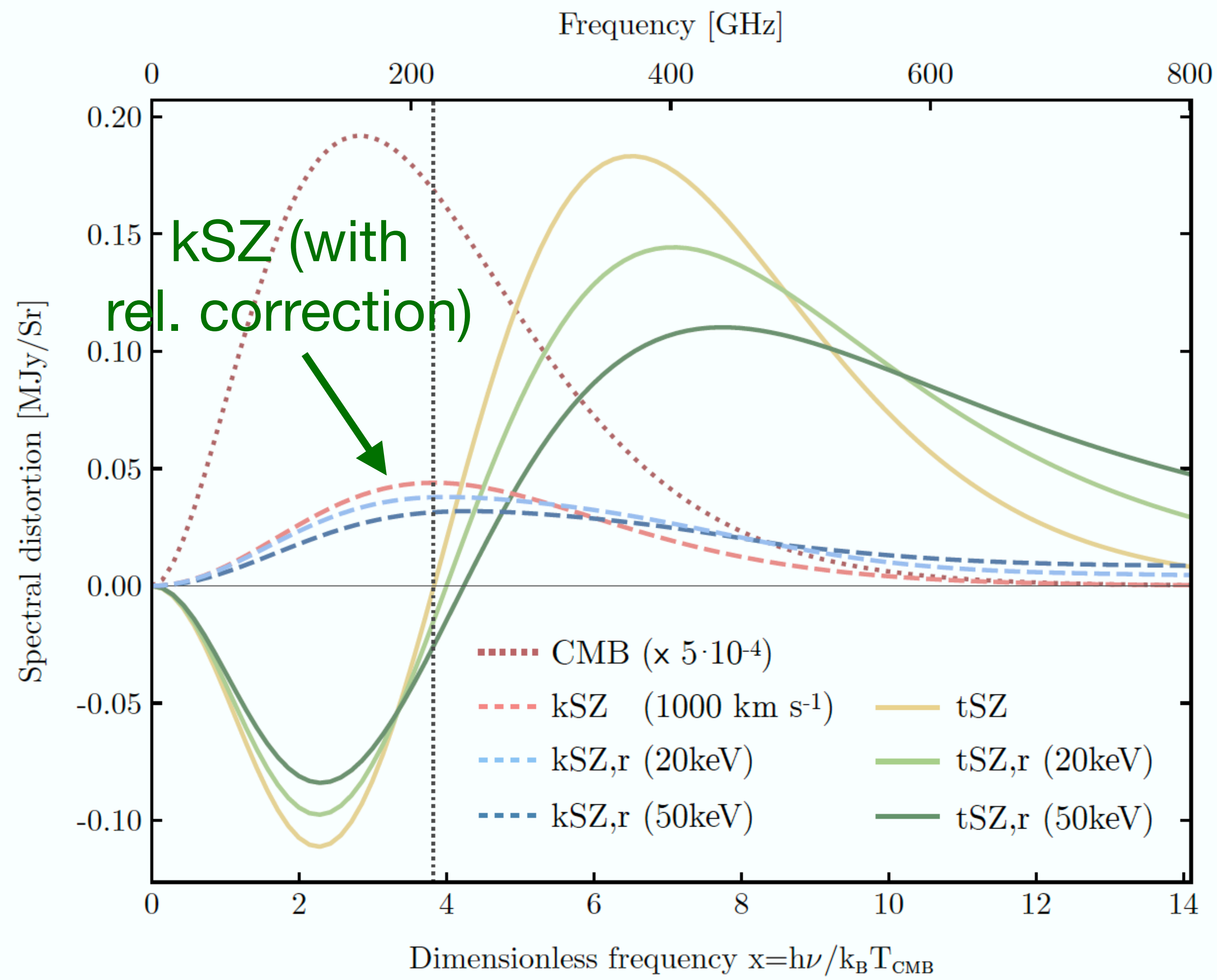

$$\frac{\Delta T_{\rm CMB}}{T_{\rm CMB}} \approx -\int \sigma_{\rm T} n_{\rm e}\, \boldsymbol{n}\cdot\boldsymbol{\beta}_{\rm p}\, {\rm d}l = -\int \boldsymbol{n}\cdot\boldsymbol{\beta}_{\rm p}\, {\rm d}\tau_{\rm e} \equiv -y_{\rm kSZ}$$

$$\Delta I_\nu \approx -I_0 \frac{x^4 e^x}{(e^x-1)^2}\, y_{\rm kSZ}$$

$\boldsymbol{n}\cdot\boldsymbol{\beta}_{\rm p}$ is the component of peculiar velocity along the line of sight

Redshift-independence of the SZ effect

Sine the SZ effect is a scattering of the background CMB photons, the effect of the cosmic expansion is the same on both the scattered and un-scattered photons. In other words, the signal is independent of redshift!

Hence if you can resolve the cluster, the total flux density within the telescope beam remains constant no matter the distance of the cluster, provided the intrinsic property of the cluster remains the same.

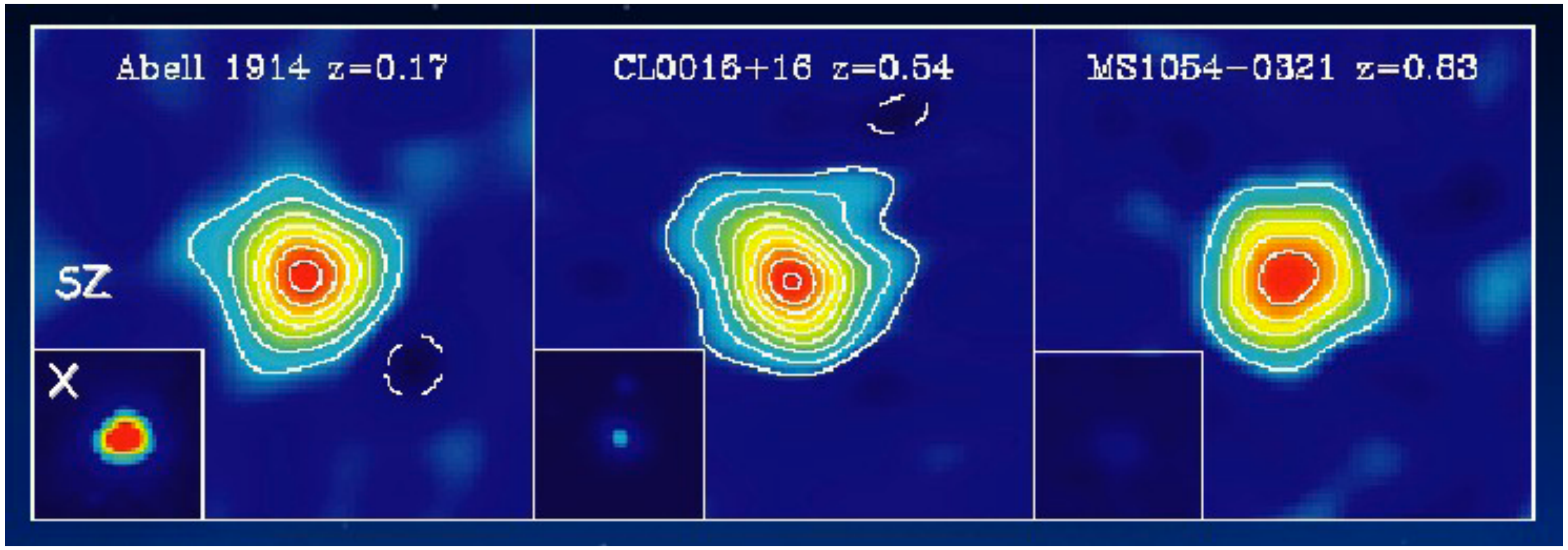

$$\Delta S_\nu = \int \Delta I_\nu \, d\Omega \propto \frac{\int n_e T_e \, dV}{D_A^2} \propto \frac{f_{\rm gas} M_{\rm tot} T_e}{D_A^2}$$

“Beam dilution” of the SZ effect

However, if the instrument beam is larger than the cluster, then the flux generated by the SZ effect gets weaker as the cluster is more distant and hence smaller in angular diameter (think of a surface with uniform brightness getting smaller). This causes a redshift-dependent selection for some SZ experiments, like Planck (upper figure on right).

For Ground-based experiments with ~1 arcmin beam size, like SPT, this is not a problem, since clusters above 2x10^{14} M$_\odot$ do not get any smaller! In fact, the mass threshold goes down slightly, as the clusters get denser and hotter at high-z.

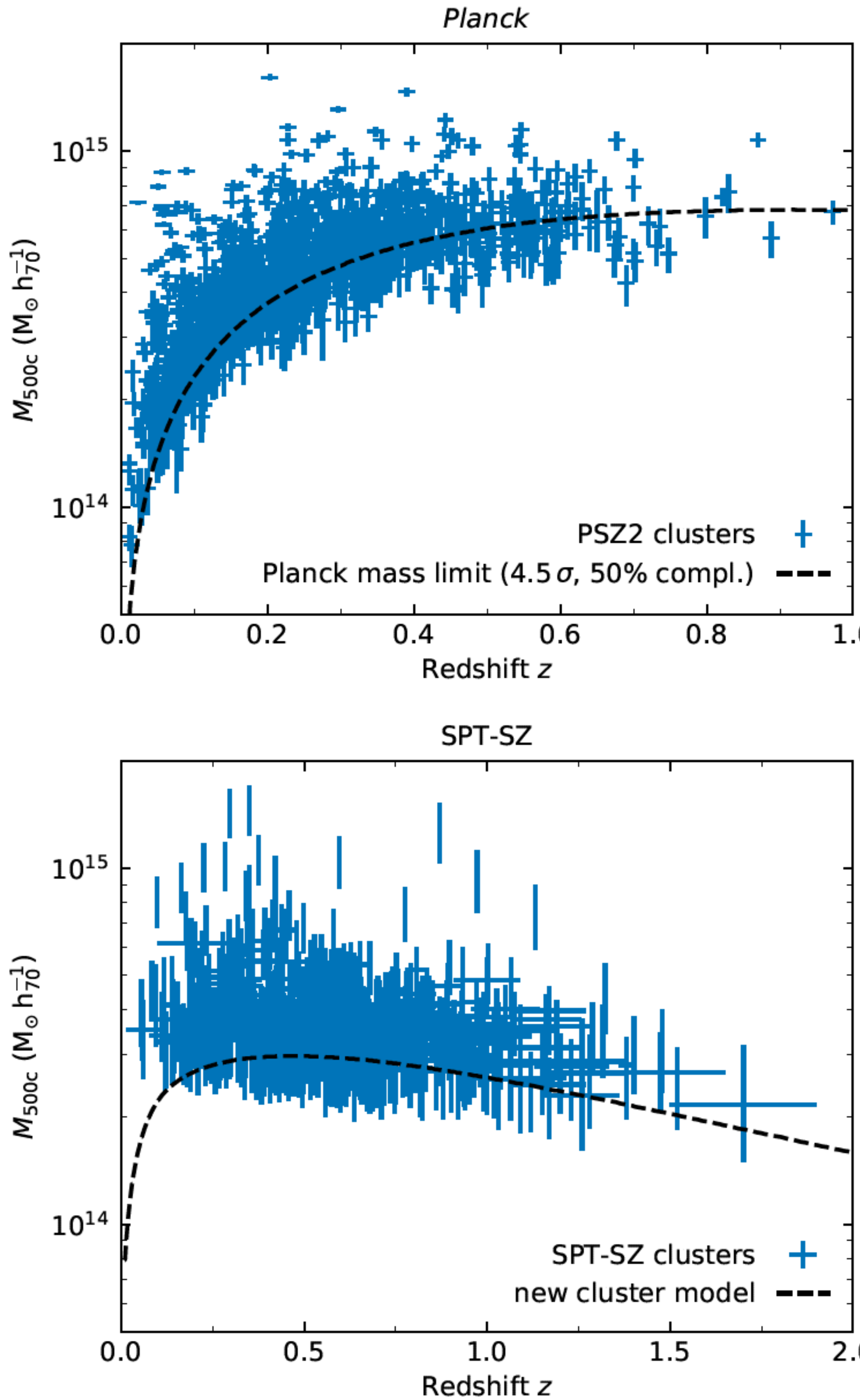

The first four SZE discovered galaxy clusters

unfiltered map (with CMB)

filtered detection maps

null maps

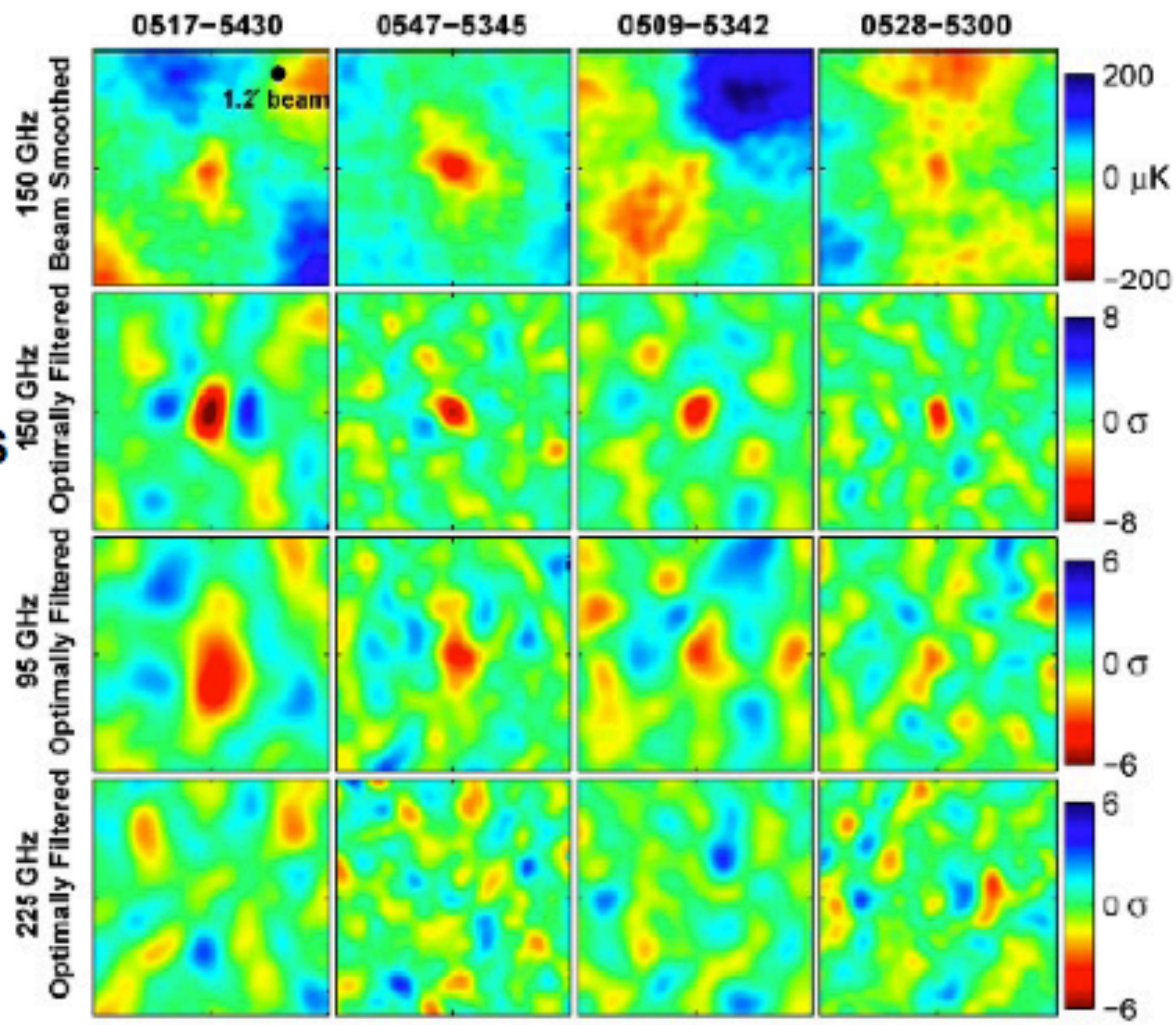

20'x20' field-of-view

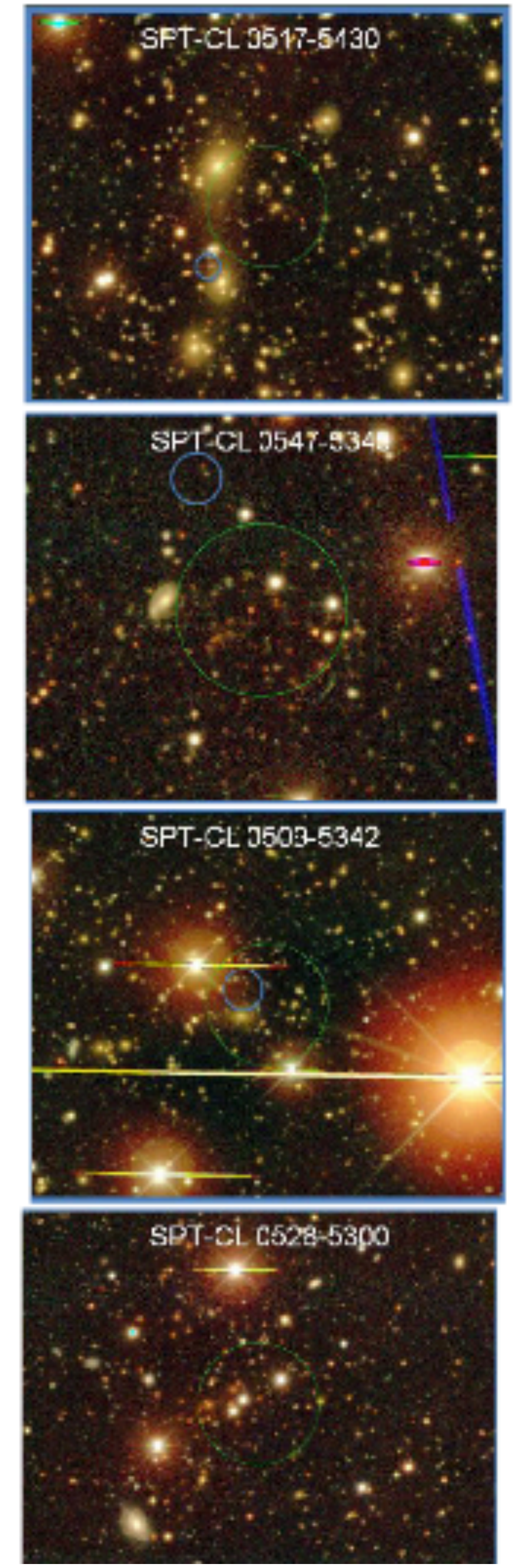

Source: Staniszewski et al. 2009

In six years (SPT alone)

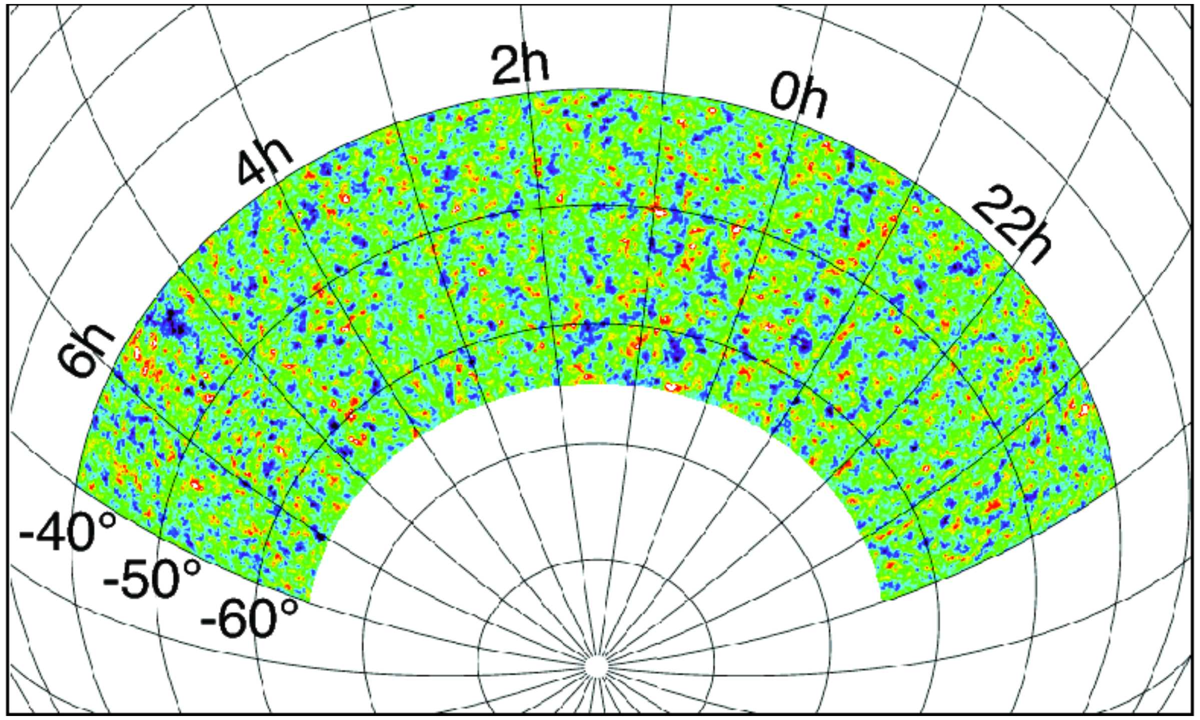

~700 confirmed galaxy clusters from the SPT 2500 deg^2 field (Bleem et al. 2015)

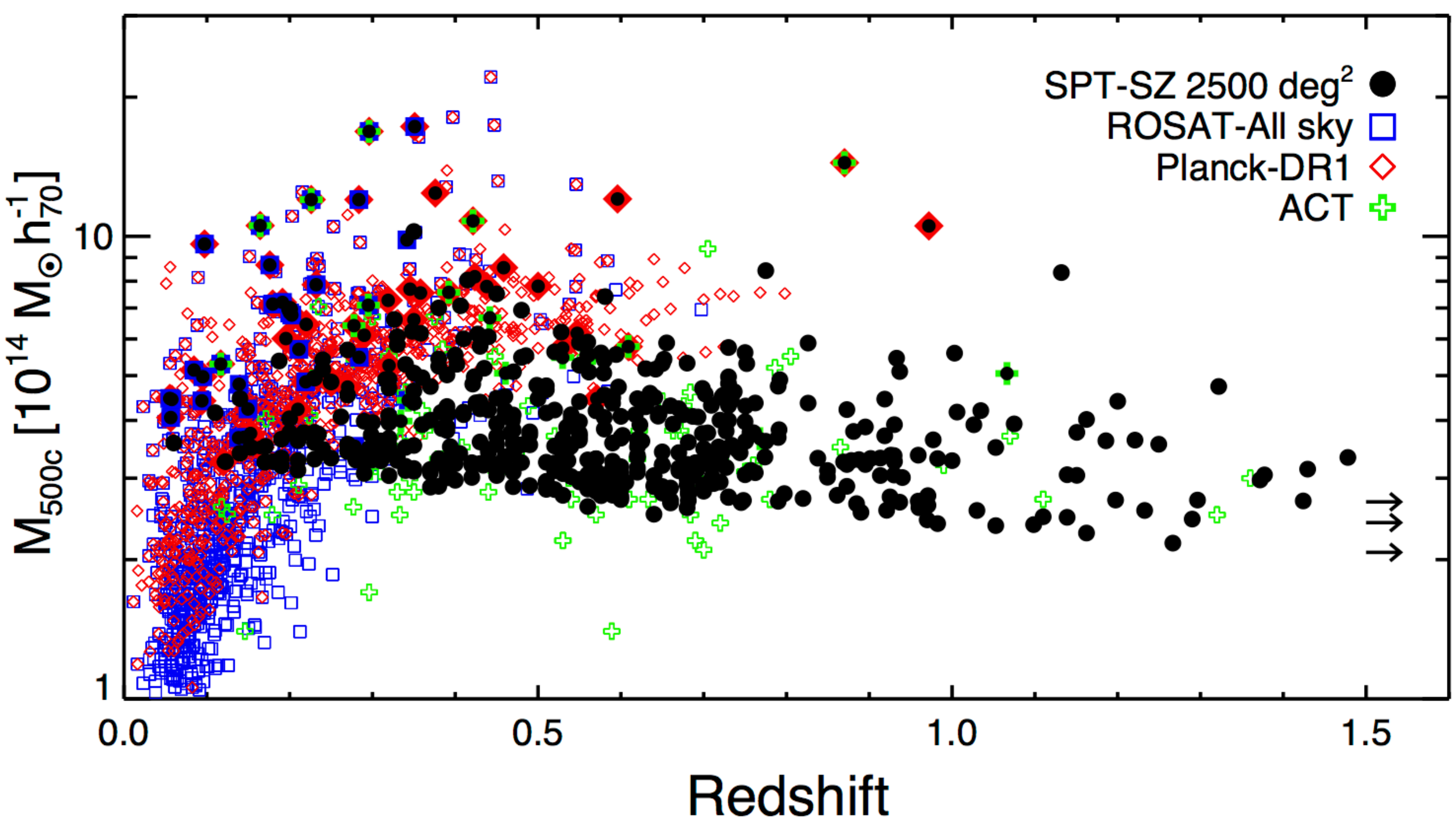

In the next few years

SPT-3G, currently taking data, is expected to find over 5000 clusters

Our own CCAT-prime project (with collaborators from US and Canada) will start taking data in 2021

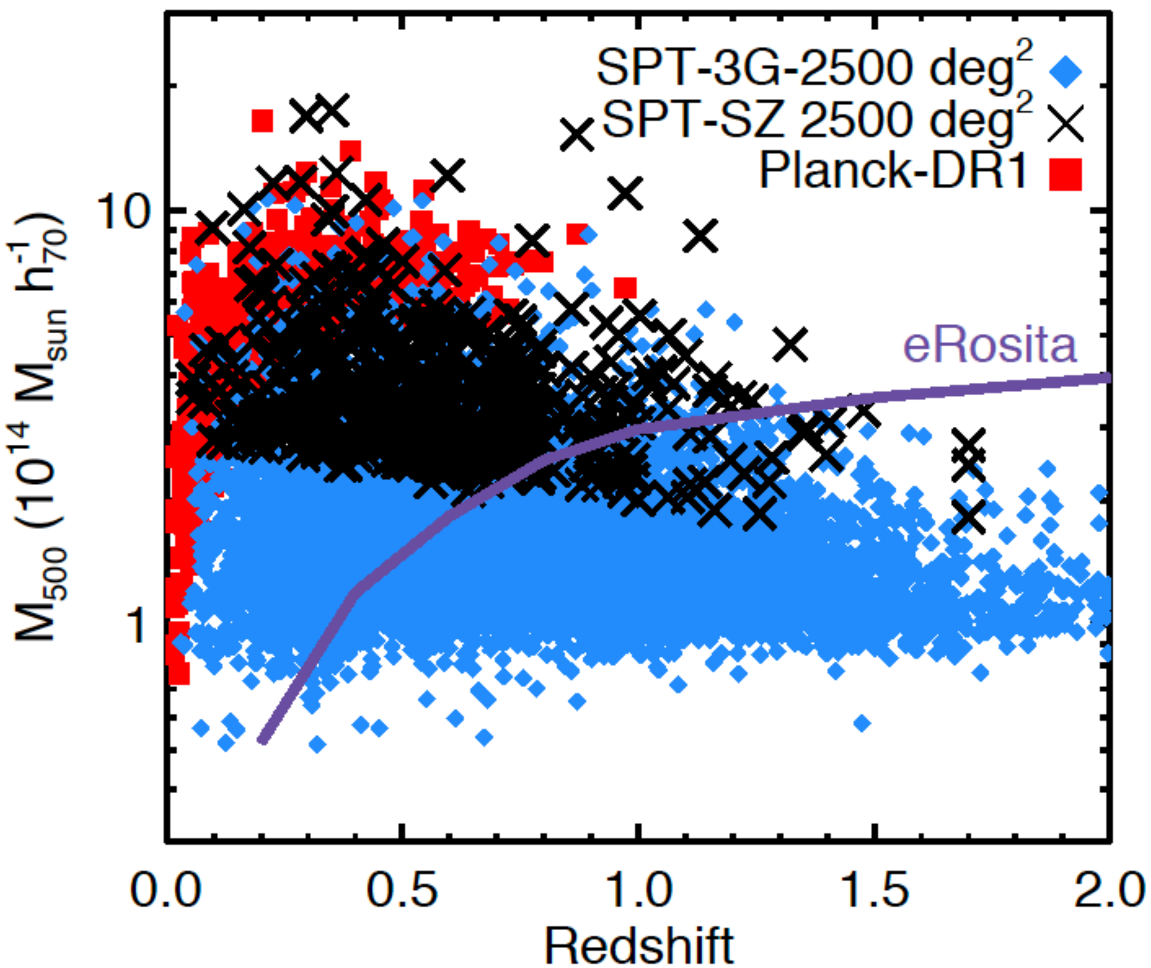

T_0 (uK)

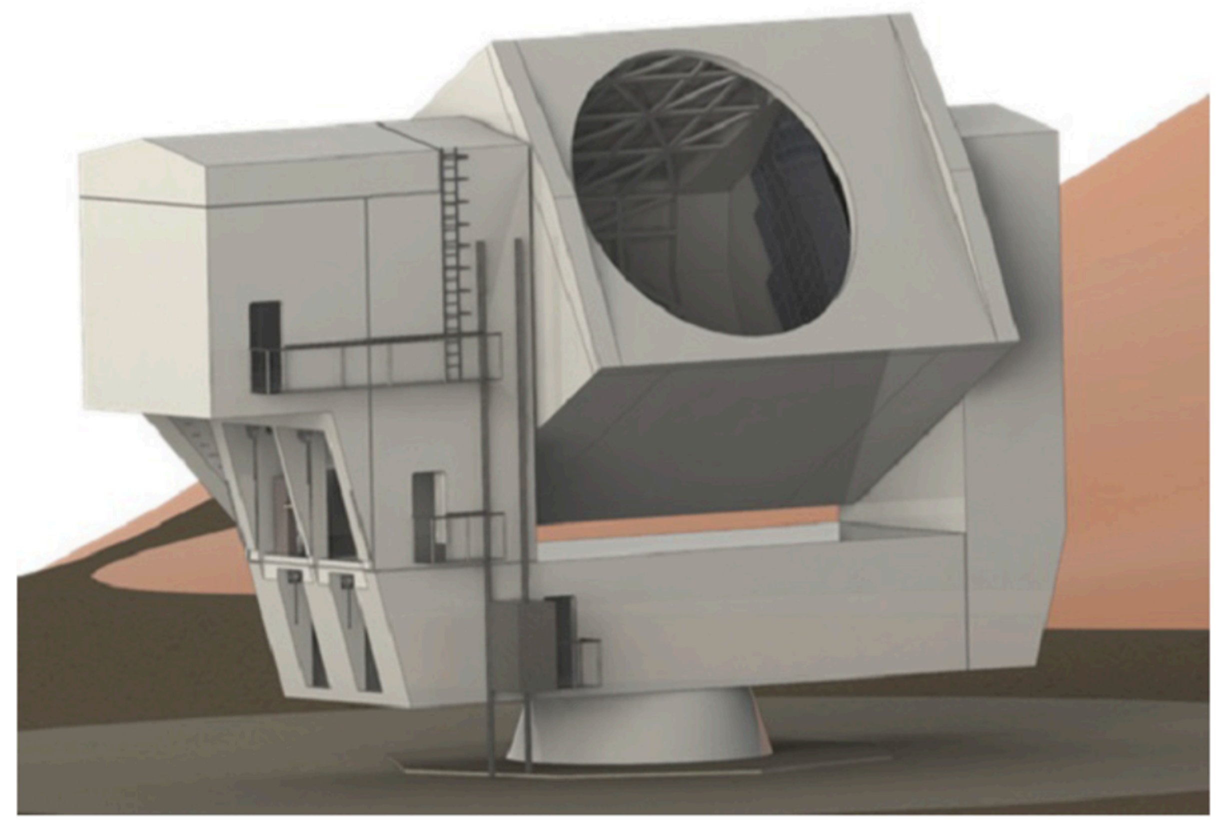

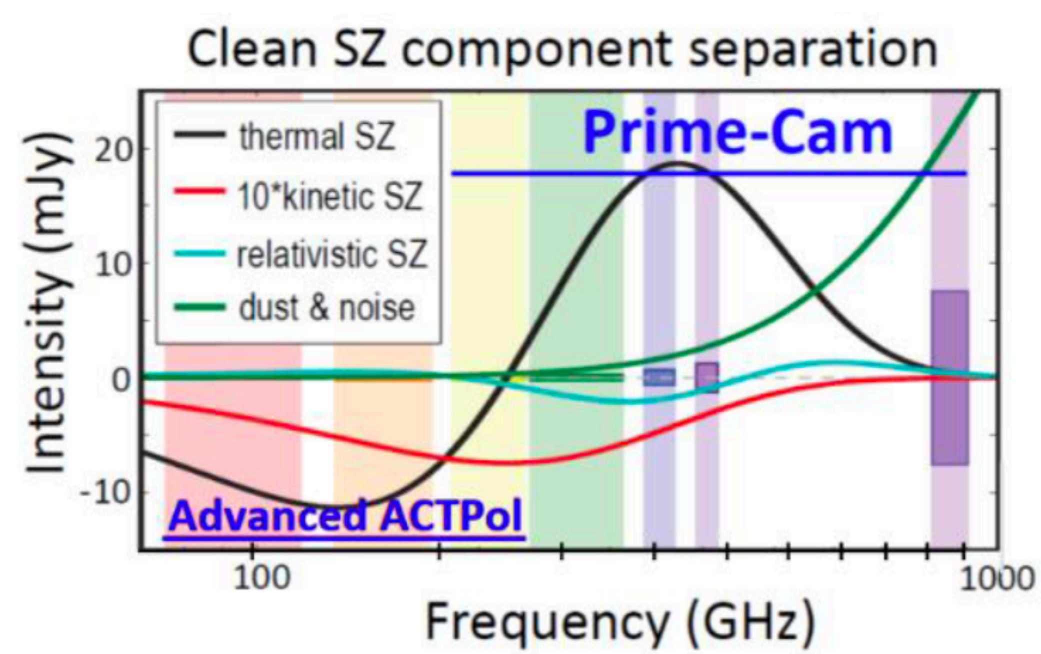

CCAT-prime's unique strength will be the separation of the tSZ, kSZ and rSZ components from multi-frequency observations

Questions?